Supplementary Information (SI) for Inorganic Chemistry Frontiers.

Supporting information

Coinage metal(I) clusters based on a $P,P'(N,N')_2$-ligand: colorful phosphorescence, abnormal thermal quenching behavior and anticounterfeiting application

Andrey Yu. Baranov,[a] Evgeniya P. Doronina,[b] Mariana I. Rakhmanova,[a] Irina Yu. Bagryanskaya,[c] Konstantin A. Brylev,[a] Taisiya S. Sukhikh,[a] Alexander V. Artem'ev*[a]

[a] *Nikolaev Institute of Inorganic Chemistry, 3, Acad. Lavrentiev Ave., 630090 Novosibirsk, Russia*
[b] *A. E. Favorsky Irkutsk Institute of Chemistry, SB RAS, 1 Favorsky Str., 664033 Irkutsk, Russia*
[c] *N. N. Vorozhtsov Novosibirsk Institute of Organic Chemistry, 9, Acad. Lavrentiev Ave., 630090 Novosibirsk, Russia*

*Author for correspondence: chemisufarm@yandex.ru (Alexander V. Artem'ev)

Table of contents

§1. General details and instrumentation

$AgNO_3$ (99%, Merck), KPF_6 (99%, Sigma-Aldrich), Celite® S (Sigma-Aldrich) and MeCN (HPLC grade, Cryochrom) were used as purchased. $[Ag(MeCN)_4]PF_6$ and $[Cu(MeCN)_4]PF_6$ were prepared by the same described method.[1] 1,2-Bis[bis(pyridin-2-ylmethyl)phosphino]ethane (**L**) was prepared as we previously described.[2] [Au(tht)Cl] and AuI were prepared using the literature methods.[3,4] Gold(I) phenylacetylide was obtained from [Au(tht)Cl] and phenylacetylene (98.0%, TCI) as described.[5] The commercially available solvents were purified by common methods before using for the synthetic procedures. All manipulations with 1,2-bis[bis(pyridin-2-ylmethyl)phosphino]ethane (**L**) were performed under an argon atmosphere using standard Schlenk equipment. All the reactions were performed at ambient temperature.

Powder X-ray diffraction analyses (PXRD) for compounds **1**, **2**, **5** and **6** were made on a Shimadzu XRD-7000 diffractometer (Cu-Kα radiation, Ni – filter, 3–35° 2θ range, 0.03° 2θ step, 5s per point).

The PXRD patterns of the compounds **3**, **4**, **7** and **8** were recorded with a Bruker D8 Venture diffractometer with a CMOS PHOTON III detector and an IμS 3.0 microfocus source (CuKα radiation, $\lambda = 1.54178$ Å, Montel mirrors) at 150K. The samples were prepared by fast grinding the powders harvested directly from mother liquor and depositing them to a glass needle with a small amount of epoxy. Debye diffraction patterns with continuous diffraction arcs were obtained by φ-scanning (360°).[6] To diminish the effect of the preferred orientations, five scans were made at different positions of a goniometer for ω from –240° to 0°. External standard (CeO_2) correction and integration were performed using the Dioptas program.[7]

CHN microanalyses were performed on a vario MICRO cube analyzer.

Thermogravimetric analyses (TGA&DTG) were carried out in a closed Al_2O_3 pan under argon flow at 10 °C/min^{-1} heating rate using a NETZSCH STA 449 F1 Jupiter STA instrument.

mid-IR spectra were recorded on a Bruker Vertex 80 FT-spectrometer in KBr pellets at ambient temperature.

^{1}H and $^{31}P\{^{1}H\}$ NMR spectra were registered using a Bruker AV-500 spectrometer at 500.13 and 202.46 MHz, respectively, at room temperature. ^{1}H NMR spectra were referenced using residual solvent peaks, and $^{31}P\{^{1}H\}$ NMR shifts are referenced respective to 85% H_3PO_4/D_2O as an external standard.

Steady-state excitation and emission spectra were recorded on a Fluorolog 3 spectrometer (Horiba Jobin Yvon) equipped with a cooled PC177CE-010 photon detection module and an R2658 photomultiplier. The emission decays were recorded on the same instrument. The absolute PLQYs were determined at 298 K using a Fluorolog 3 Quanta-phi integrating sphere. Temperature-dependent excitation and emission spectra as well as emission decays were recorded using an Optistat DN optical cryostat (Oxford Instruments) integrated with above spectrometer.

Electronic absorption spectra were recorded on a SF-2000 spectrophotometer (OKB Spectr).

ESI-MS spectra were recorded on the Shimadzu LCMS-9030 instrument using direct injection of a MeOH solution (10^{-3} M) of the sample.

§2. Synthesis and characterization data

[Au_2L_2](PF_6)$_2$ (**1**)

A solution of KPF_6 (40 mg, 0.218 mmol) in MeCN (2 mL) was added to **L** (101 mg, 0.218 mmol). To the resulting solution, a solution of [Au(tht)Cl] (70 mg, 0.218 mmol) in CH_2Cl_2 (3 mL) was then added while stirring. The reaction mixture was stirred for 6 h. The resulting mixture was centrifuged, filtered through a Celite pad and evaporated to give a yellow oil, which was triturated with Et_2O and dried under vacuum to give a yellowish powder. Yield: 133 mg (76%). X-Ray quality crystals of **1** were grown by Et_2O vapor diffusion into a MeCN solution of **1** at ambient temperature. Anal. Calc. for $C_{52}H_{56}Au_2F_{12}N_8P_6$: C, 39.0; H, 3.5; N, 7.0. Found: C, 39.1; H, 3.7; N, 6.8%. FT-IR (KBr, cm^{-1}): 403 (w), 496 (w), 557 (s), 752 (m), 841 (vs), 899 (m), 995 (m), 1155 (w), 1310 (w), 1404 (m), 1435 (s), 1472 (s), 1568 (m), 1587 (s), 2911 (w), 3009 (w), 3055 (w). ^{1}H NMR (500.13 MHz, DMSO-d_6, ppm), δ: 8.34 (d, J = 4.2 Hz, 8H, H-6 in Py), 7.67 (td, J = 7.6 Hz, J = 1.7 Hz, 8H, H-4 in Py), 7.24 (dd, J = 4.2 Hz, 8H, J = 7.6 Hz, 8H, H-5 in Py), 7.21 (d, J = 7.6 Hz, 8H, H-3 in Py), 3.62 (d, J = 14.3 Hz, 8H, in CH_aH_bPy), 3.55 (d, J = 14.3 Hz, 8H, in CH_aH_bPy), 2.54 (unres. t, 8H, in PCH_2CH_2P). ^{31}P{^{1}H} NMR (202.47 MHz, DMSO-d_6, ppm), δ: 33.24 (s, P from L), –144.18 (sept., J = 711 Hz, PF_6^-).

[$Au_2L_2I_2$] (**2**)

A solution of **L** (62 mg, 0.135 mmol) in CH_2Cl_2 (3 mL) was added to AuI (43 mg, 0.133 mmol) and the mixture was stirred for 10 h under an argon atmosphere in the dark. The resulting yellowish solution was filtered through a cotton wool. To the filtrate, Et_2O (20 mL) was then added and the mixture was kept at 4 °C for several days. The mother liquor containing a small amount of an amorphous precipitate was decanted. The colorless crystals of **2** were washed with Et_2O (2 × 3 mL) and dried under vacuum. Yield: 64 mg (61%). Anal. Calc. for $C_{52}H_{56}Au_2I_2N_8P_4$: C, 39.9; H, 3.6; N, 7.2. Found: C, 39.7; H, 3.5; N, 7.0. FT-IR (KBr, cm^{-1}): 405 (m), 488 (m), 583 (w), 625 (w), 664 (w), 752 (m), 783 (m), 793 (m), 806 (m), 837 (m), 870 (s), 993 (m), 1049 (w), 1082 (m), 1132 (w), 1150 (w), 1198 (w), 1256 (m), 1308 (w), 1398 (m), 1414 (m), 1433 (vs), 1472 (s), 1568 (s), 1587 (s), 1638 (w), 2901 (w), 3005 (w), 3042 (w). ^{1}H NMR (500.13 MHz, $CDCl_3$, ppm), δ: 8.34 (d, J = 4.8 Hz, 8H, H-6 in Py), 7.59 (d, J = 7.8 Hz, 8H, H-3 in Py), 7.51 (td, J = 7.7 Hz, J = 1.7 Hz, 8H, H-4 in Py), 7.05 (dd, J = 4.8 Hz, J = 7.8 Hz, H-5 in Py), 3.78 (d, J = 14.0 Hz, 8H, in CH_aH_bPy), 3.73 (d, J = 14.0 Hz, 8H, in CH_aH_bPy), 2.53 (br. s, 8H, in PCH_2CH_2P). ^{31}P{^{1}H} NMR (202.47 MHz, $CDCl_3$, ppm), δ: 24.80 (s).

[Au_2L_2(C≡CPh)$_2$]·EtOH (**3a**) and [AuL(C≡CPh)]$_n$ (**3b**)

A solution of **L** (70 mg, 0.153 mmol) in CH_2Cl_2 (4 mL) was added to gold(I) phenylacetylide (90 mg, 0.302 mmol) and the mixture was stirred overnight. The solution obtained was then filtered through a Celite pad and evaporated to give a yellow oil, which was triturated with Et_2O to give a yellowish powder. The obtained powder was washed with Et_2O (2 mL) and dried under vacuum. Yellowish powder. Yield: 136 mg (85%). The vapor diffusion of Et_2O into a solution of **3** in EtOH-CH_2Cl_2 (6:2, v/v) results in formation of crystals **3a**·EtOH contaminated by a small fraction of crystals of **3**. Crystals **3b** were mechanically separated from crystals **3a**·EtOH with tweezers. Anal. Calc. for $C_{44}H_{44}Au_2N_4P_2O$ (**3a**·EtOH): C, 48.0; H, 4.0; N, 5.1. Found: C, 48.1; H, 3.8; N, 5.2. FT-IR (KBr, cm^{-1}): 405 (w), 486 (m), 528 (w), 627 (w), 694 (s), 756 (vs), 797 (m), 841 (m), 858 (m), 995 (m), 1049 (w), 1080 (w), 1153 (w), 1209 (m), 1256 (w), 1308 (w), 1400 (m), 1435 (vs), 1470 (s), 1485 (s), 1568 (s), 1587 (vs), 2112 (w), 2909 (w), 2951 (vw), 3007 (w), 3048 (w). ^{1}H NMR (500.13 MHz, $CDCl_3$, ppm), *δ*: 8.56 (d, *J* = 4.4 Hz, 4H, H-6 in Py), 7.67 (td, *J* = 7.6 Hz, *J* = 1.6 Hz, 4H, H-4 in Py), 7.50 (d, *J* = 7.8 Hz, 4H, H-3 in Py), 7.45 (m, 4H, *o*-H in Ph), 7.25−7.16 (m, 6H, from Ph – *m*- and *p*-H and 4H from Py – H-5), 3.50 (t, *J* = 4.8 Hz, 8H, in CH_2Py), 2.35 (s, 4H, in PCH_2CH_2P). $^{31}P\{^1H\}$ NMR (202.47 MHz, $CDCl_3$, ppm), *δ*: 36.53 (s).

$[Ag_4L_2](PF_6)_4·2Me_2CO$ (**4**)

A solution of $[Ag(MeCN)_4]PF_6$ (210 mg, 0.50 mmol) in acetone (2 mL) was added to **L** (124 mg, 0.27 mmol), and the mixture was stirred for 3 h. The resulting solution was diluted with Et_2O (3 mL) and stirred for another 2 h. The presipitate formed was triturated with Et_2O. The obtained beige powder was dried under vacuum. Yield: 204 mg (80%). X-Ray quality single crystals of **4**·$2Me_2CO$ formulation (sc-XRD data) were grown by slow diffusion of Et_2O vapor into an acetone solution of **4**. Anal. Calc. for $C_{58}H_{68}Ag_4N_8P_8O_2F_{24}$: C, 34.1; H, 3.3; N, 5.5. Found: C, 33.9; H, 3.2; N, 5.6. FT-IR (KBr, cm^{-1}): 405 (w), 488 (w), 557 (s), 750 (m), 839 (vs), 1001 (w), 1053 (w), 1094 (w), 1161 (w), 1252 (w), 1315 (w), 1408 (m), 1418 (m), 1439 (m), 1479 (m), 1570 (m), 1601 (m), 1707 (w), 2928 (w), 2974 (w), 3015 (vw), 3075 (w). ^{1}H NMR (500.13 MHz, CD_3CN, ppm), *δ*: 8.33–8.05 (br. s, 8H, H-6 in Py), 7.69 (t, *J* = 7.5 Hz, 8H, H-4 in Py), 7.27 (d, *J* = 7.7 Hz 8H, H-3 in Py), 7.23–7.15 (m, 8H, H-5 in Py) 3.47–3.33 (m, 16H, CH_aH_bPy), 2.35 (br. s, 8H, PCH_2CH_2P). $^{31}P\{^1H\}$ NMR (202.47 MHz, CD_3CN, ppm), *δ*: –6.50 (br. s, **L**), –144.53 (sept, *J* = 704 Hz, PF_6^-).

$[Ag_9L_3(NO_3)_3](NO_3)_6·8H_2O$ (**5**)

A solution of $AgNO_3$ (86 mg, 0.504 mmol) in MeCN (4 mL) was added to **L** (77 mg, 0.168 mmol), and the mixture was stirred for 5 h in the dark. The precipitate formed was then centrifuged, washed with MeCN (3 mL) and dried under vacuum. The obtained powder (115 mg) was then dissolved in water (20 mL) under (50–60 °C) and filtered through a Celite pad. The filtrate was slowly evaporated at ambient temperature to give brownish crystals of **5**·$8H_2O$ formulation (sc-XRD data). Yield: 60 mg (35%). Anal. Calc. for $C_{78}H_{100}Ag_9N_{21}P_6O_{35}$: C, 30.7; H, 3.3; N, 9.6. Found: C, 31.0; H, 3.2; N, 9.6%. FT-IR (KBr, cm^{-1}): 496 (w), 758 (w), 789 (m), 826 (w), 1022 (w), 1161 (w), 1339 (vs), 1373 (vs), 1385 (vs), 1412 (s), 1441 (m), 1481 (m), 1570 (m), 1601 (s), 1634 (w), 2909 (w), 2955 (w), 3032 (vw), 3067 (vw), 3447 (m). ^{1}H NMR (500.13 MHz, DMSO-*d*$_6$, ppm), *δ*: 8.52 (d, *J* = 3.8 Hz, 12H, H-6 in Py), 7.83 (td, *J* = 7.7 Hz, *J* = 1.4 Hz, 12H, H-4 in Py), 7.41 (d, *J* = 7.8 Hz, 12H, H-3 in Py), 7.37 (m, 12H, H-5 in Py), 3.61–3.58 (m, 24H, in CH_2Py), 2.60–2.54 (br. s, 12H, in PCH_2CH_2P). $^{31}P\{^1H\}$ NMR (202.47 MHz, DMSO-*d*$_6$, ppm), *δ*: –3.47 (s).

$[Au_2Ag_4L_2(NO_3)_2(H_2O)](NO_3)_4\cdot H_2O$ (**6**)

Au(tht)Cl (11 mg, 0.017 mmol) in CH_2Cl_2 (2 mL) was added to a solution of **5**$\cdot 8H_2O$ (34 mg, 0.011 mmol) in H_2O (8 mL) while stirring vigorously. The mixture was stirred for 2 h in the dark. The precipitate formed was centrifuged off, and the water phase was separated, washed with CH_2Cl_2 (3 × 2 mL) and filtered through a Celite pad. The filtrate was slowly evaporated at ambient temperature to give the crystals of **6**$\cdot 2H_2O$ formulation (sc-XRD data). Off-white needles. Yield: 17 mg (48%). Anal. Calc. for $C_{52}H_{60}Ag_4Au_2N_{14}O_{20}P_4$: C, 29.0; H, 2.8; N, 9.1. Found: C, 28.9; H, 2.9; N, 9.1%. FT-IR (KBr, cm^{-1}): 417 (m), 496 (m), 756 (m), 789 (m), 826 (m), 868 (w), 1018 (m), 1038 (w), 1059 (w), 1090 (m), 1159 (m), 1337 (vs), 1414 (s), 1443 (s), 1481 (s), 1570 (m), 1599 (s), 1641 (w), 2905 (w), 2951 (w), 3030 (vw), 3073 (wv). $^{31}P\{^1H\}$ NMR (202.47 MHz, D_2O, ppm), δ: 41.76 (s, P from L), 28.13 (s, P from L).

$[Au_2Cu_4L_2Cl_2](PF_6)_4\cdot 2Me_2CO$ (**7**)

A solution of [Au(tht)Cl] (58 mg, 0.181 mmol) in CH_2Cl_2 (3 mL) was added to **L** (83 mg, 0.181 mmol). The resulting solution was stirred for 3 h. Hexane (10 mL) was then added to the solution to precipitate an intermediate product. The precipitate was triturated with Et_2O (2 × 3 mL) and dried under vacuum to afford a yellowish powder (110 mg). The powder was dissolved in the mixture of Me_2CO (11 mL) and MeCN (3.5 mL). $[Cu(MeCN)_4]PF_6$ (117 mg) was then added to the solution. The reaction mixture was stirred for 3 h. Et_2O (10 mL) was then added and the mixture was additionally stirred for 5 h. The precipitate formed was centrifuged, washed with Et_2O (5 mL) and dried. Yellow powder. Yield: 143 mg (67%). X-Ray quality crystals of **7**$\cdot 4Me_2CO\cdot 2EtOH$ formulation (sc-XRD data) were obtained by Et_2O vapor diffusion into a solution of **7** in MeCN-Me_2CO-EtOH mixed solvent at ambient temperature. Anal. Calc. for $C_{58}H_{68}Au_2Cl_2Cu_4N_8P_8F_{24}O_2$: C, 29.9; H, 2.9; N, 4.8. Found: C, 29.8; H, 2.8; N, 5.0%. FT-IR (KBr, cm^{-1}): 419 (vw), 496 (vw), 557 (m), 760 (w), 795 (m), 841 (vs), 878 (m), 1022 (vw), 1096 (vw), 1165 (vw), 1227 (vw), 1321 (w), 1366 (vw), 1408 (w), 1418 (w), 1443 (w), 1481 (w), 1570 (w), 1601 (m), 1709 (w), 2903 (vw), 2970 (vw), 3107 (vw). ^1H NMR (500.13 MHz, CD_3CN, ppm), δ: 8.40 (unres. m, , 8H, H-6 in Py), 7.70 (t, J = 7.5 Hz, 8H, H-4 in Py), 7.31–7.21 (m, 16H, H-3 and H-5 in Py), 3.79 (br. s, 16H, in CH_2Py), 2.53 (br. s, 8H, in CH_2CH_2). $^{31}P\{^1H\}$ NMR (202.47 MHz, CD_3CN, ppm), δ: 29.27 (s, P from L), –144.61 (sept., J = 704 Hz, PF_6^-).

$[Au_2Cu_4L_2I_2(MeCN)_4](PF_6)_4$ (**8**)

$[Cu(MeCN)_4]PF_6$ (20 mg, 0.0537 mmol) was added to a suspension of compound **2** (21 mg, 0.0134 mmol) in a mixture of MeCN (0.5 mL) and acetone (4 mL) while stirring. The solution was stirred for 3 h. The resulting yellow solution was filtered through a small celite pad. Et_2O was added dropwise to the filtrate until it became cloudy while stirring vigorously. The suspension formed was additionally stirred for another 2 h. The precipitate formed was centrifuged, washed with Et_2O (4 mL) and dried under vacuum. Yellow powder. Yield: 31 mg (90%). X-Ray quality single crystals of **8**$\cdot 10MeCN$ formulation (sc-XRD data) were grown by Et_2O vapor diffusion into a solution of **8** in a MeCN-acetone mixed solvent at 4 °C. Anal. Calc. for

$C_{60}H_{68}Au_2Cu_4F_{24}I_2N_{12}P_8$: C, 28.1; H, 2.7; N, 6.6. Found: C, 28.1; H, 2.8; N, 6.8%. FT-IR (KBr, cm^{-1}): 422 (w), 494 (w), 559 (s), 662 (vw), 758 (m), 793 (m), 843 (vs), 1018 (w), 1061 (w), 1082 (w), 1094 (w), 1165 (w), 1250 (w), 1314 (w), 1412 (m), 1441 (m), 1477 (s), 1568 (w), 1599 (s), 2253 (vw), 2270 (vw), 2903 (vw), 2941 (vw), 2968 (vw), 3075 (vw). $^{31}P\{^1H\}$ NMR (202.47 MHz, $(CD_3)_2CO$, ppm), δ: 29.03 (br. s, P from L), 17.60 (br. s, P from L), –143.49 (sept, J = 708 Hz, PF_6^-).

§3. Single crystal X-ray crystallography

The data for **1**, **2**, **3a**·EtOH, **3b** and **7**·$4Me_2CO$·2EtOH were collected on a Bruker Kappa Apex II CCD diffractometer using φ,ω-scans of narrow (0.5°) frames with MoKα radiation (λ = 0.71073 Å) and a graphite monochromator. The data for **4**·$2Me_2CO$, **5**·$8H_2O$, **6**·H_2O and **8**·3MeCN were collected with a Bruker D8 Venture diffractometer with a CMOS PHOTON III detector and IμS 3.0 source [λ(MoKα) = 0.71073 Å, mirror optics]. The structures were solved by direct methods SHELXL97 and refined by a full matrix least-squares anisotropic-isotropic (for H atoms) procedure using SHELXL-2014/7 programs set.[8] Absorption corrections were applied using the empirical multiscan method with the SADABS program.[9] The positions of the hydrogen atoms were calculated with the riding model. Free solvent accessible volume in **3a**·EtOH derived from PLATON[10] routine analysis was found to be 11.6% (990.0 $Å^3$). This volume is occupied by highly disordered solvent molecules EtOH that could not be modeled as a set of discrete atomic sites. We employed PLATON/SQUEEZE procedure to calculate the contribution to the diffraction from the solvent region and thereby produced a set of solvent-free diffraction intensities.

Table S1. Table of SC-XRD experimental details for **1–4**.

	1	**2**	**3a**·EtOH	**3b**	**4**·2Me$_2$CO
CCDC number	2265012	2292654	2265013	2265014	2420289
Chemical formula	$C_{52}H_{56}Au_2N_8P_6F_{12}$	$C_{52}H_{56}Au_2I_2N_8P_4$	$C_{42}H_{38}Au_2N_4P_2$	$C_{42}H_{38}Au_2N_4P_2$	$C_{58}H_{68}Ag_4N_8P_8O_2F_{24}$
M_r	1600.80	1564.66	1054.63	1054.63	2044.44
Crystal system, space group	Monoclinic, $P2_1/c$	Monoclinic, $C2/c$	Monoclinic, $C2/c$	Triclinic, $P\bar{1}$	Triclinic, $P\bar{1}$
Temperature (K)	296	296	296	200	150
a, b, c (Å)	26.3706 (11), 11.0301 (4), 21.6082 (10)	44.2073 (19), 13.8208 (6), 18.4512 (9)	25.724 (7), 13.051 (3), 26.005 (6)	10.6314 (6), 12.0455 (7), 16.7803 (10)	12.3098 (7), 13.8300 (7), 24.1177 (13)
α, β, γ (°)	111.895 (2)	93.978 (3)	102.025 (13)	89.945 (2), 74.808 (2), 68.814 (2)	99.914 (2), 91.989 (2), 115.002 (2)
V (Å^3)	5831.8 (4)	11246.2 (9)	8539 (4)	1923.1 (2)	3638.9 (3)
Z	4	8	8	2	2
μ (mm^{-1})	5.27	6.47	6.97	7.74	1.35
Crystal size (mm)	0.40 × 0.10 × 0.05	0.40 × 0.20 × 0.10	0.40 × 0.15 × 0.05	0.80 × 0.30 × 0.10	0.13 × 0.08 × 0.05
T_{min}, T_{max}	0.698, 0.928	0.552, 0.801	0.422, 0.862	0.325, 0.802	0.679, 0.746
No. of measured, independent and observed [$I > 2s(I)$] reflections	105340, 17133, 13209	70766, 12957, 9047	41762, 8577, 4609	20524, 8818, 7204	34258, 15812, 12410
R_{int}	0.071	0.067	0.109	0.050	0.032
(sin θ/λ)$_{max}$ (Å^{-1})	0.706	0.652	0.623	0.649	0.641
$R[F^2>2s(F^2)]$, $wR(F^2)$, S	0.033, 0.079, 1.01	0.042, 0.097, 1.02	0.073, 0.194, 1.06	0.036, 0.108, 1.05	0.063, 0.169, 1.06
No. of reflections	17133	12957	8577	8818	15812
No. of parameters	721	613	379	451	942
$\Delta\rho_{max}$, $\Delta\rho_{min}$ (e Å^{-3})	1.02, -0.62	1.51, -1.06	1.78, -1.16	2.13, -1.95	1.83, -0.80

Table S2. Table of SC-XRD experimental details for **5**–**8**.

	5·$8H_2O$	**6**·H_2O	**7**·$4Me_2CO$·$2EtOH$	**8**·$3MeCN$
CCDC number	2420290	2420291	2265015	2453798
Chemical formula	$C_{78}H_{100}Ag_9N_{21}O_{35}P_6$	$C_{52}H_{60}Ag_4Au_2N_{14}O_{20}P_4$	$C_{68}H_{92}Au_2Cl_2Cu_4N_8P_8F_{24}O_6$	$C_{60}H_{68}Au_2Cu_4I_2N_{12}P_4\cdot 4(F_6P)\cdot 3[C_2H_3N]$
M_r	3048.43	2150.43	2540.24	2686.07
Crystal system, space group	Monoclinic, $C2/c$	Triclinic, $P\bar{1}$	Triclinic, $P\bar{1}$	Orthorhombic, $Pcca$
Temperature (K)	150	150	200	150
a, b, c (Å)	21.358 (2), 19.231 (2), 27.464 (3)	16.345 (13), 18.847 (14), 20.584 (16)	12.3615 (5), 14.0830 (7), 15.0530 (7)	39.4826 (13), 16.0227 (5), 28.5922 (10)
α, β, γ (°)	109.293 (3)	89.015 (18), 88.86 (2), 89.472 (17)	67.048 (2), 86.616 (2), 70.550 (1)	
V (Å^3)	10646 (2)	6339 (8)	2267.78 (18)	18087.9 (10)
Z	4	4	1	8
μ (mm^{-1})	1.80	6.01	4.44	14.54
Crystal size (mm)	0.08 × 0.08 × 0.08	0.07 × 0.02 × 0.02	0.40 × 0.20 × 0.04	0.14 × 0.09 × 0.04
T_{min}, T_{max}	0.543, 0.745	0.368, 0.745	0.759, 0.928	0.417, 0.753
No. of measured, independent and observed [$I > 2s(I)$] reflections	23081, 8594, 4802	21055, 6038, 3272	24288, 10407, 8347	121814, 15958, 12954
R_{int}	0.092	0.193	0.046	0.102
$(\sin \theta/\lambda)_{max}$ (Å^{-1})	0.582	0.385	0.652	0.596
$R[F^2>2s(F^2)]$, $wR(F^2)$, S	0.060, 0.155, 0.99	0.090, 0.260, 1.04	0.041, 0.106, 1.08	0.091, 0.254, 1.04
No. of reflections	8594	6038	10407	15958
No. of parameters	646	698	554	1014
$\Delta\rho_{max}$, $\Delta\rho_{min}$ (e Å^{-3})	1.02, -1.08	1.14, -1.15	1.96, -0.96	5.18, -2.49

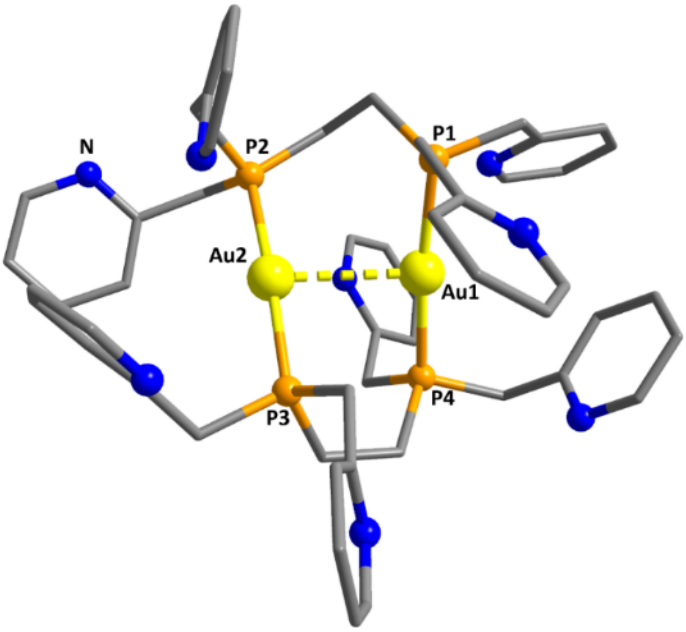

Figure S1. The structure of **1** (H atoms and uncoordinated anions are omitted for clarity). Selected interatomic distances (Å) and angles (°): Au1–Au2 2.9447(2), Au1–P4 2.2873(9), Au1–P1 2.3050(9), Au2–P3 2.3120(9), Au2–P2 2.3152(9), P4–Au1–P1 174.08(3), P3–Au2–P2 176.06(3).

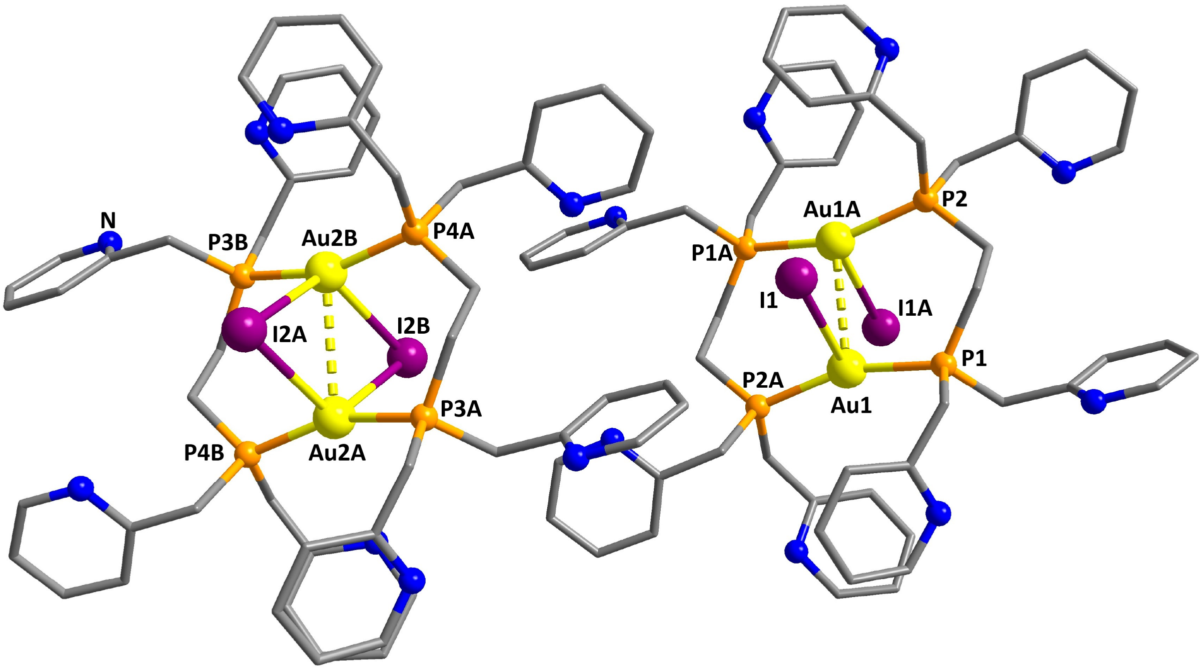

Figure S2. The structure of **2** (one of the two independent units, H atoms are omitted for clarity). Selected interatomic distances (Å) and angles (°): Au2B–Au2A 3.1324(5), Au1–Au1A 3.0695(5), Au2B–P4A 2.2919(13), Au2B–P3B 2.2913(13), Au2B–I2B 3.2009(5), Au1–P2A 2.2946(14), Au1–P1 2.2961(14), Au1–I1 3.2365(6), I1–Au1–Au1A 68.993(14), P4B–Au2A–P3A 159.27(5), P4A–Au2B–Au2A 100.66(4), P3B–Au2B–Au2A 99.78(4), P4A–Au2B–I2B 93.71(4), P3B–Au2B–I2B 92.19(4), Au2A–Au2B–I2B 63.734(12). Symmetry codes: A (1–*x*; 1–*y*; 1–*z*), B (0.5–*x*, 1.5–*y*, 1–*z*).

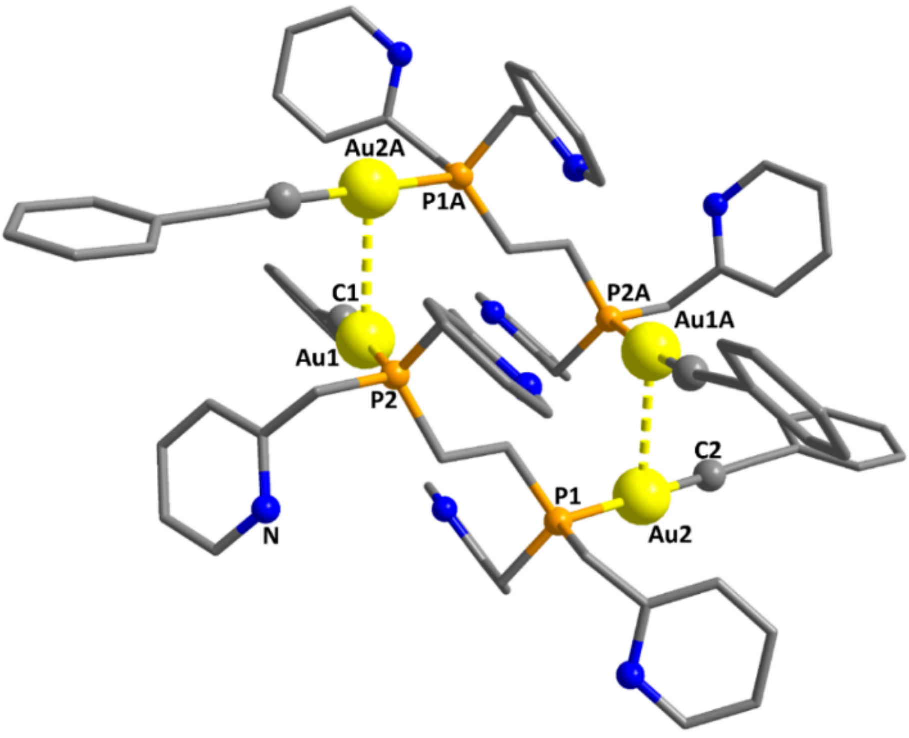

Figure S3. The structure of **3a** (two symmetrically dependent units are presented to show metallophilic interactions, H atoms are omitted for clarity). Selected interatomic distances (Å) and angles (°): Au1–Au2A 3.0717(11), Au1–C1 1.95(2), Au1–P2 2.254(5), Au2–C2 2.011(16), Au2–P1 2.262(4), C1–Au1–P2 174.3(5), C1–Au1–Au2A 92.8(5), P2–Au1–Au2A 92.82(12), C2–Au2–P1 178.8(5), C2–Au2–Au1A 88.2(5), P1–Au2–Au1A 92.20(13), P1A–Au2A–Au1–P2 110.6(2). Symmetry code: A (–*x*; 2–*y*; –*z*).

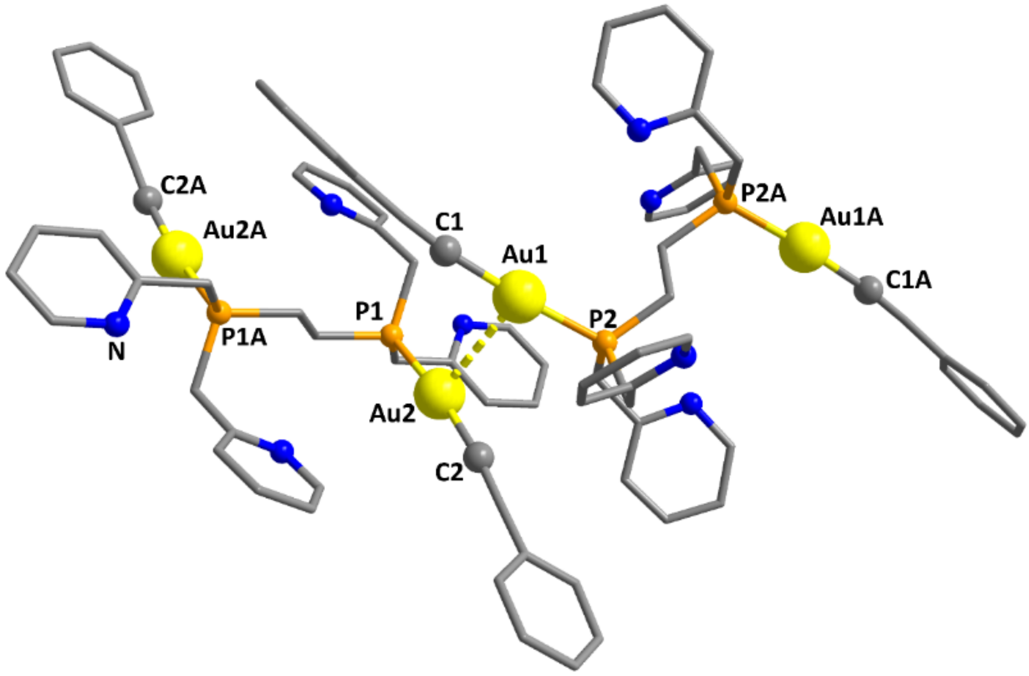

Figure S4. The structure of **3b** (two symmetrically dependent units are presented to show metallophilic interactions). The H atoms are omitted for clarity. Selected interatomic distances (Å) and angles (°): Au1–Au2 3.2029(3), Au1–C1 2.010(6), Au1–P2 2.2797(14), Au2–C2 2.018(5), Au2–P1 2.2793(13), C1–Au1–P2 175.80(16), C1–Au1–Au2 91.09(16), P2–Au1–Au2 93.07(4), C2–Au2–P1 172.45(16), C2–Au2–Au1 87.56(16), P1–Au2–Au1 99.96(4), P1–Au2–Au1–P2 122.8(6). Symmetry code: A (1–*x*; 1–*y*; –*z*).

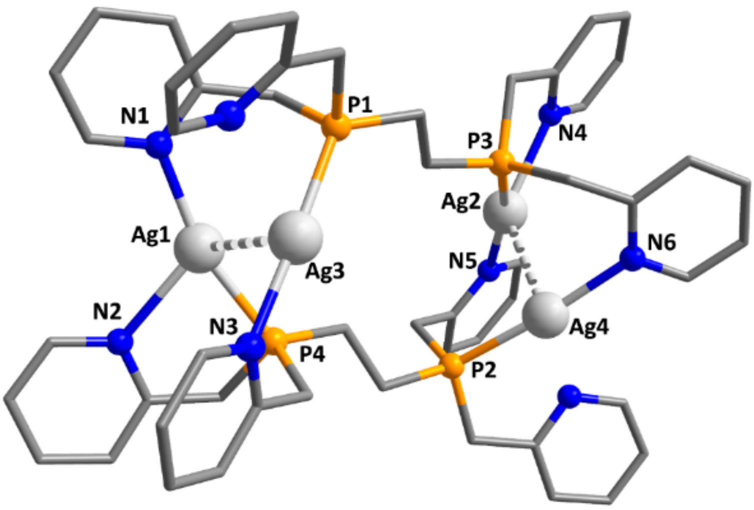

Figure S5. The structure of **4** (H atoms, solvate molecules and anions are omitted for clarity). Selected interatomic distances (Å) and angles (°): Ag1–Ag3 2.9168(7), Ag2–Ag4 2.9037(7), Ag1–N1 2.178(5), Ag1–N2 2.506(6), Ag1–P4 2.3880(17), Ag3–N3 2.209(6), Ag3–P1 2.3811(17), Ag2–N4 2.427(6), Ag2–N5 2.196(6), Ag2–P3 2.4236(18), Ag4–N6 2.203(6), Ag4–P2 2.3785(17), N1–Ag1–N2 120.4(2), N1–Ag1–P4 162.74(15), N2–Ag1–P4 76.81(14), N3–Ag3–P1 176.92 (16), N6–Ag4–P2 175.27(16), N4–Ag2–N5 121(1), N5–Ag2–P3 160.80(14), N4–Ag2–P3 77.54(17).

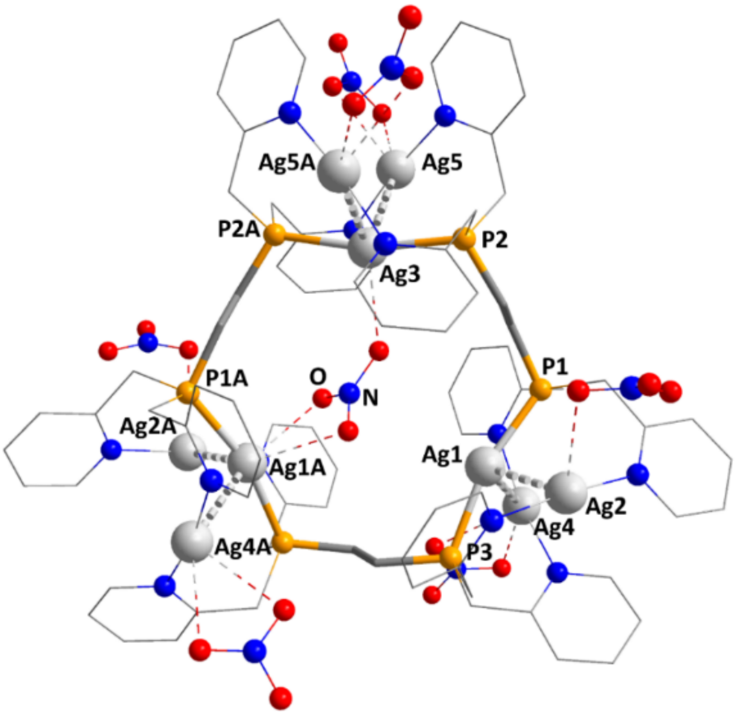

Figure S6. The structure of **5** (H atoms, uncoordinated anions, and solvate molecules are omitted for clarity). Selected interatomic distances (Å) and angles (°): Ag1–Ag2 2.9892(12), Ag1–Ag4 3.0245(13), Ag3–Ag5 3.0262(12), Ag1–P1 2.407(3), Ag1–P3 2.404(3), Ag3–P2 2.395(3), Ag–N_{Py} 2.161–2.191, Ag–O 2.661–2.914, Ag2–Ag1–Ag4 113.38(4), P3–Ag1–P1 164.90(10), P2A–Ag3–P2 166.93(15), Ag5–Ag3–Ag5A 103.43(5), N_{Py}–Ag–N_{Py} 169.06–175.02. Symmetry code: A (1–*x*; *y*; 1.5–*z*).

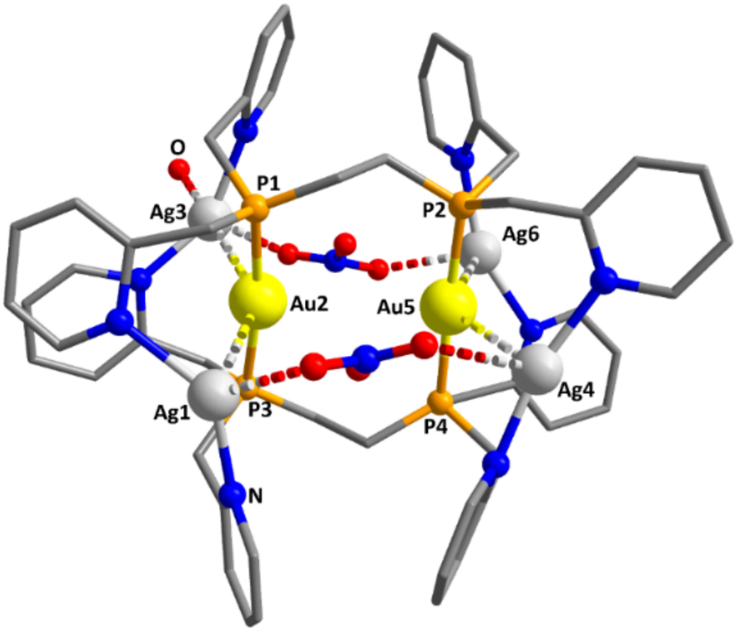

Figure S7. The structure of **6** (one of the two independent unit, H atoms, uncoordinated anions, and solvate molecules are omitted for clarity). Selected interatomic distances (Å) and angles (°): Au2–Ag1 3.054(7), Au2–Ag3 3.001(6), Au5–Ag4 2.967(6), Au5–Ag6 2.961(6), Au2–P1 2.326(17), Au2–P3 2.318(16), Au5–P2 2.290(16), Au5–P4 2.291(17), Ag–N_{Py} 2.01–2.26, Ag–O_{NO3} 2.48–2.85, Ag3–Au2–Ag1 143.74(19), Ag6–Au5–Ag4 131.18(19), P3–Au2–P1 171.9(6), P2–Au5–P4 177.6(6), N_{Py}–Ag1–N_{Py} 133.7(17), N_{Py}–Ag3–N_{Py} 146.0(19), N_{Py}–Ag4–N_{Py} 165.0(17), N_{Py}–Ag6–N_{Py} 156.8(18).

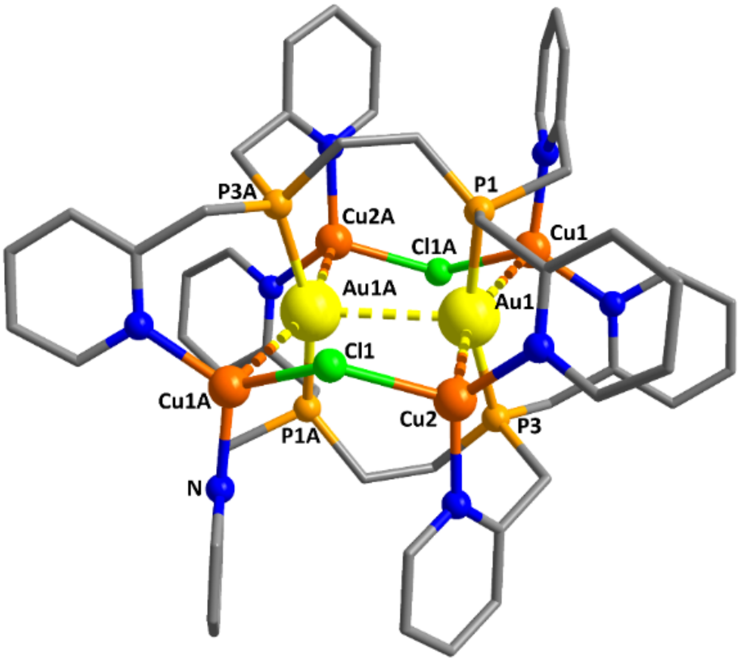

Figure S8. The structure of **7** (H atoms, uncoordinated anions, and solvate molecules are omitted for clarity). Selected interatomic distances (Å) and angles (°): Au1–Cu1 2.7896(7), Au1–Cu2 2.8282(7), Au1–Au1A 3.0640(4), Au1–P1 2.3090(13), Au1–P3 2.3179(14), Cu1–Cl1A 2.2551(15), Cu2–Cl1 2.3335(16), Cu–N (av.) 1.987, P1–Au1–P3 161.39(5), P1–Au1–Cu1 86.00(4), P3–Au1–Cu1 89.15(4), P1–Au1–Cu2 89.65(3), P3–Au1–Cu2 87.95(4), Cu1–Au1–Cu2 157.37(2), P1–Au1–Au1A 94.51(4), P3–Au1–Au1A 103.88(4), Cu1–Au1–Au1A 113.616(17), Cu2–Au1–Au1A 88.851(17), Cu1A–Cl1–Cu2 128.65(7). Symmetry code: A (1–*x*; 1–*y*; 1–*z*).

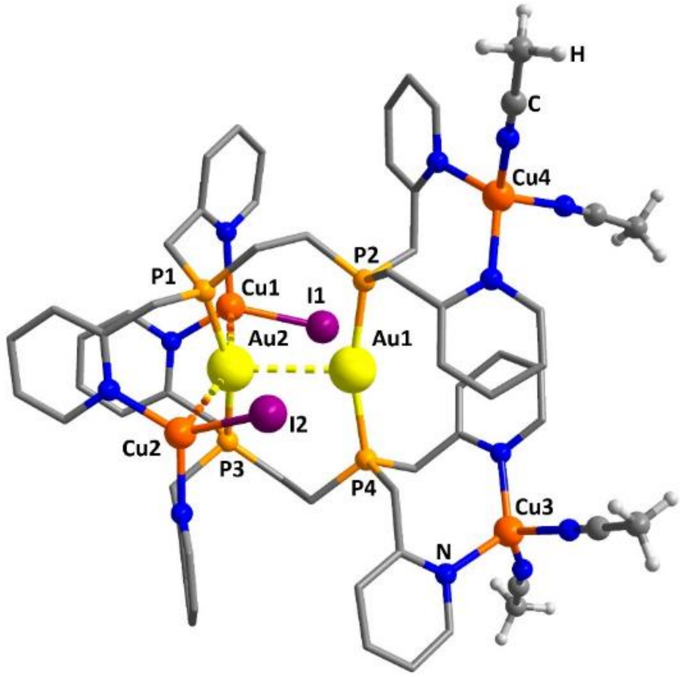

Figure S9. The structure of **8** (H atoms, uncoordinated anions, and solvate molecules are omitted for clarity). Selected interatomic distances (Å) and angles (°): Au1–Au2 3.1600(8), Au2–Cu1 2.776(2), Au2–Cu2 2.773(2), Au2–P1 2.313(4), Au2–P3 2.302(3), Au1–P2 2.309(3), Au1–P4 2.306(3), I1–Cu1 2.521(2), I2–Cu2 2.518(2), Cu1–N$_{Py}$ 1.98–2.01, Cu2–N$_{Py}$ 1.98–2.02, Cu4–N$_{Py}$ 2.042–2.053, Cu4–N$_{MeCN}$ 1.990–2.062, Cu3–N$_{Py}$ 2.038–2.041, Cu3–N$_{MeCN}$ 2.012–2.059, Cu1–Au2–Au1 100.87(5), Cu1–Au2–Cu2 159.63(7), Cu2–Au2–Au1 99.49(5), P1–Au2–Au1 100.16(9), P1–Au2–Cu1 85.34(10), P1–Au2–Cu2 90.80(10), P1–Au2–P3 160.91(13), N$_{Py}$–Cu1–N$_{Py}$ 116.2(5), N$_{Py}$–Cu2–N$_{Py}$ 115.4(5), N$_{Py}$–Cu3–N$_{Py}$ 120.0(5), N$_{Py}$–Cu4–N$_{Py}$ 119.6(5), N$_{MeCN}$–Cu3–N$_{MeCN}$ 100.0(6), N$_{MeCN}$–Cu4–N$_{MeCN}$ 102.8(6).

§4. Powder X-ray diffraction data

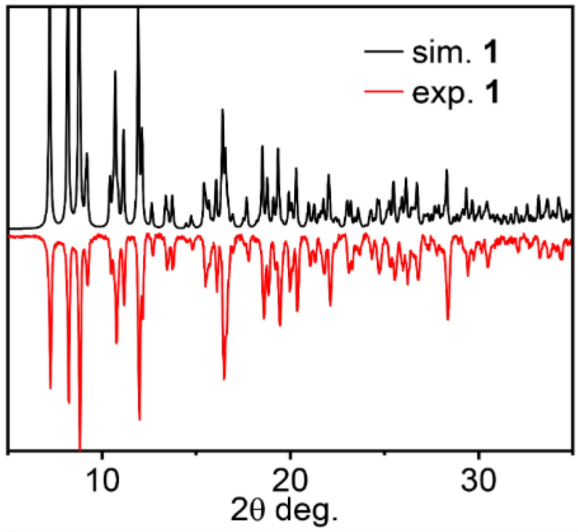

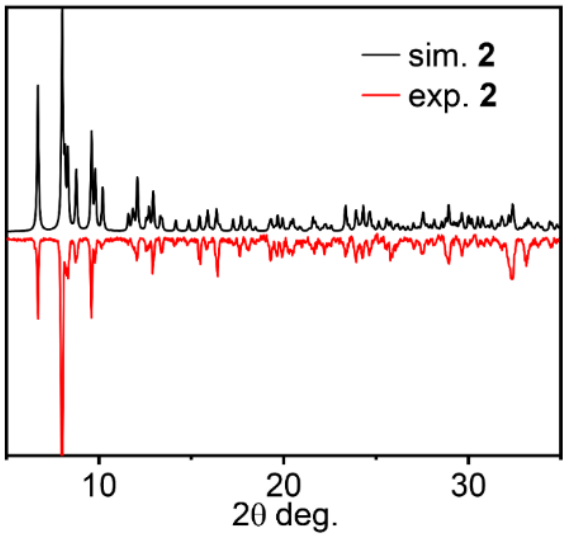

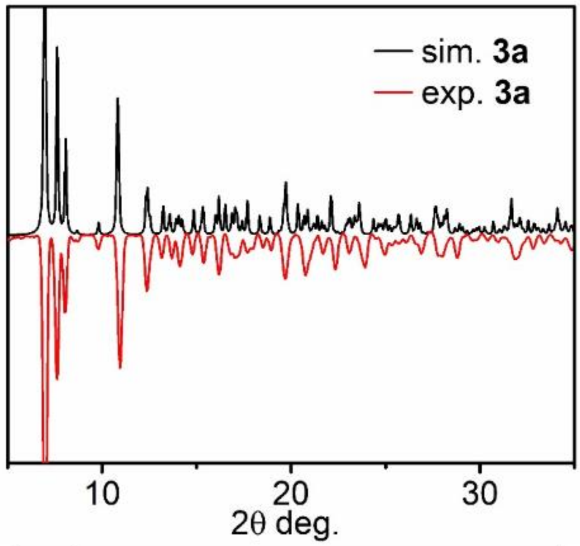

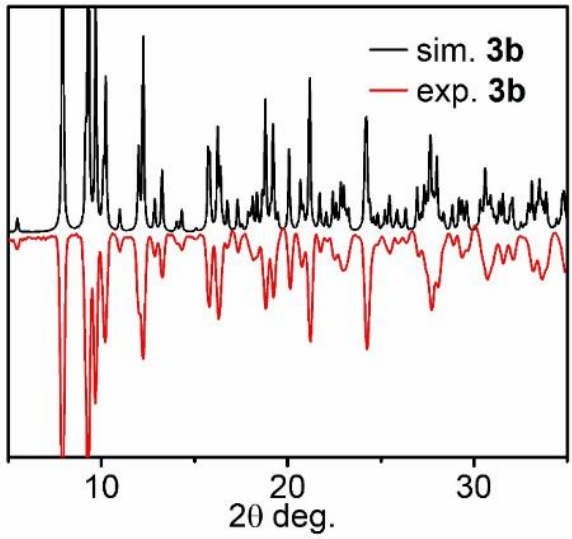

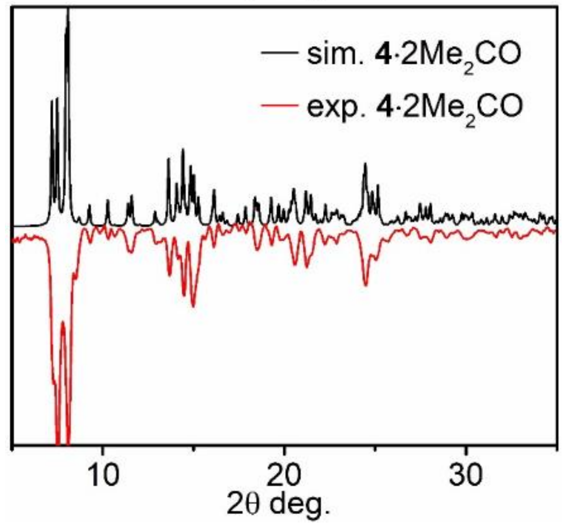

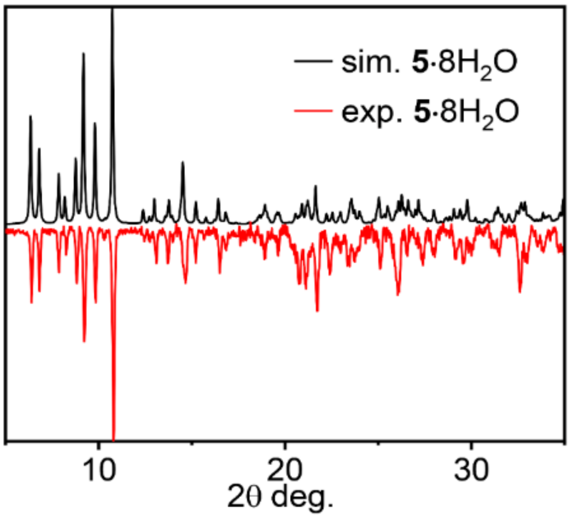

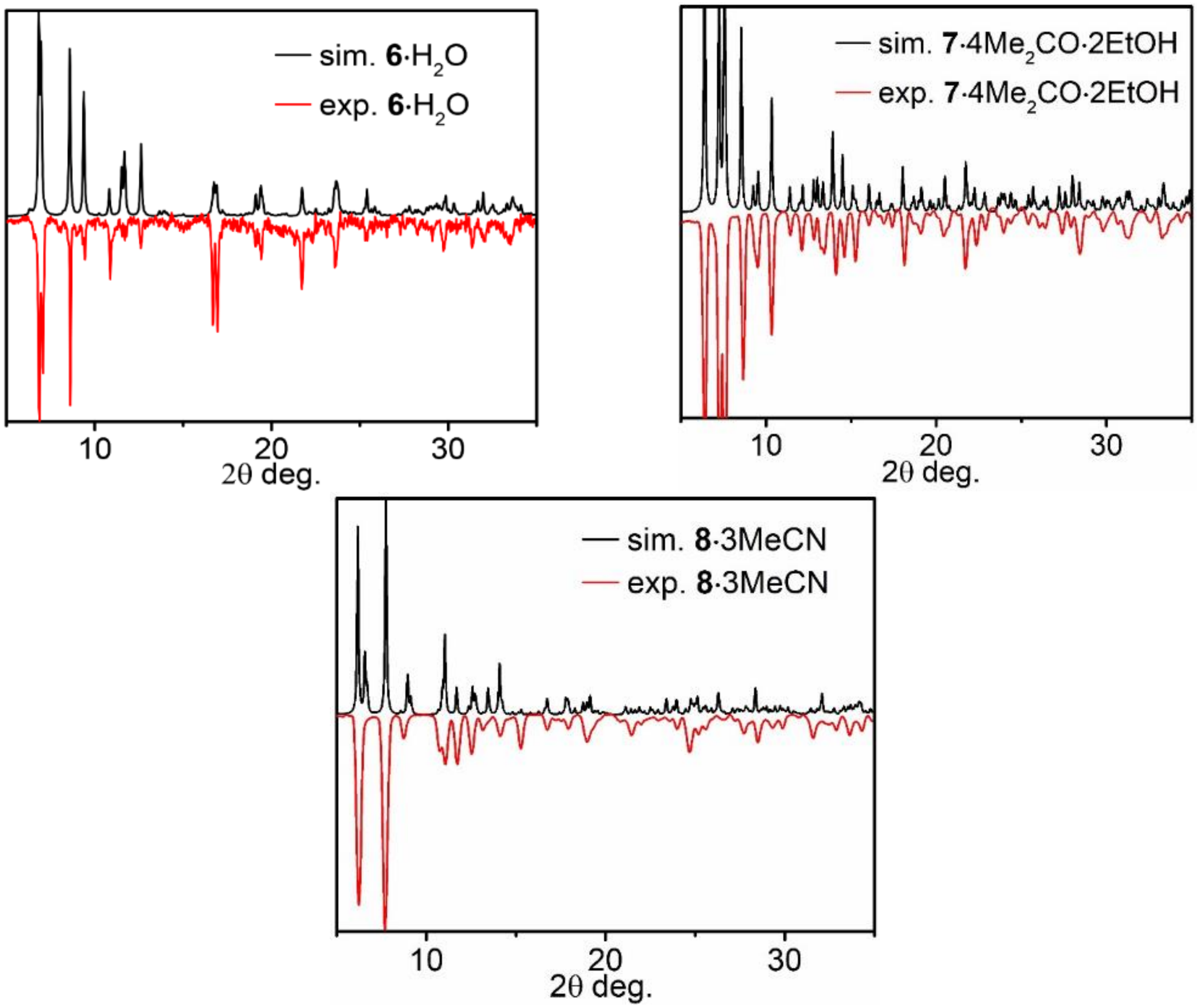

Figure S10. Simulated and experimental PXRD patterns of the compounds **1**–**8**.

§5. NMR spectra

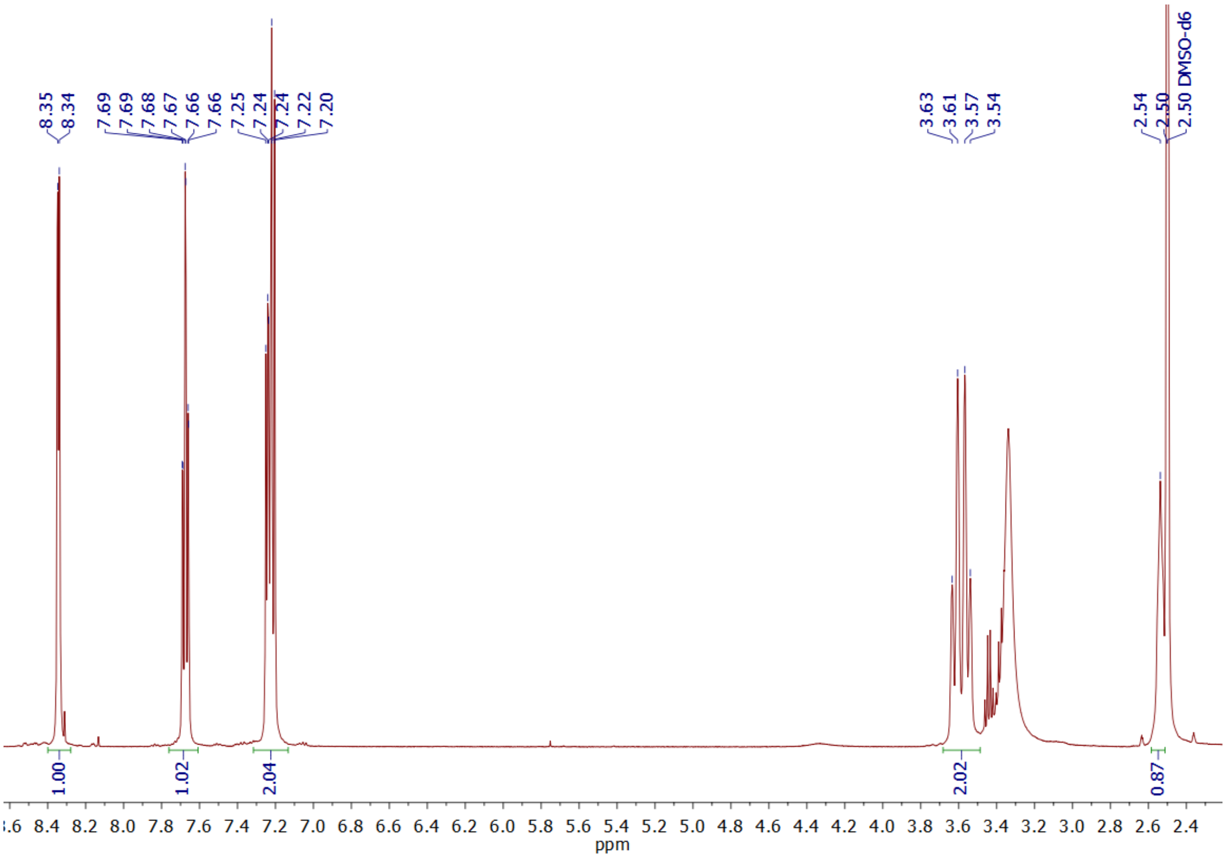

Figure S11. ^{1}H NMR spectrum of **1** in DMSO-d_6.

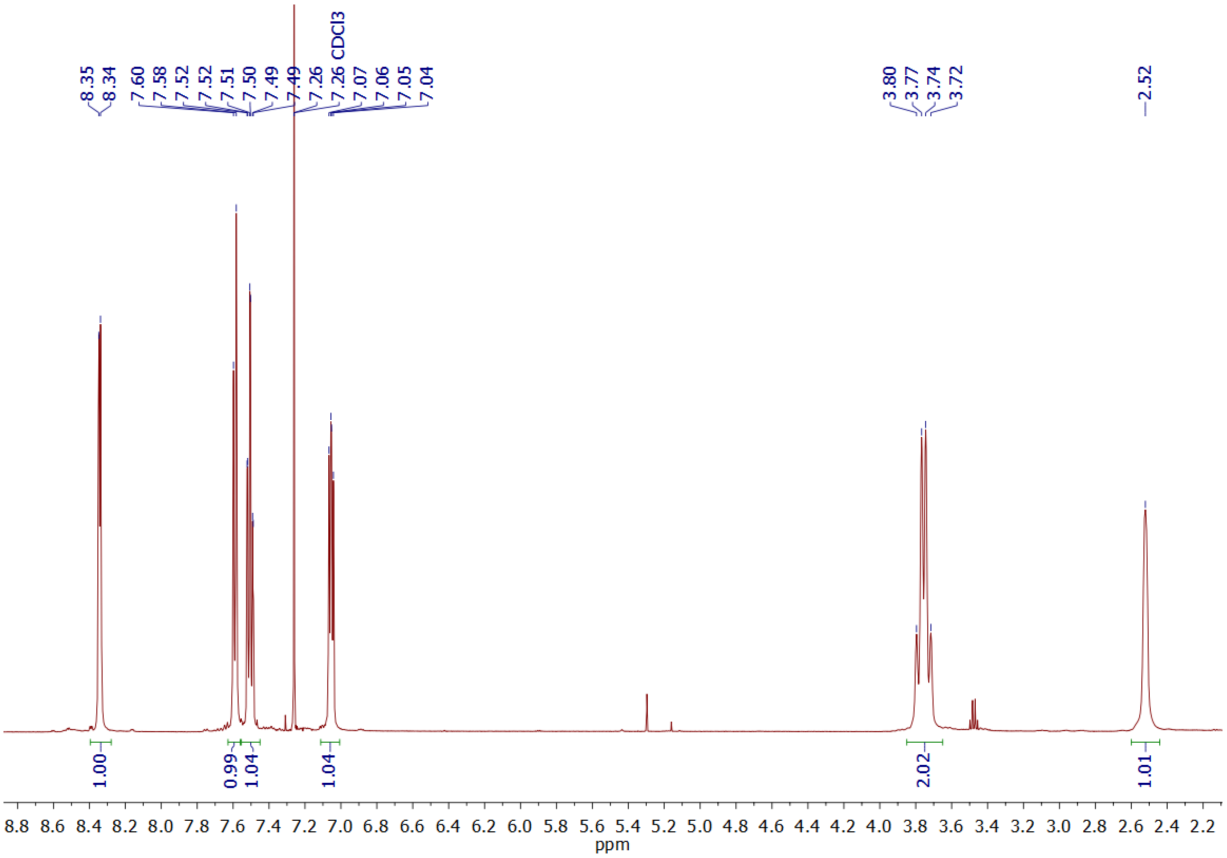

Figure S12. ^{1}H NMR spectrum of **2** in $CDCl_3$.

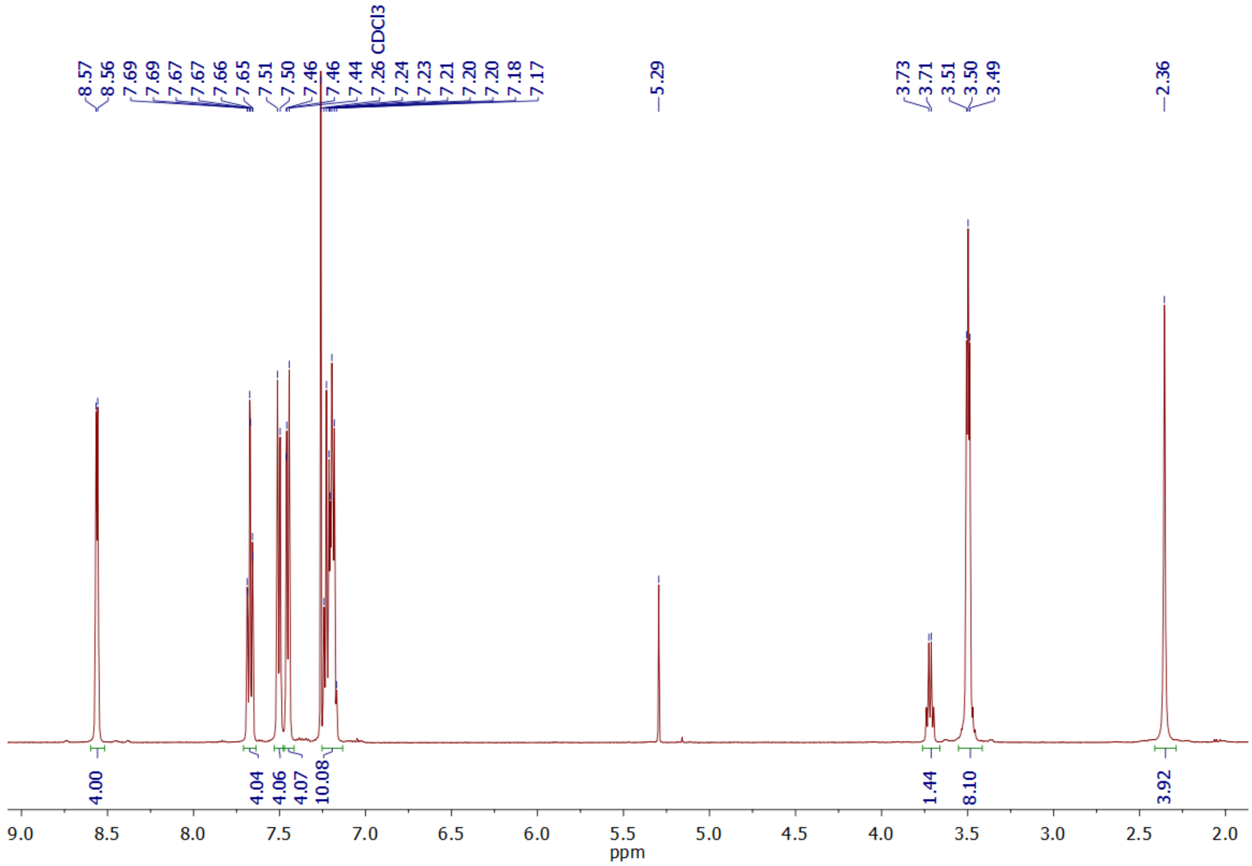

Figure S13. ^{1}H NMR spectrum of **3** in $CDCl_3$.

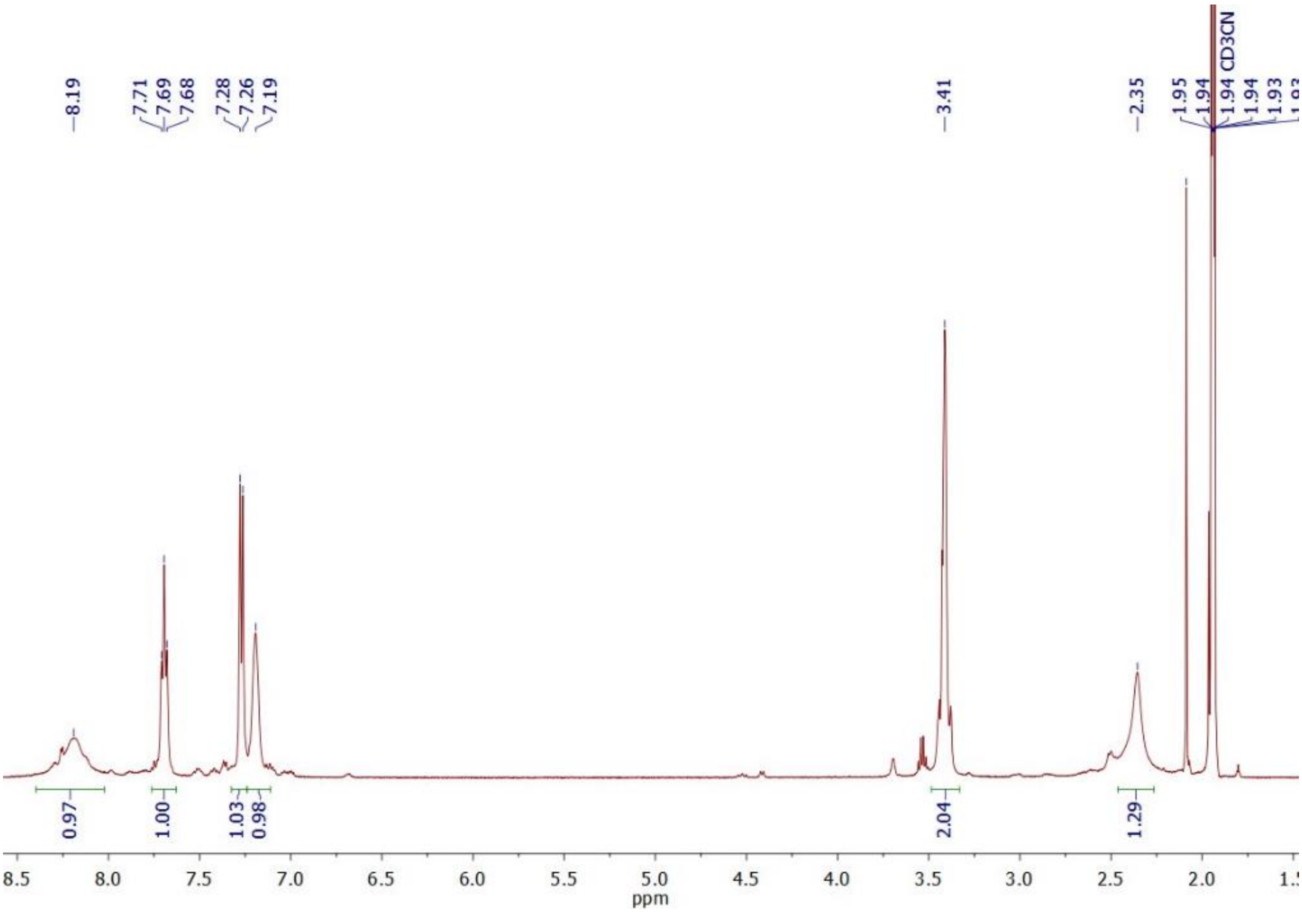

Figure S14. ^{1}H NMR spectrum of **4** in CD_3CN.

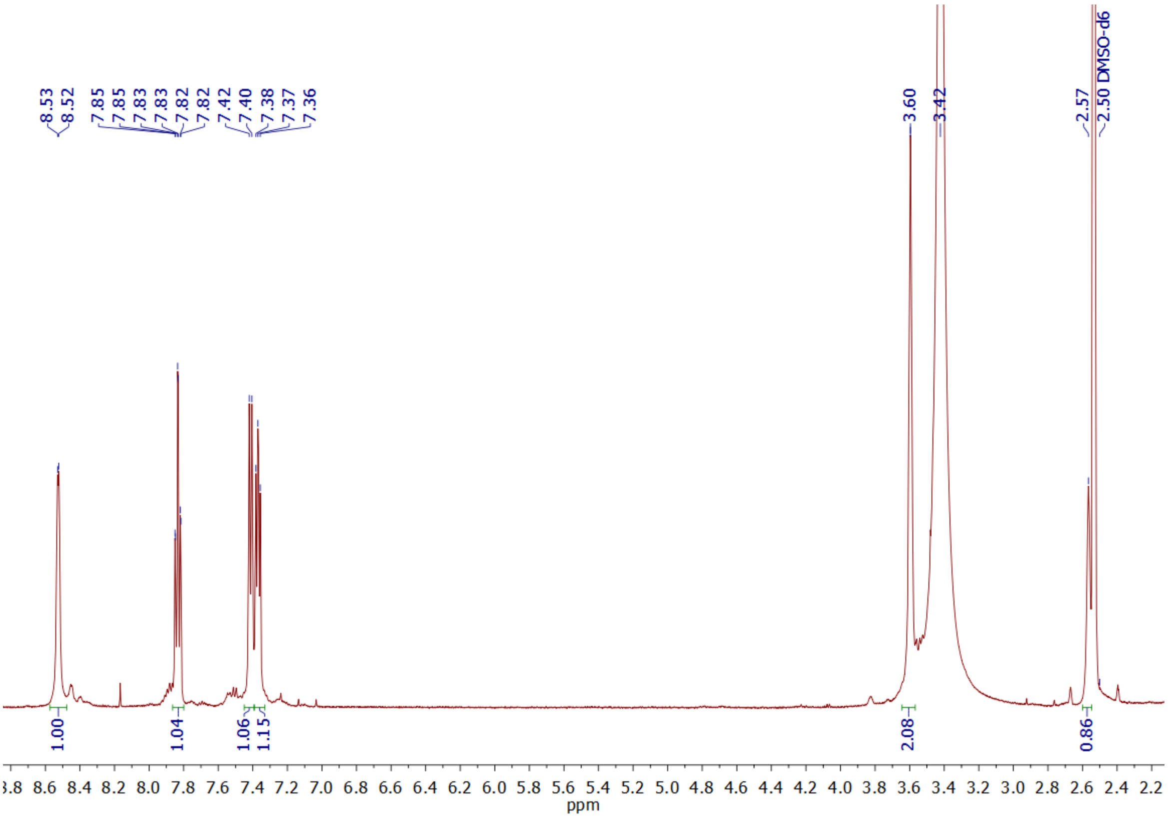

Figure S15. ^{1}H NMR spectrum of **5** in DMSO-d_6.

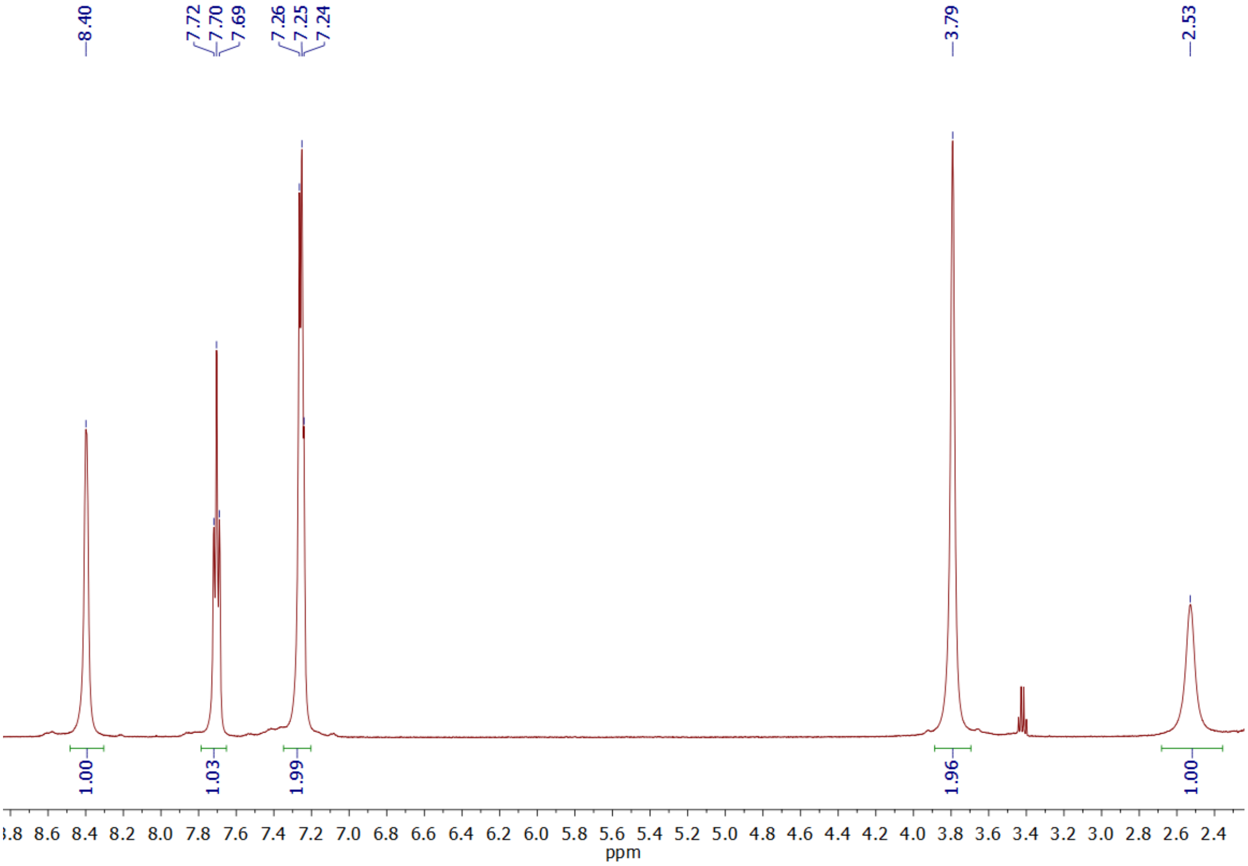

Figure S16. ^{1}H NMR spectrum of **7** in CD_3CN.

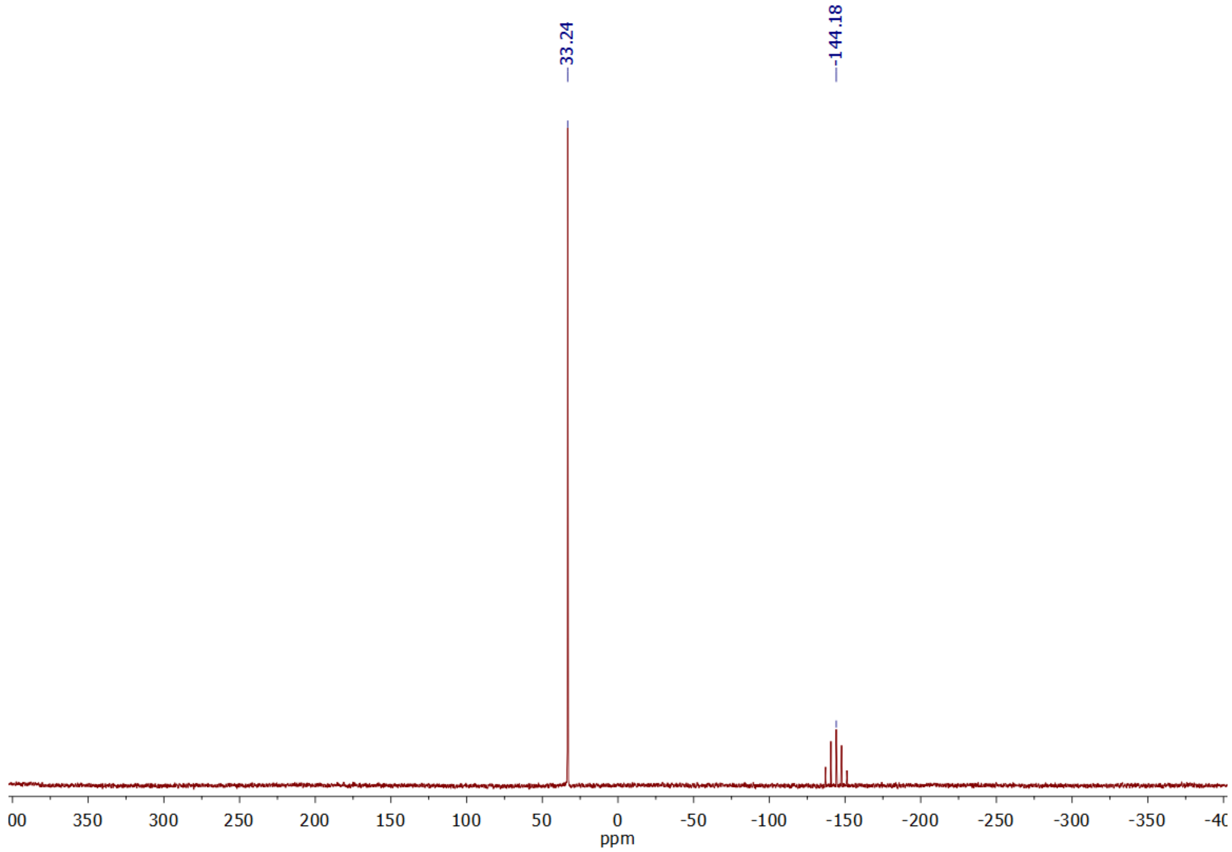

Figure S17. $^{31}P\{^1H\}$ NMR spectrum of **1** in DMSO-d_6.

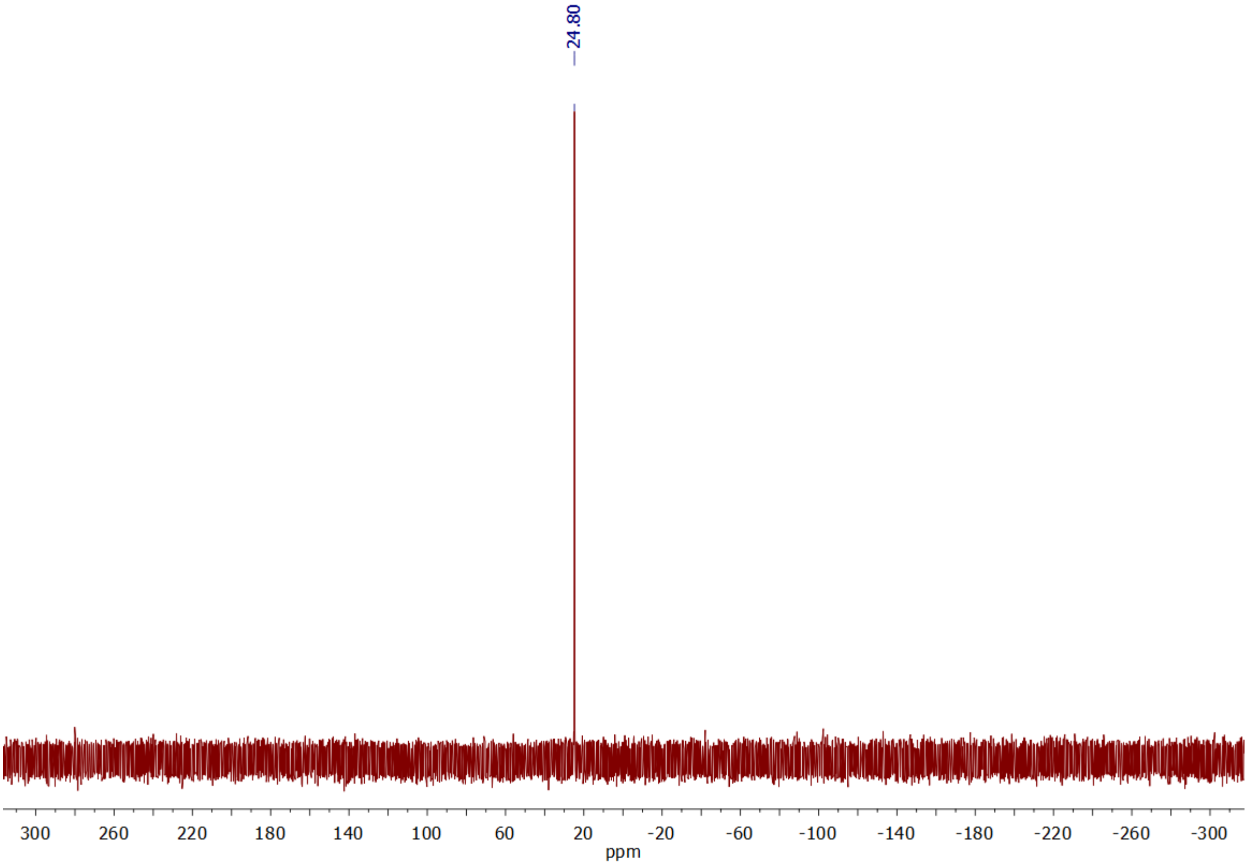

Figure S18. $^{31}P\{^1H\}$ NMR spectrum of **2** in $CDCl_3$.

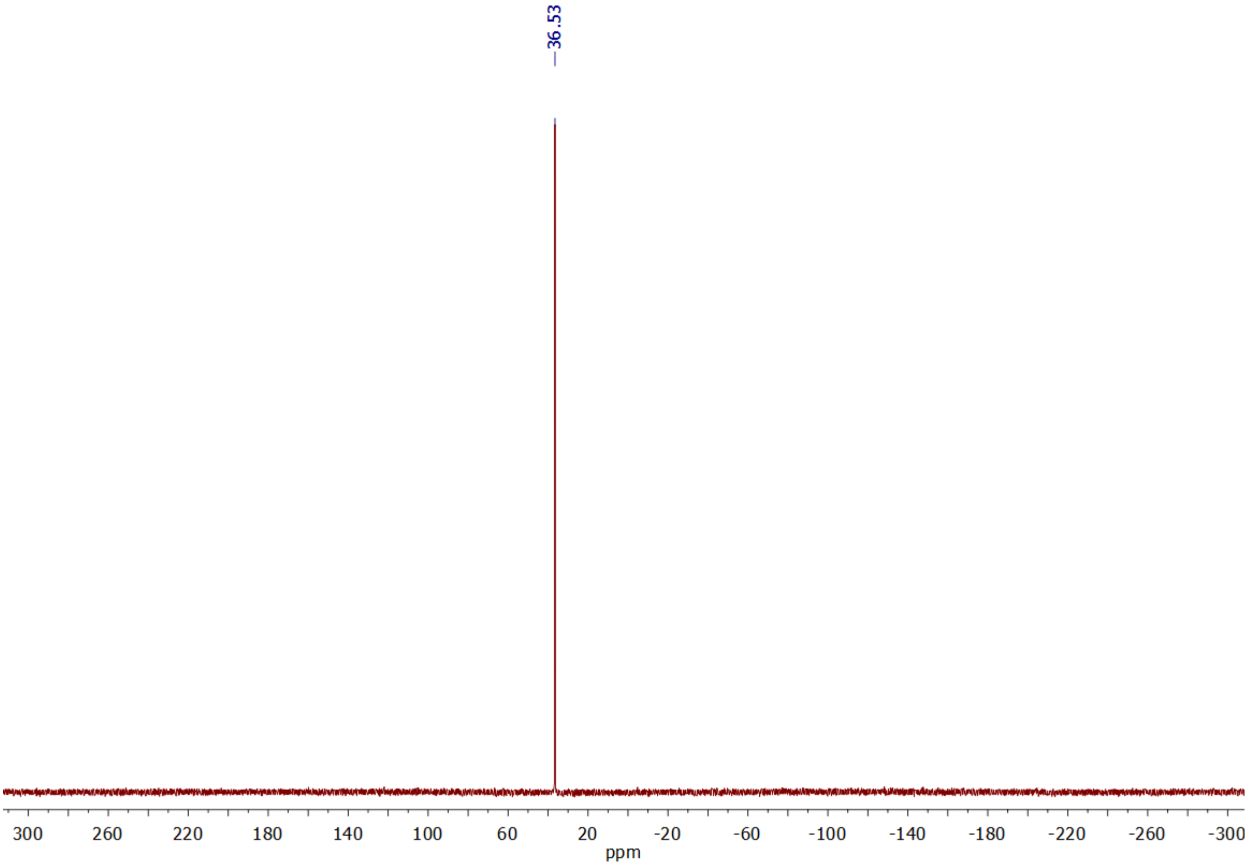

Figure S19. $^{31}P\{^1H\}$ NMR spectrum of **3** in $CDCl_3$.

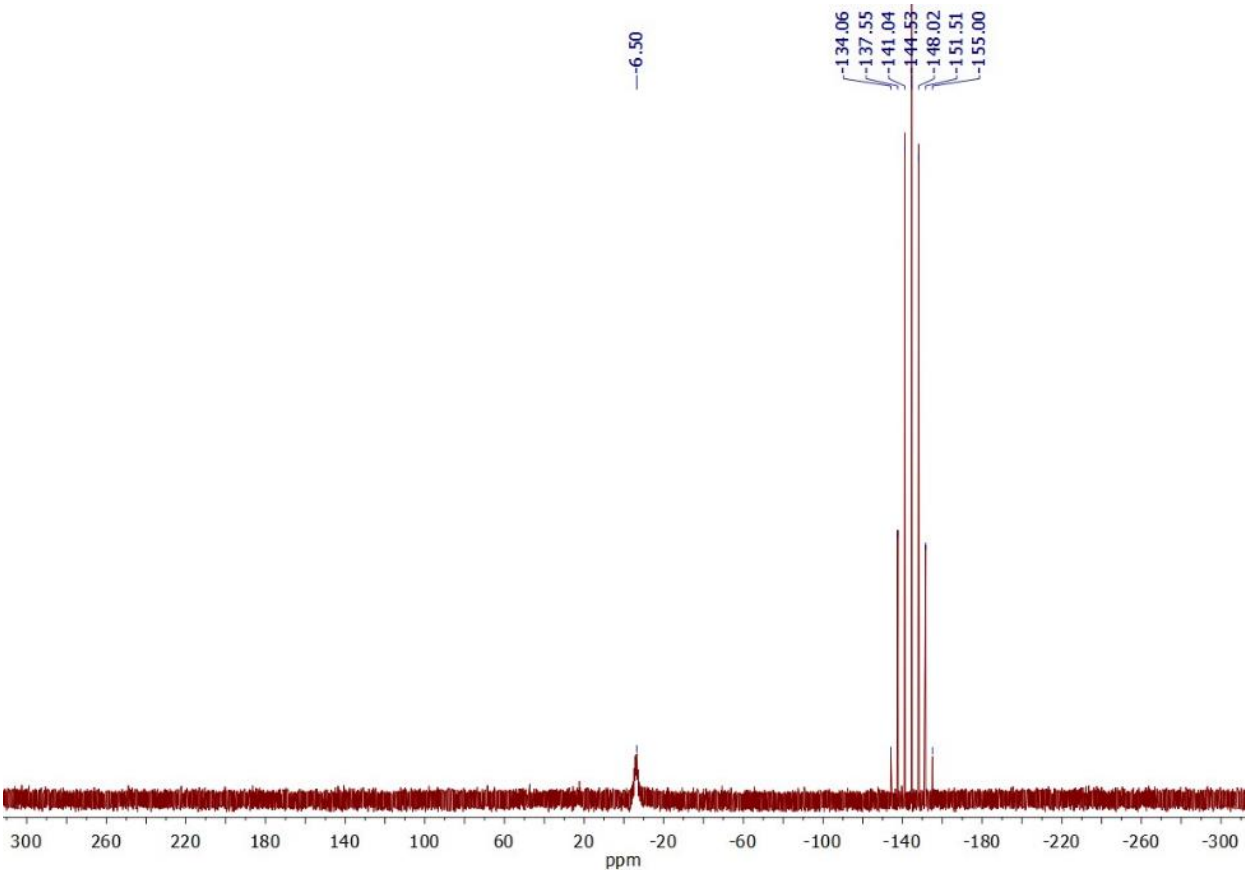

Figure S20. $^{31}P\{^1H\}$ NMR spectrum of **4** in CD_3CN.

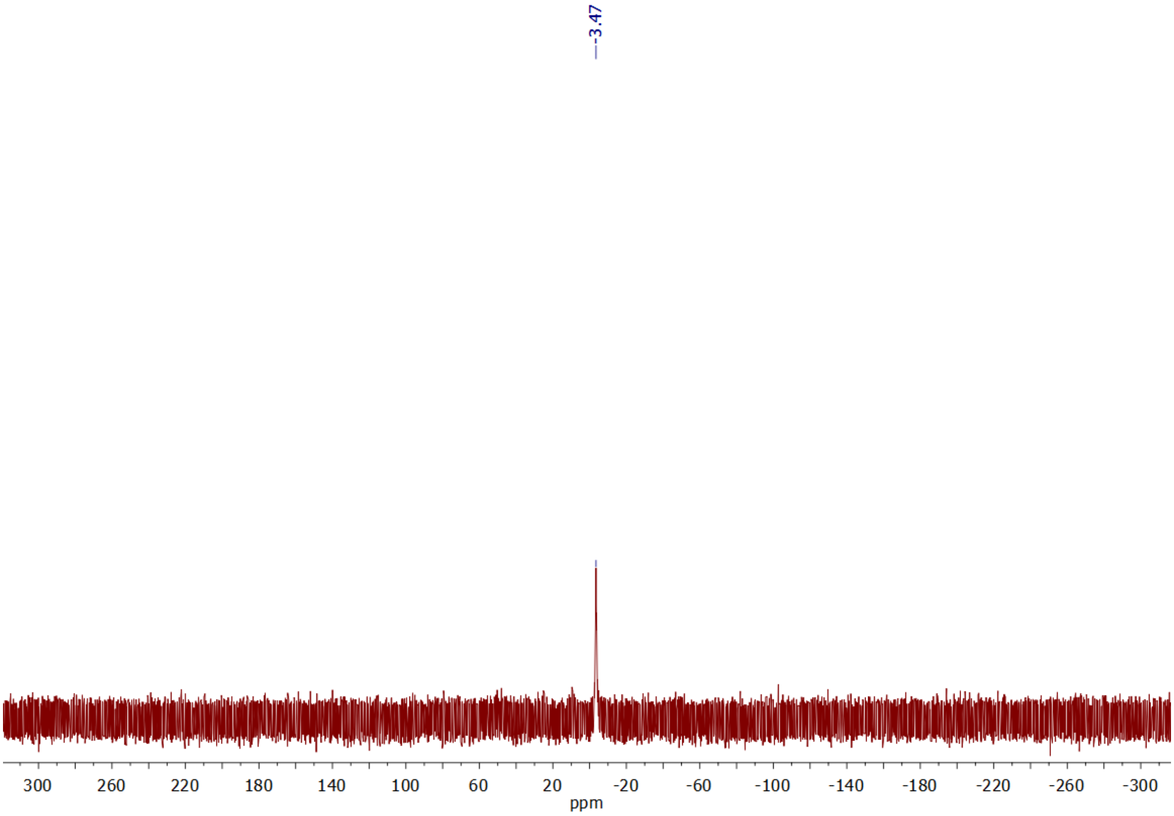

Figure S21. $^{31}P\{^{1}H\}$ NMR spectrum of **5** DMSO-d_6.

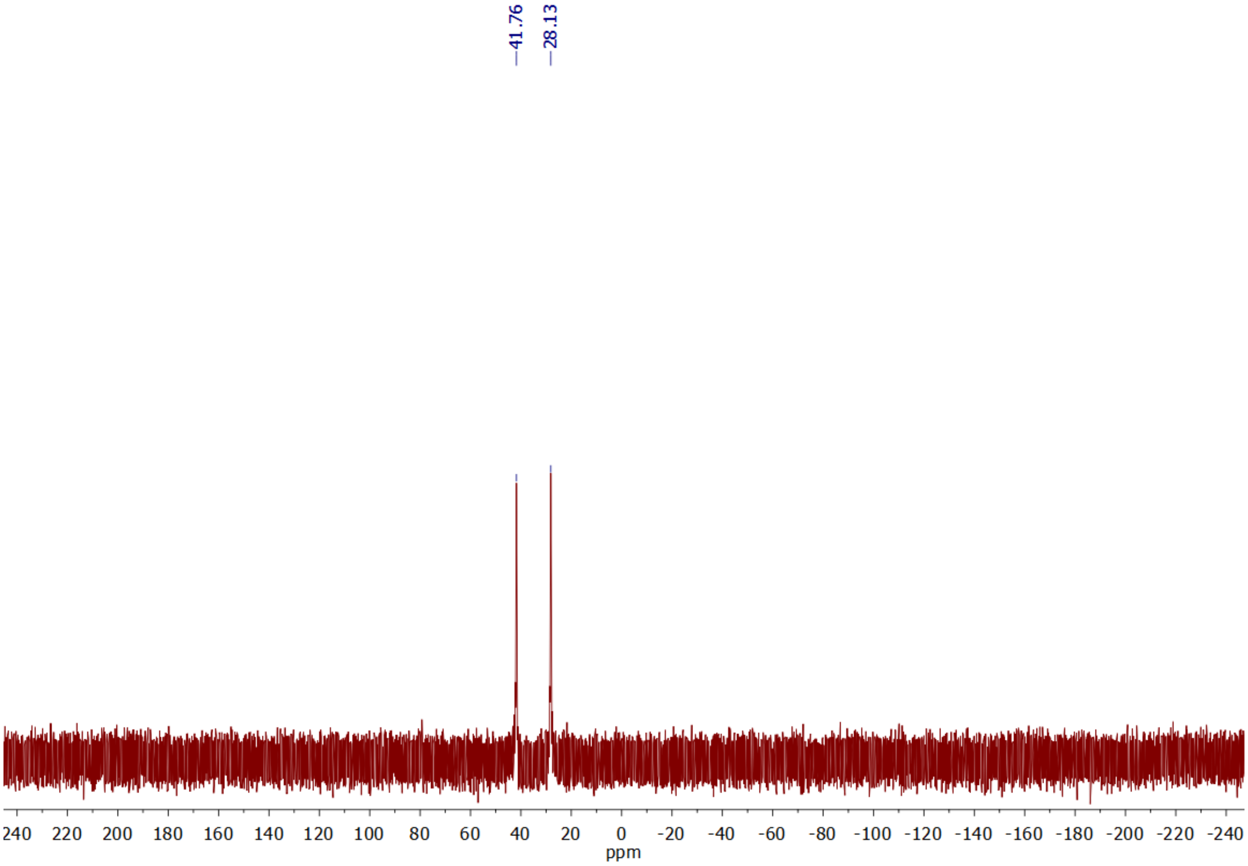

Figure S22. $^{31}P\{^{1}H\}$ NMR spectrum of **6** in D_2O.

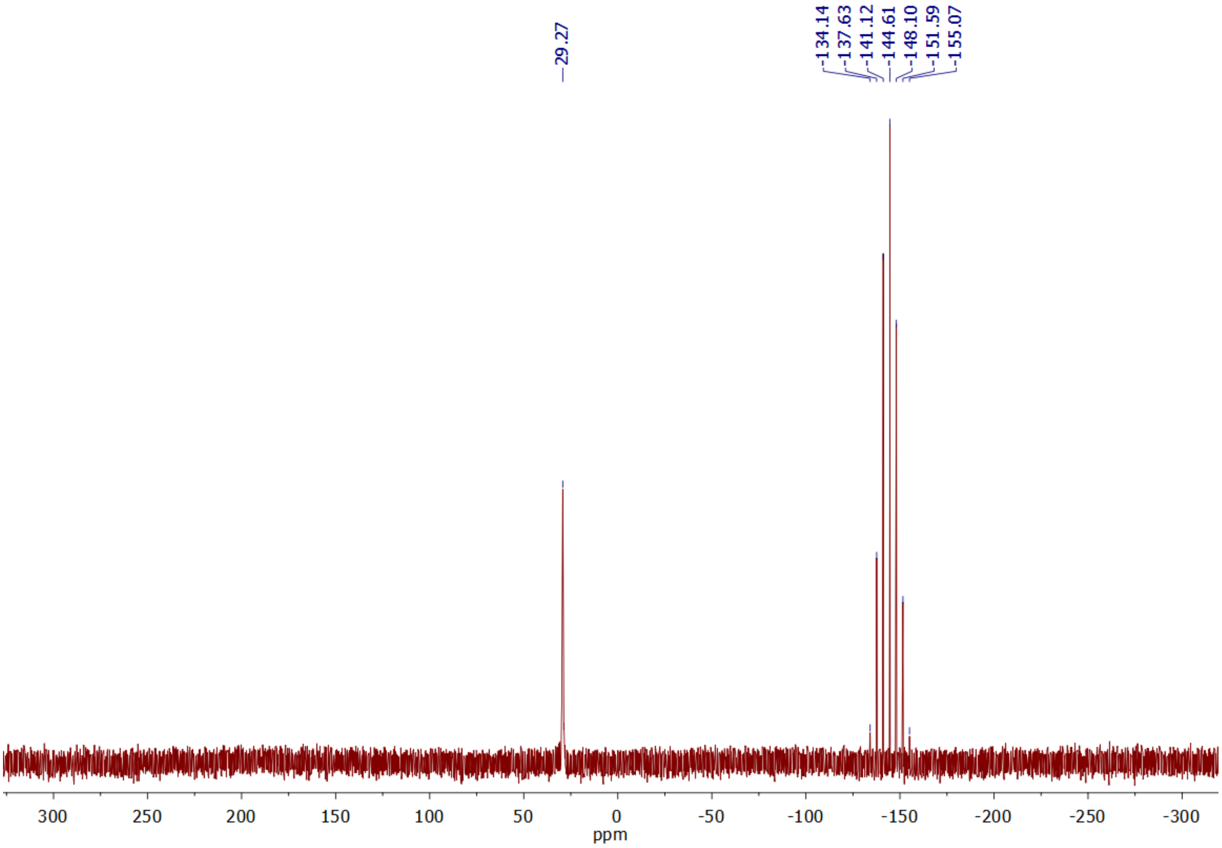

Figure S23. $^{31}P\{^{1}H\}$ NMR spectrum of **7** in CD_3CN.

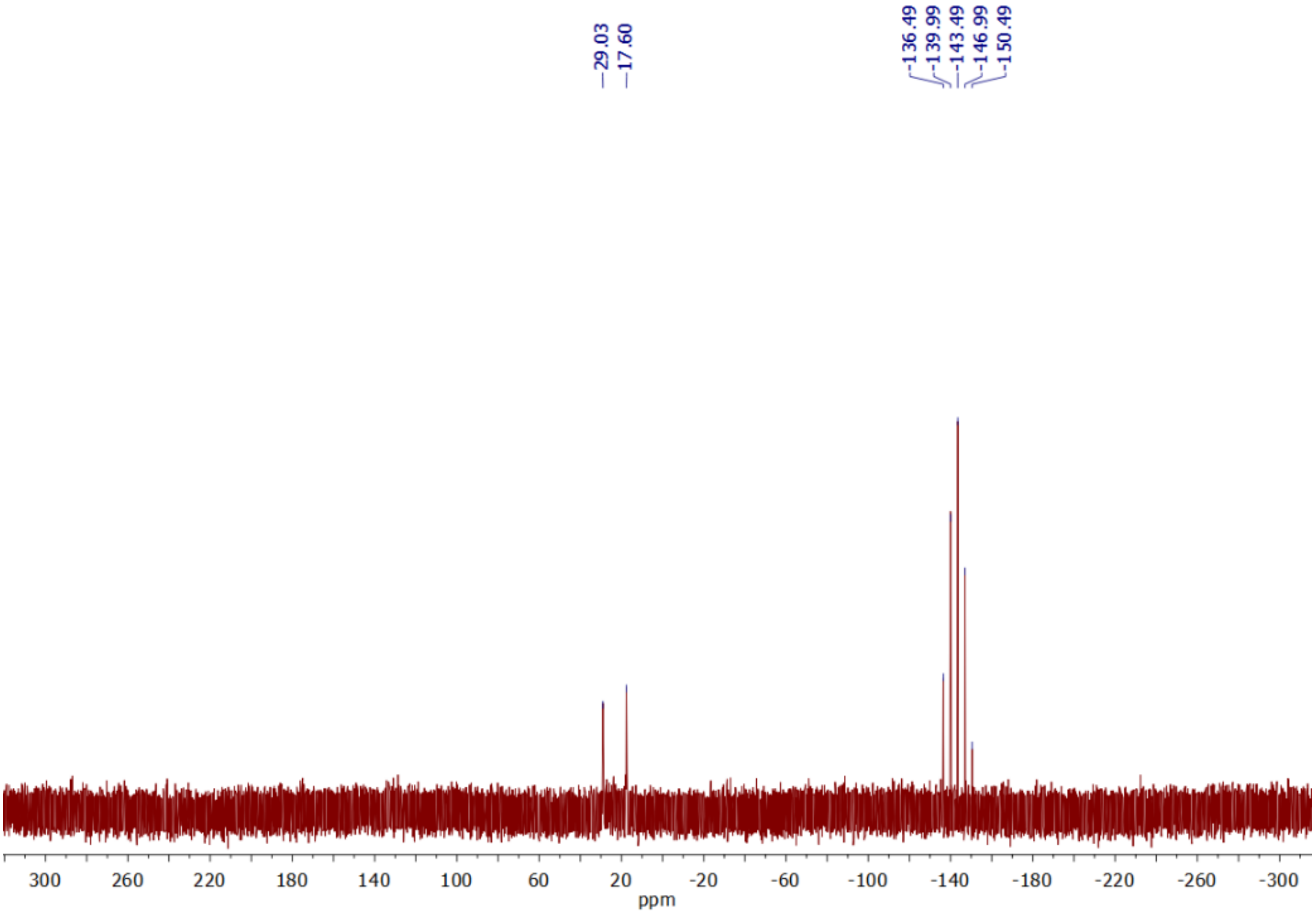

Figure S24. $^{31}P\{^{1}H\}$ NMR spectrum of **8** in acetone-d_6.

§6. *mid*-IR spectra

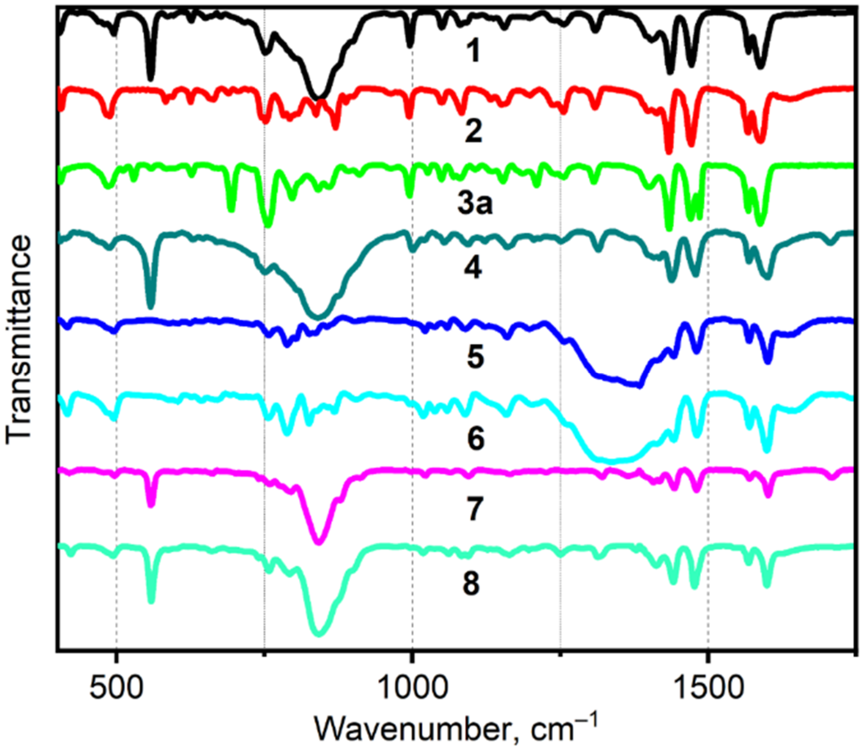

Figure S25. *mid*-IR spectra of **1**–**8** (KBr, fingerprint range).

§7. TGA&DTA curves

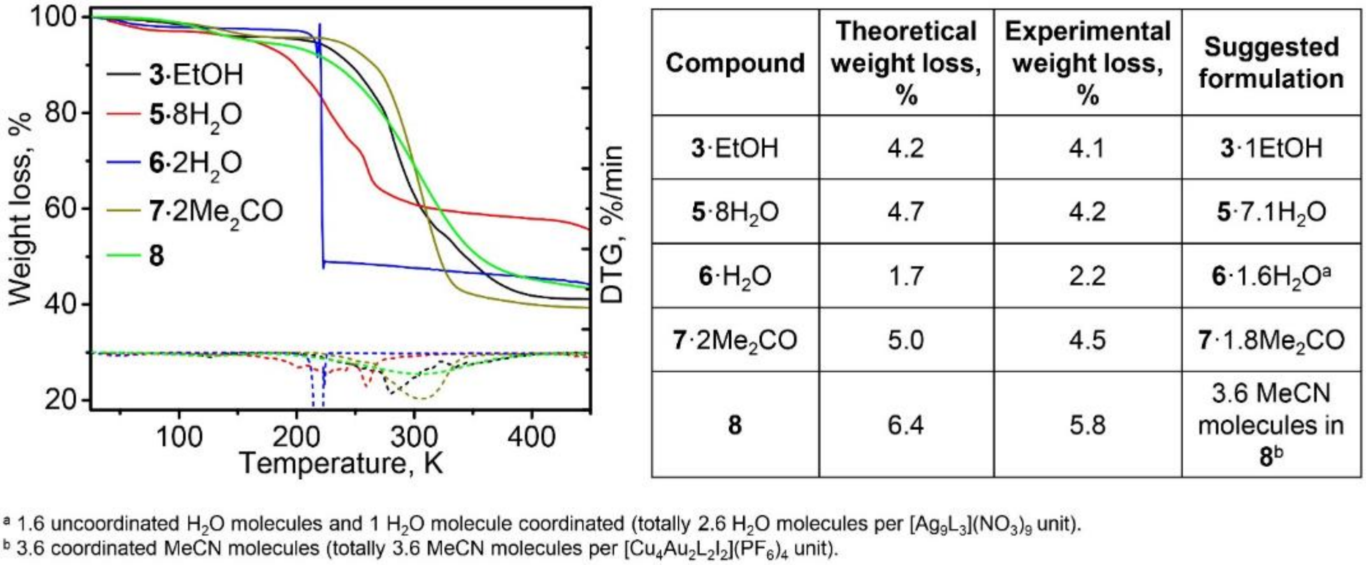

Compound	Theoretical weight loss, %	Experimental weight loss, %	Suggested formulation
3·EtOH	4.2	4.1	**3**·1EtOH
5·8H_2O	4.7	4.2	**5**·7.1H_2O
6·H_2O	1.7	2.2	**6**·1.6H_2O[a]
7·2Me_2CO	5.0	4.5	**7**·1.8Me_2CO
8	6.4	5.8	3.6 MeCN molecules in **8**[b]

[a] 1.6 uncoordinated H_2O molecules and 1 H_2O molecule coordinated (totally 2.6 H_2O molecules per $[Ag_9L_3](NO_3)_9$ unit).

[b] 3.6 coordinated MeCN molecules (totally 3.6 MeCN molecules per $[Cu_4Au_2L_2I_2](PF_6)_4$ unit).

Figure S26. TGA and DTG curves for **3**·EtOH, **5**·8H_2O, **6**·H_2O, **7**·2Me_2CO and **8**.

§8. ESI-MS data

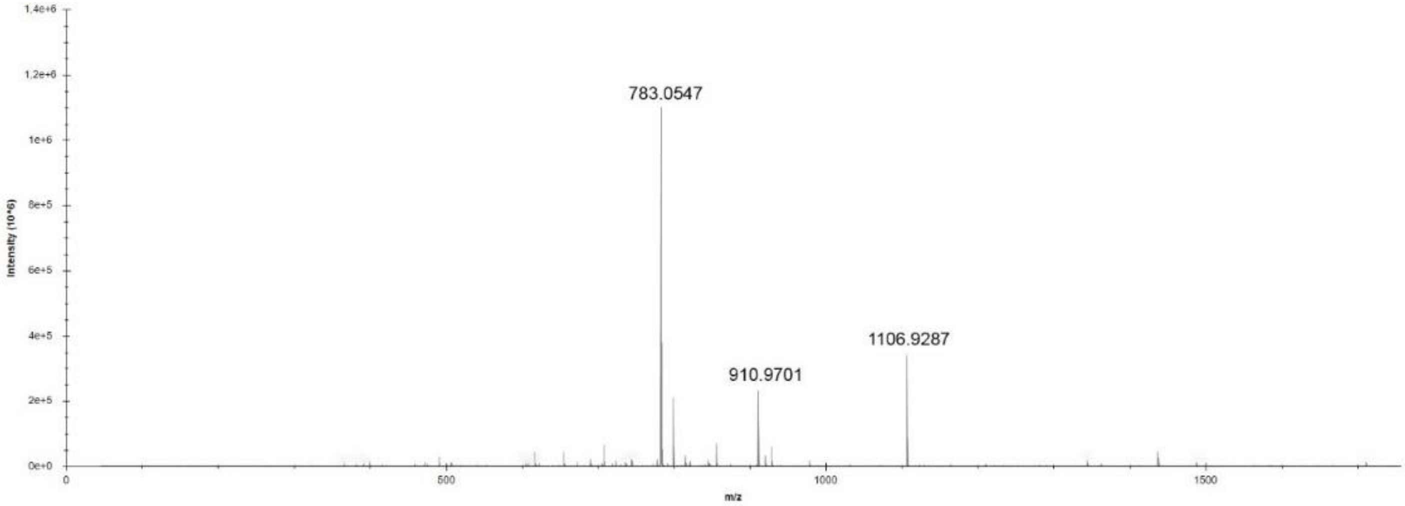

Figure S27. ESI-MS spectrum of **1** in MeOH, positive ions.

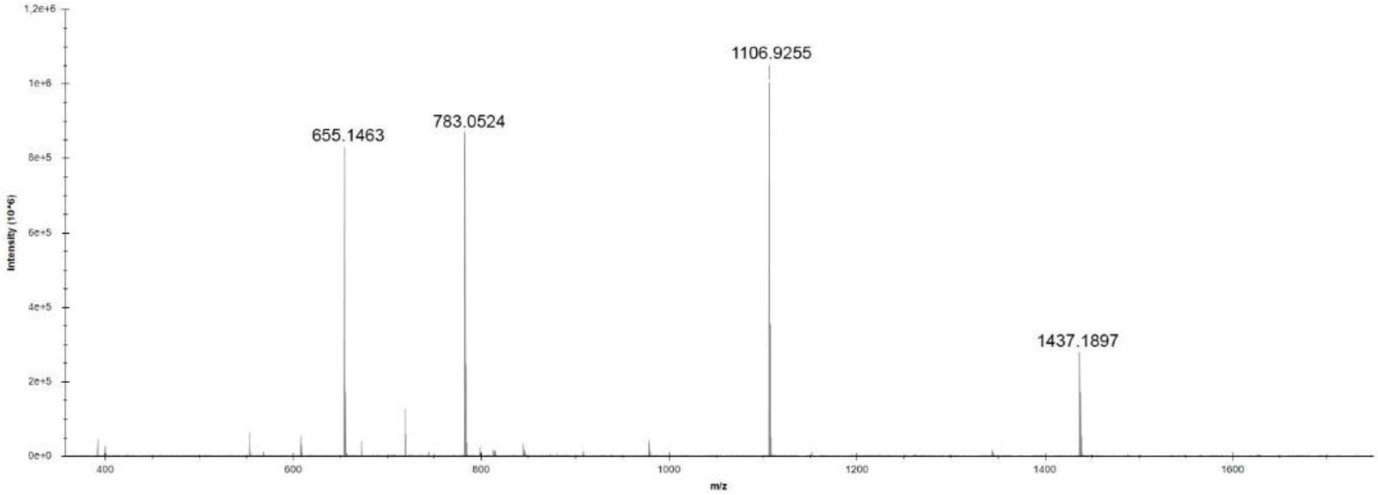

Figure S28. ESI-MS spectrum of **2** in MeOH, positive ions.

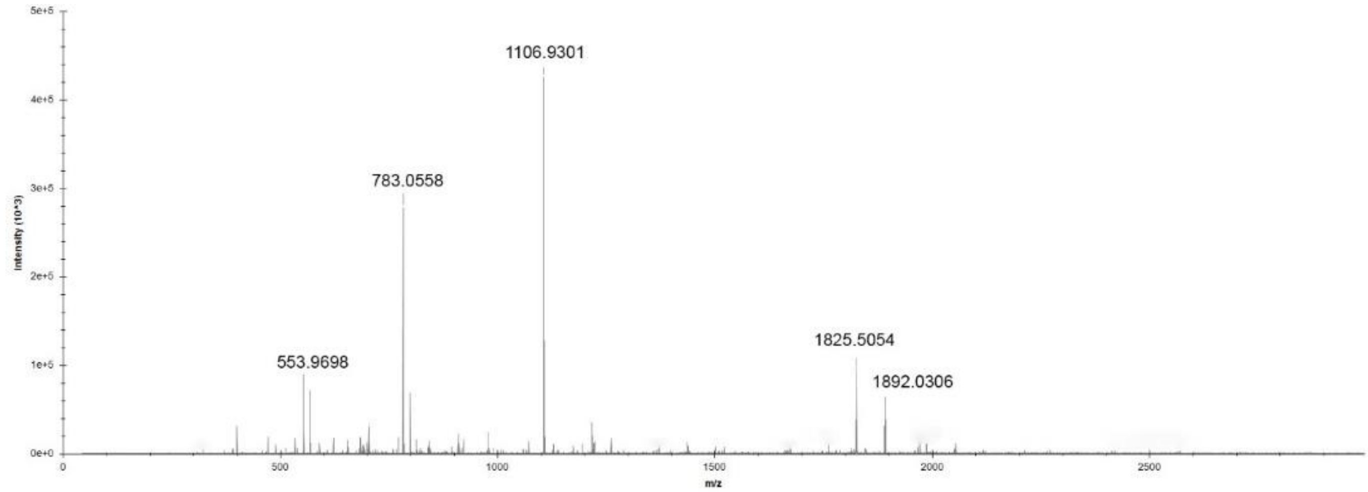

Figure S29. ESI-MS spectrum of **3** in MeOH, positive ions.

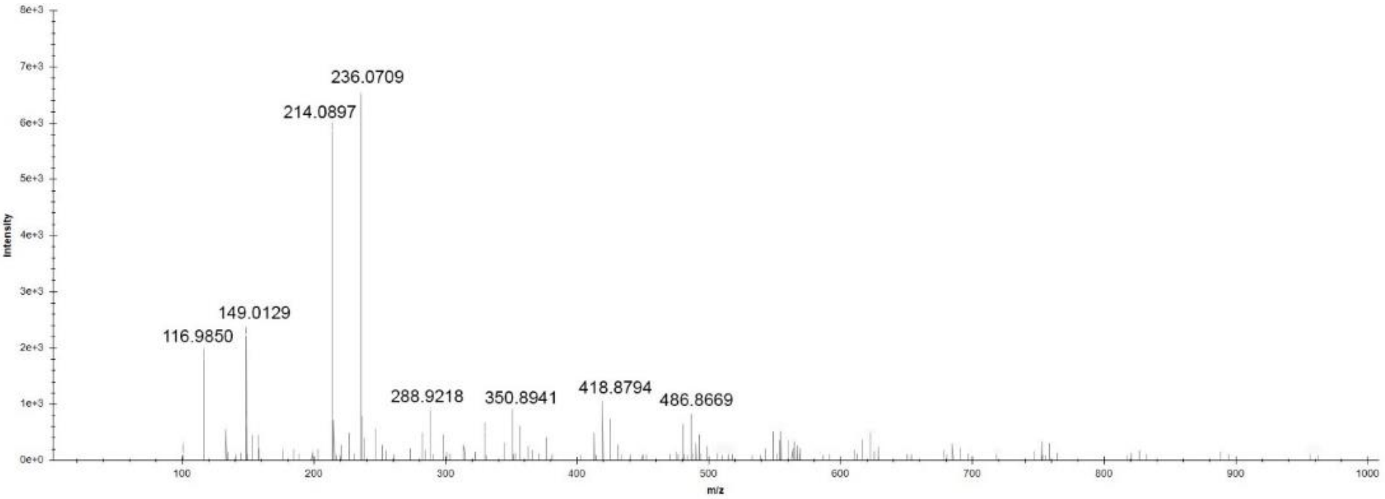

Figure S30. ESI-MS spectrum of **4** in MeOH, positive ions.

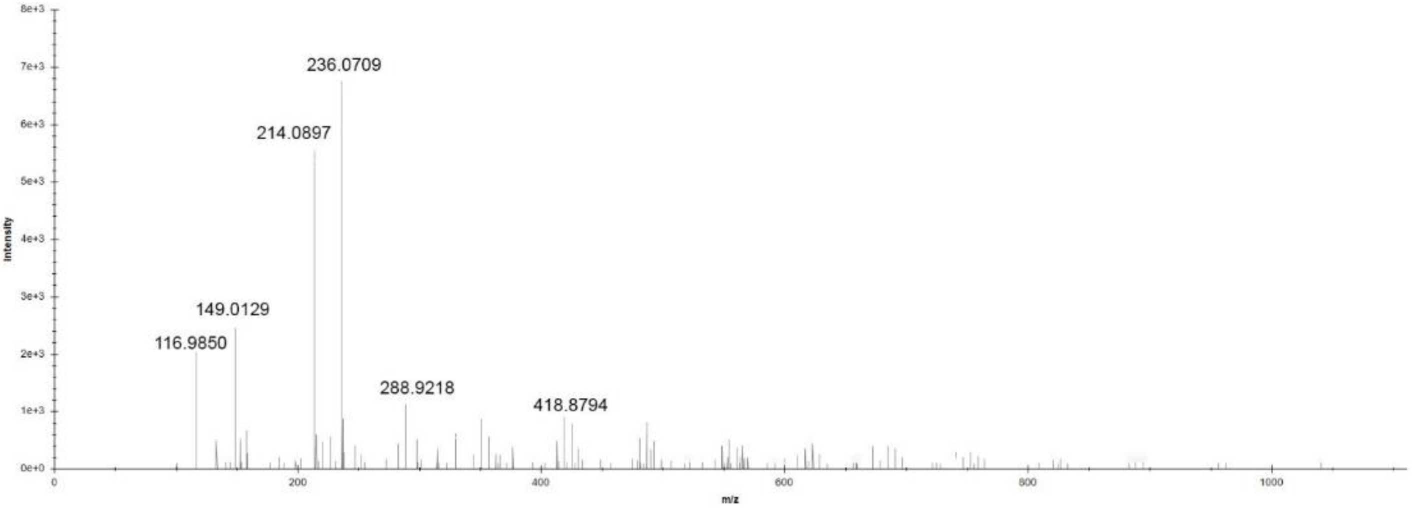

Figure S31. ESI-MS spectrum of **5** in MeOH, positive ions.

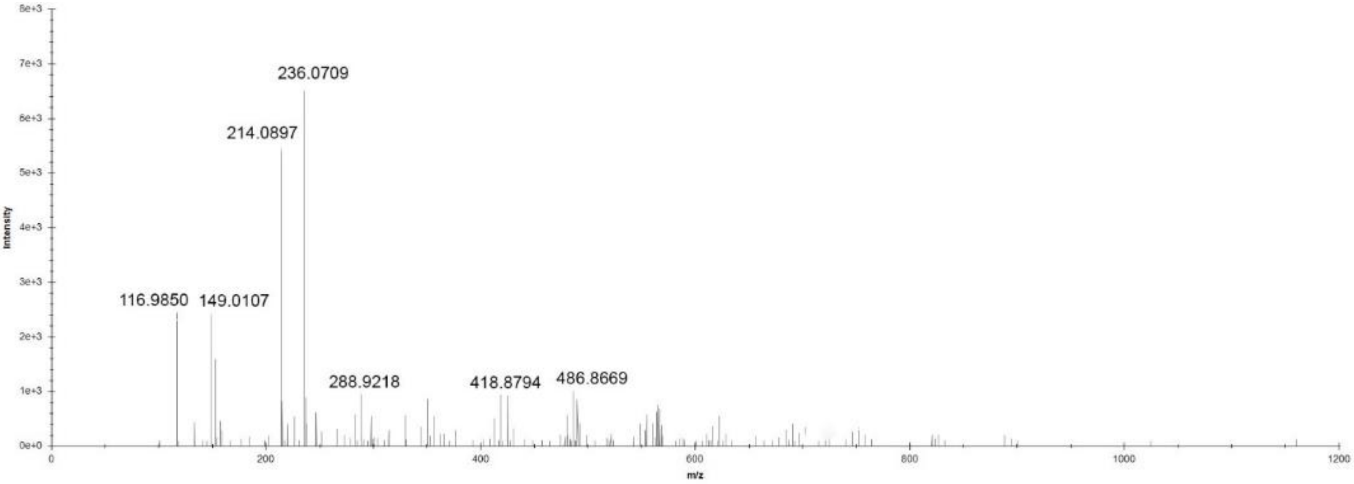

Figure S32. ESI-MS spectrum of **6** in MeOH, positive ions.

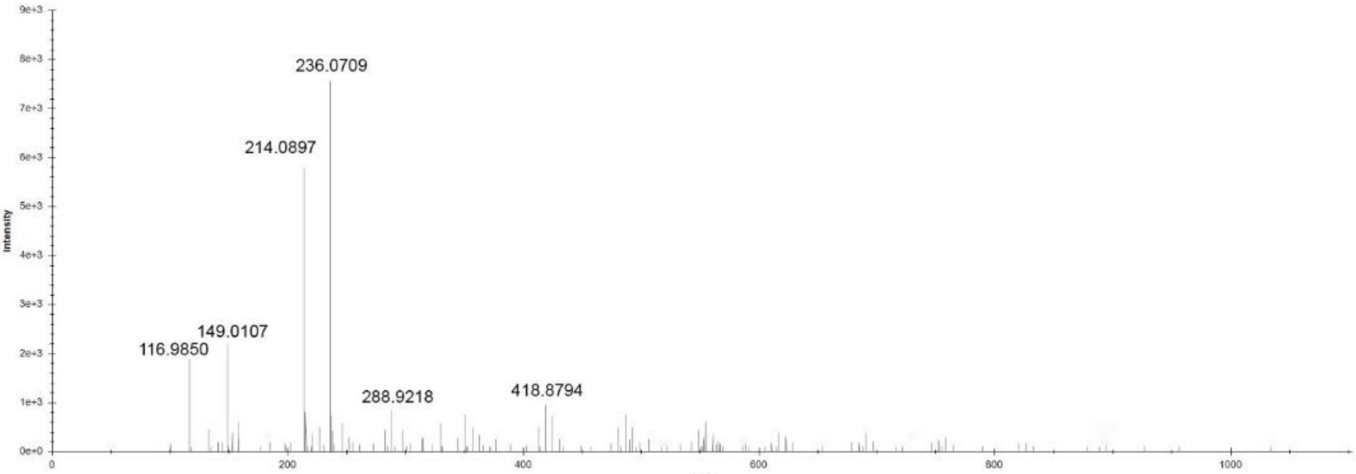

Figure S33. ESI-MS spectrum of **7** in MeOH, positive ions.

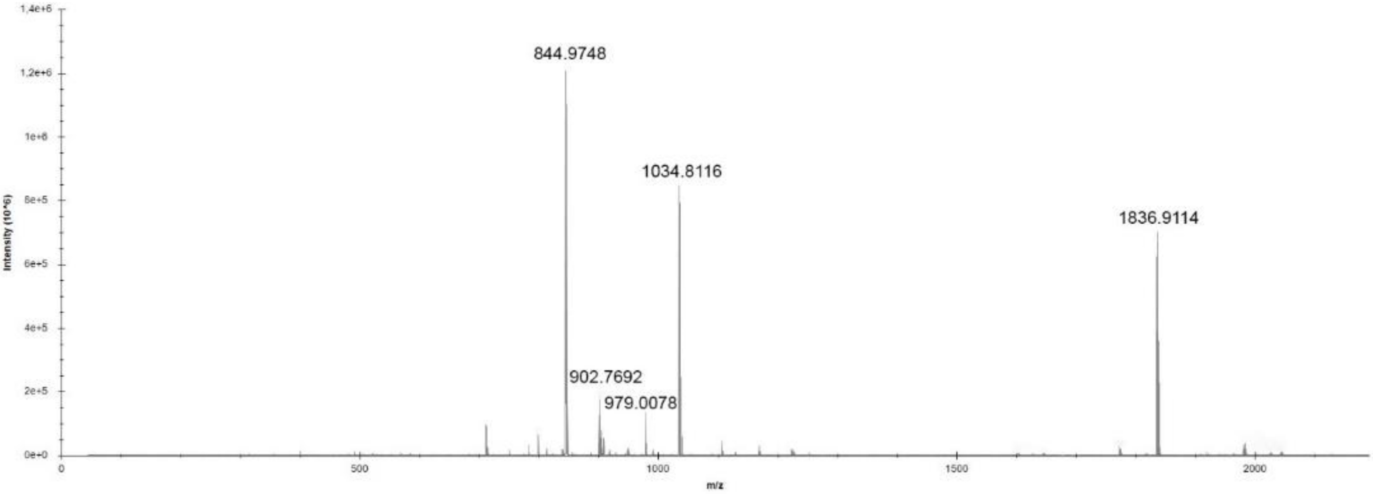

Figure S34. ESI-MS spectrum of **8** in MeOH, positive ions.

§9. DFT and TD-DFT calculation details

DFT and TD-DFT computations were performed in gas phase using Gaussian suite.[11] Computation modeling of **2** and **3a** was carried out for the neutral [$Au_2I_2L_2$] and [$Au_2(C{\equiv}CPh)_2L]_2$ molecules. In the case of **1** and **4**–**8**, the corresponding cations were computed, i.e. $[Au_2L_2]^{2+}$ (**1**), $[Ag_4L_2]^{4+}$ (**4**), $[Ag_9L_3(NO_3)]^{8+}$ (**5**), $[Au_2Ag_4L_2(NO_3)_2(H_2O)]^{4+}$ (**6**), $[Au_2Cu_4L_2(\mu_2\text{-}Cl)_2]^{4+}$ (**7**) and $[Au_2Cu_4L_2I_2(MeCN)_4]^{4+}$ (**8**). The PBE0 hybrid functional[12] combined with the LANL2DZ[13] (for metal atoms and I) and 6-31+G(d,p)[14] [for the rest atoms] basis sets were used for the calculations. The starting coordinates of the non-H atoms were taken from X-ray geometries of **1**–**8**. TD-DFT calculations[15] were performed at the same theory level with the optimized ground state (S_0) structures.

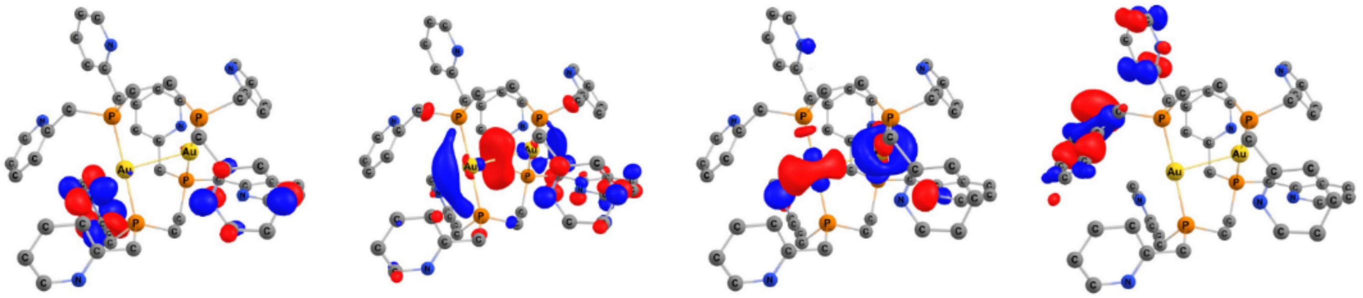

LUMO+1 (–5.51 eV) **LUMO** (–5.61 eV) **HOMO** (–10.98 eV) **HOMO-1** (–11.29 eV)

Figure S35. Selected molecular orbitals (isovalue = 0.04) for the optimized S_0 state geometry of **1**.

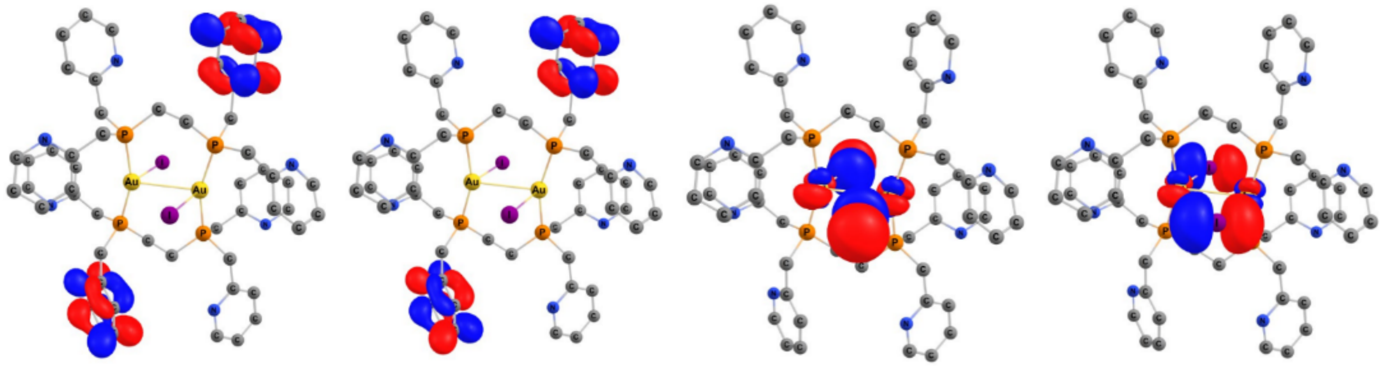

LUMO+1 (–0.87 eV) **LUMO** (–0.88 eV) **HOMO** (–4.66 eV) **HOMO-1** (–4.99 eV)

Figure S36. Selected molecular orbitals (isovalue = 0.04) for the optimized S_0 state geometry of **2**.

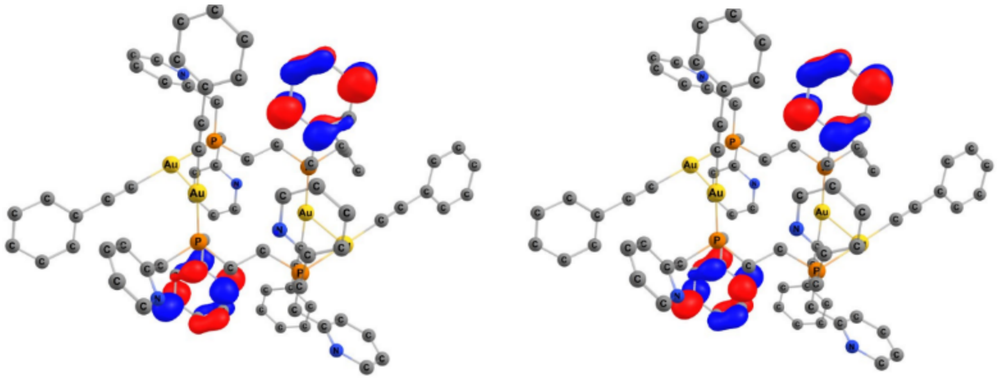

LUMO (–1.16 eV) **LUMO+1** (–1.12 eV)

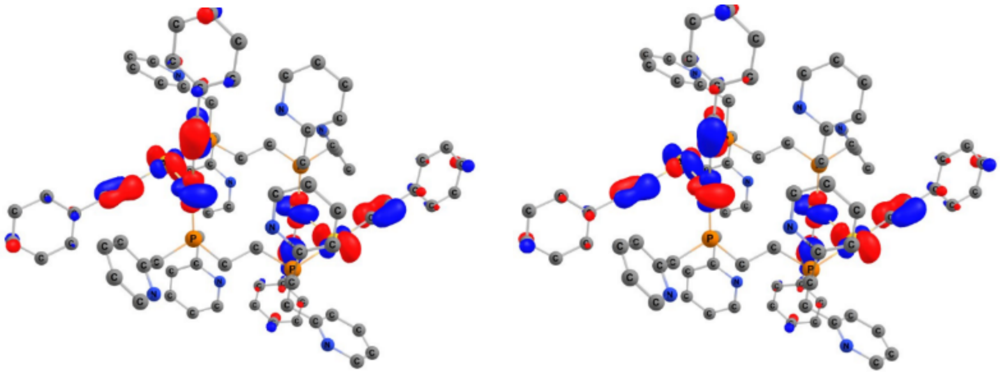

HOMO (–6.00 eV) **HOMO-1** (–6.01 eV)

Figure S37. Selected molecular orbitals (isovalue = 0.04) for the optimized S_0 state geometry of **3a**.

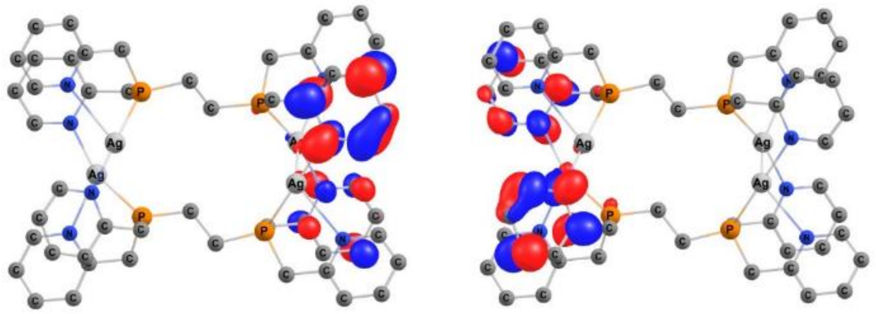

LUMO (–9.75 eV) **LUMO+1** (–9.68 eV)

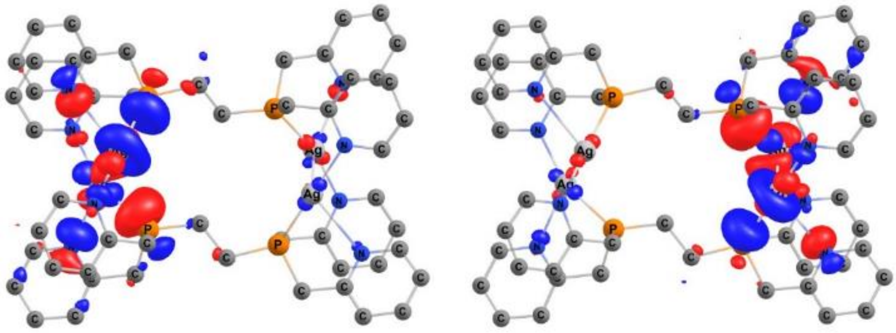

HOMO (–14.38 eV) **HOMO-1** (–14.82 eV)

Figure S38. Selected molecular orbitals (isovalue = 0.04) for the optimized S_0 state geometry of **4**.

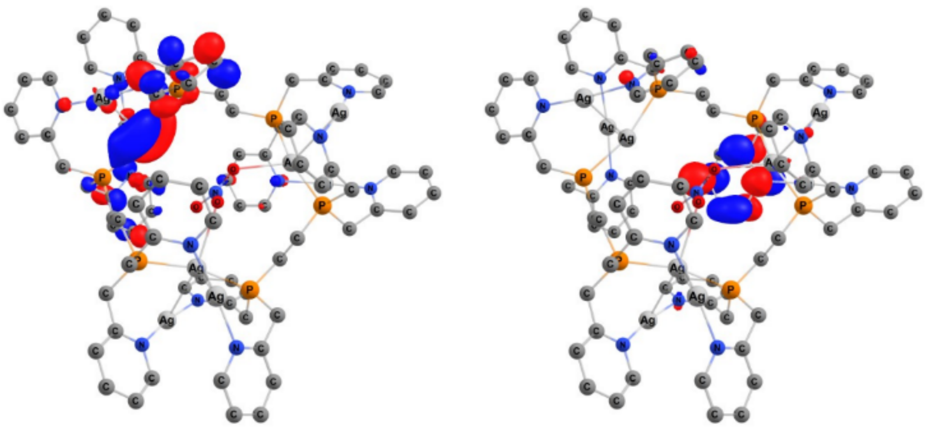

LUMO (–6.78 eV) **LUMO+1** (–16.71 eV)

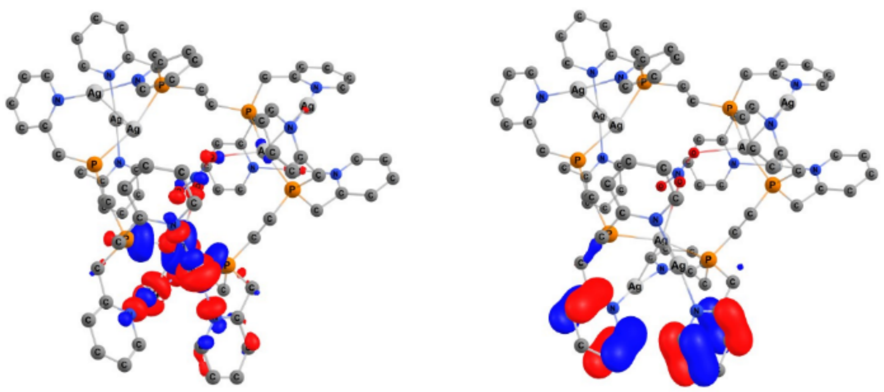

HOMO (–21.75 eV) **HOMO-1** (–21.87 eV)

Figure S39. Selected molecular orbitals (isovalue = 0.04) for the optimized S_0 state geometry of **5**.

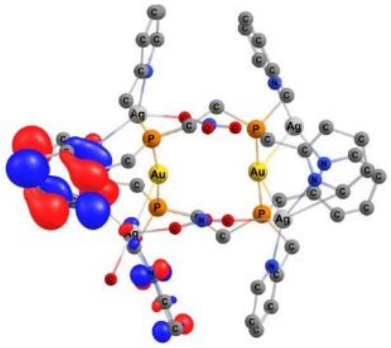

LUMO (–10.23 eV) **LUMO+1** (–10.15 eV)

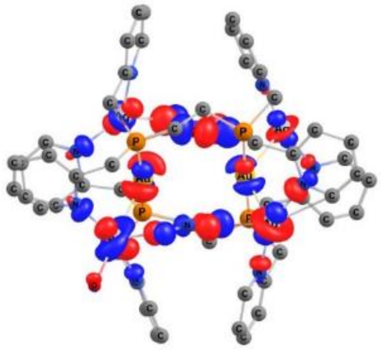

HOMO (–14.73 eV) **HOMO-1** (–14.97 eV)

Figure S40. Selected molecular orbitals (isovalue = 0.04) for the optimized S_0 state geometry of **6**.

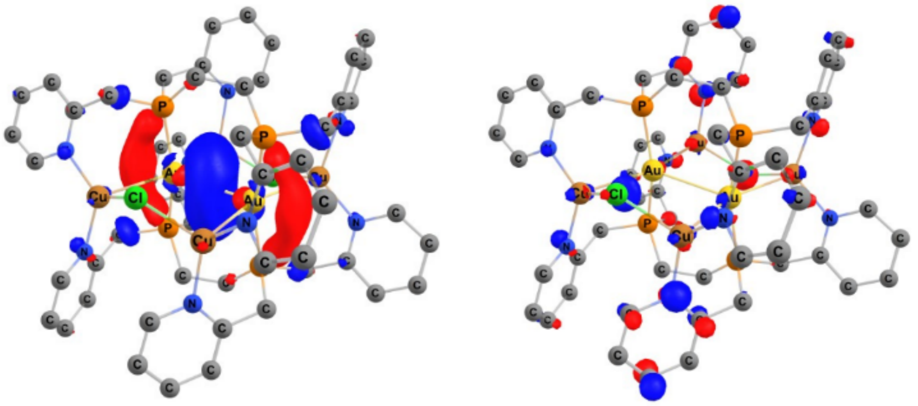

LUMO (–10.53 eV) **LUMO+1** (–10.36 eV)

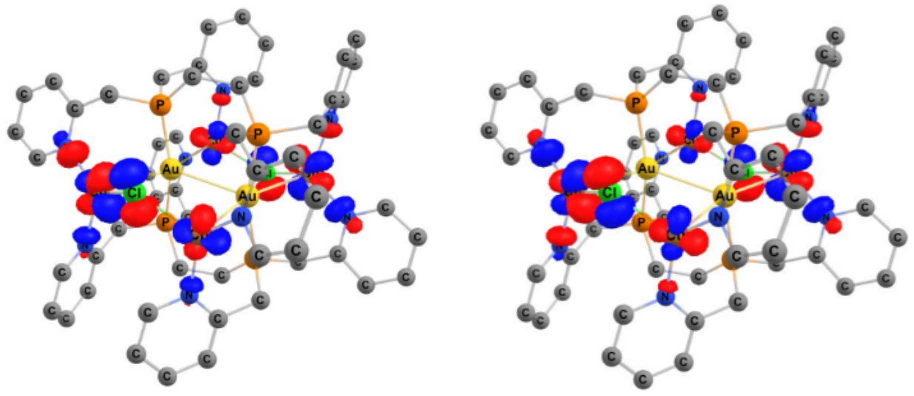

HOMO (–14.58 eV) **HOMO-1** (–14.59 eV)

Figure S41. Selected molecular orbitals (isovalue = 0.04) for the optimized S_0 state geometry of **7**.

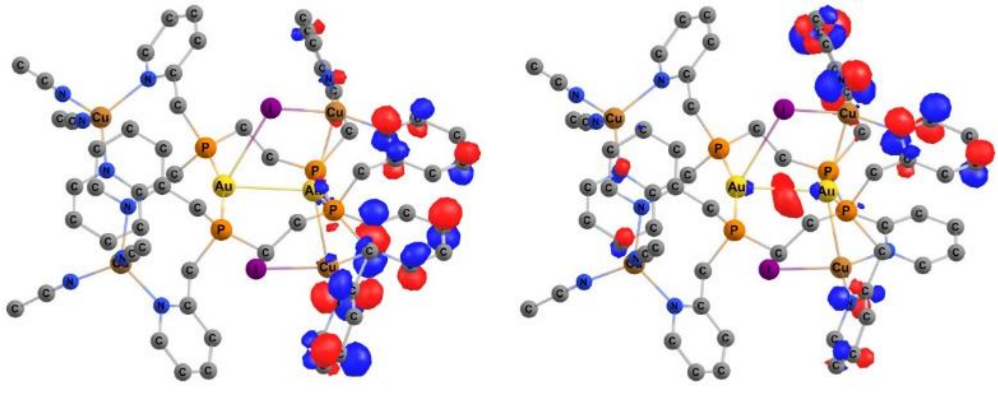

LUMO (–9.38 eV) **LUMO+1** (–9.29 eV)

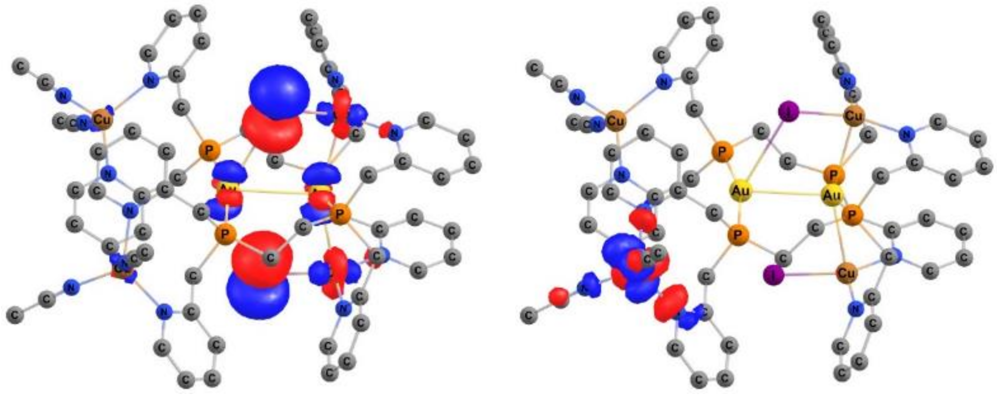

HOMO (–13.31 eV) **HOMO-1** (–13.36 eV)

Figure S42. Selected molecular orbitals (isovalue = 0.04) for the optimized S_0 state geometry of **8**.

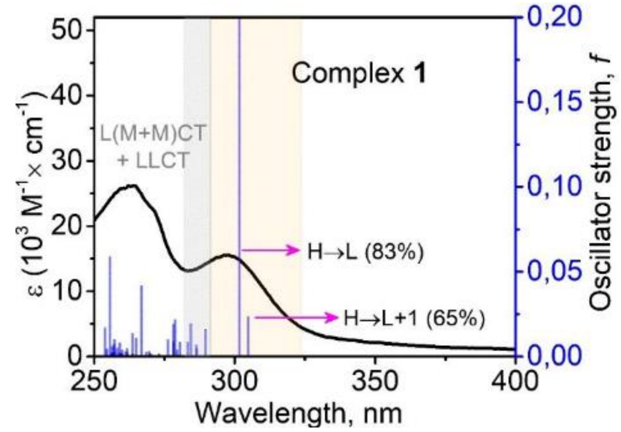

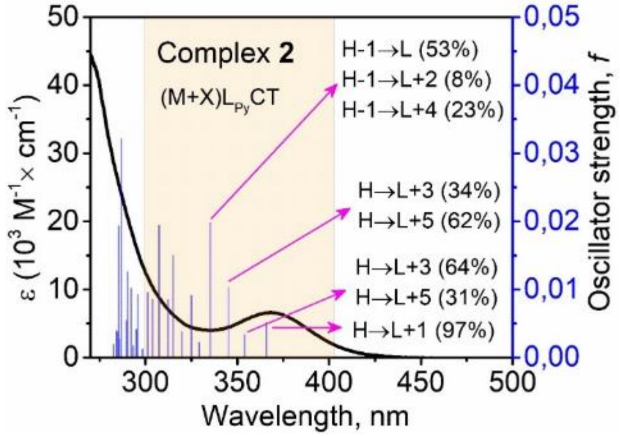

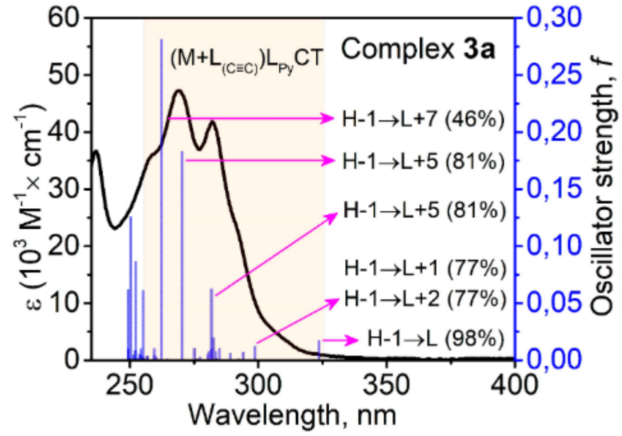

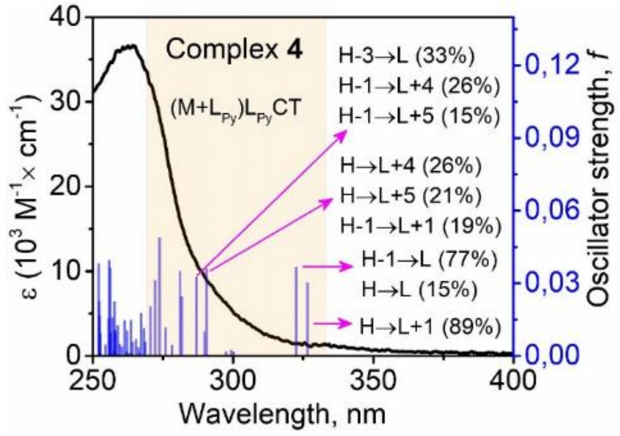

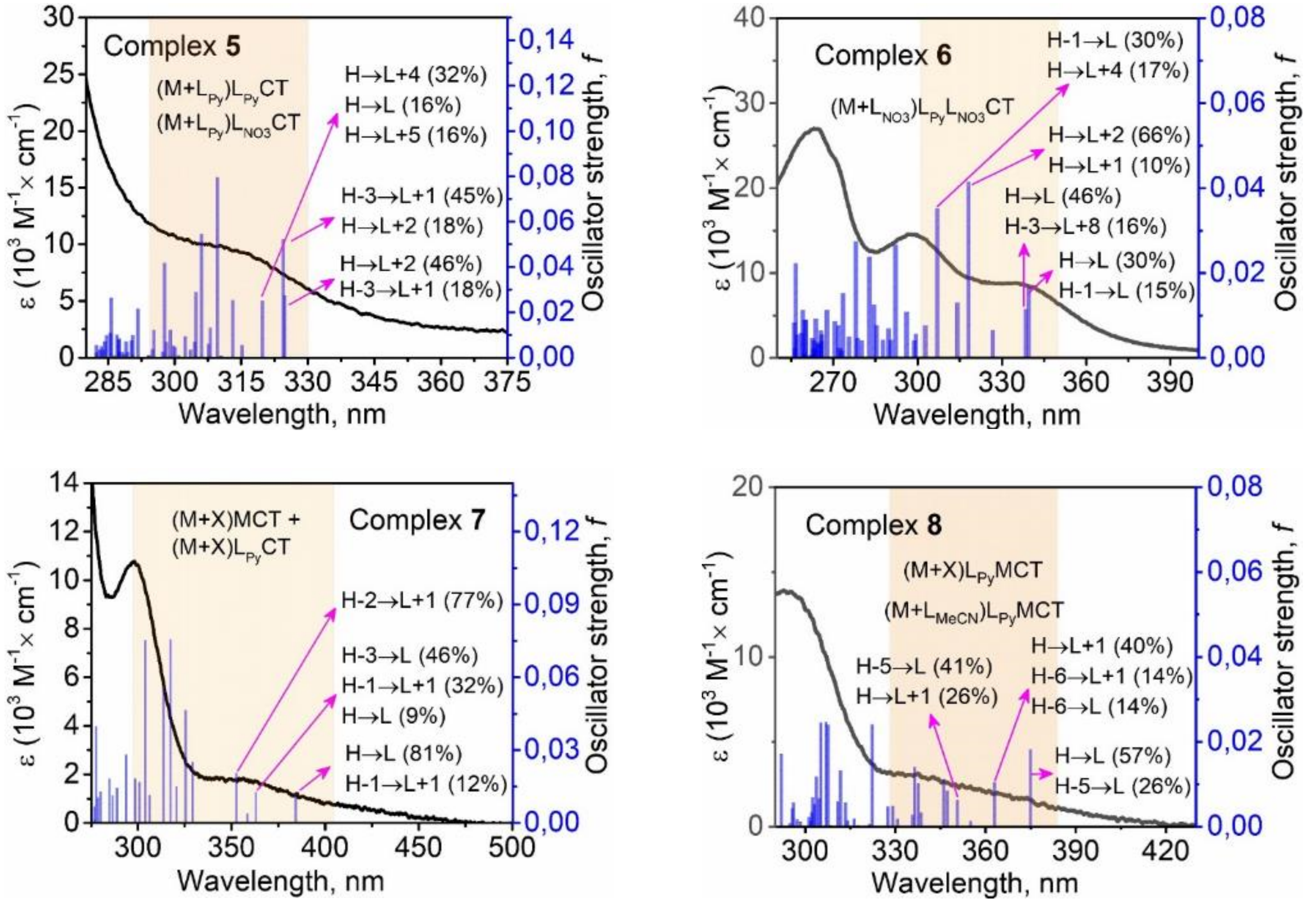

Figure S43. UV-Vis spectra of **1**–**8** and TD-DFT derived absorption patterns (vertical bars).

Table S3. The dominant NTO pairs for the excited singlet states of complex **1**.

Excited state number	W	Hole	Particle
S_1	0.93	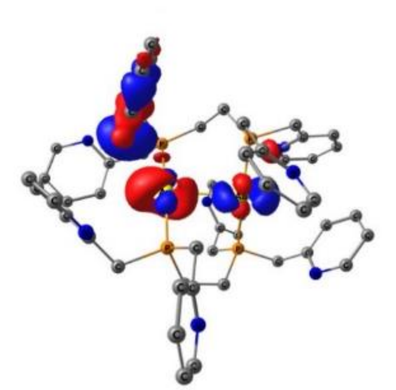	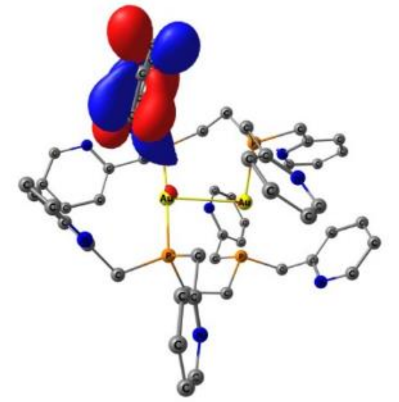
S_2	0.91	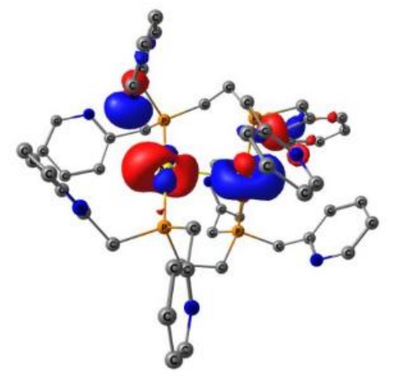	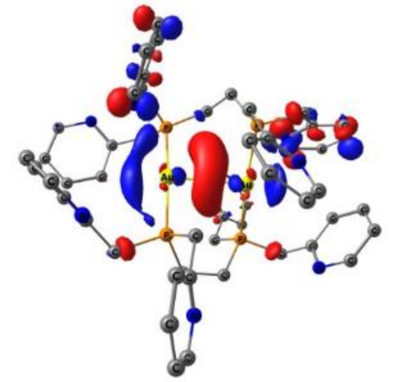

Table S4. The dominant NTO pairs for the excited singlet states of complex **2**.

Excited state number	W	Hole	Particle
S_1 ($f = 0$)	0.99	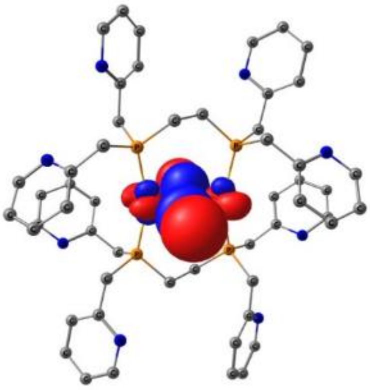	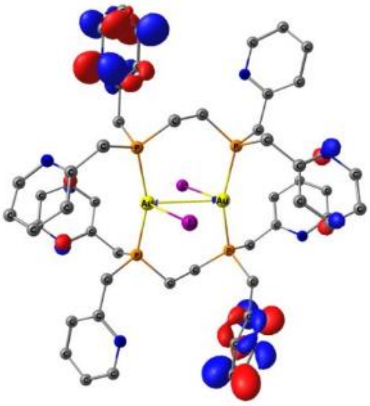
S_2	1.00	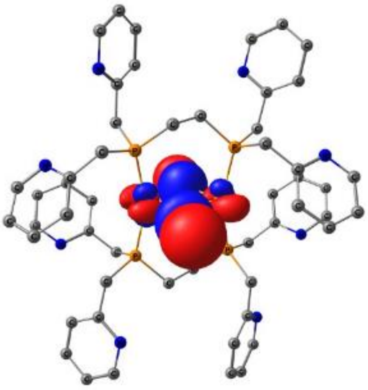	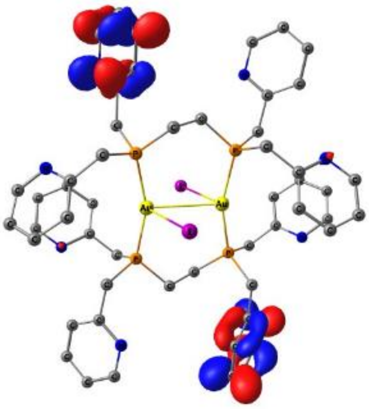
S_4	0.98	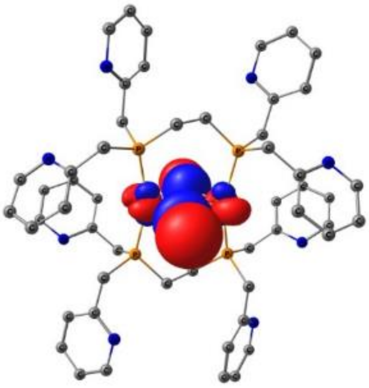	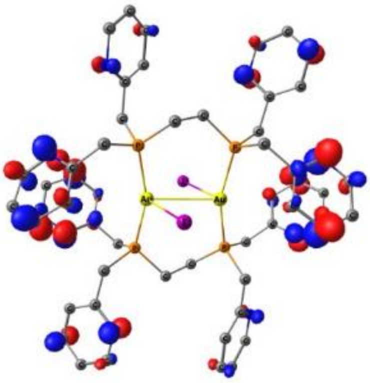
S_6	0.97	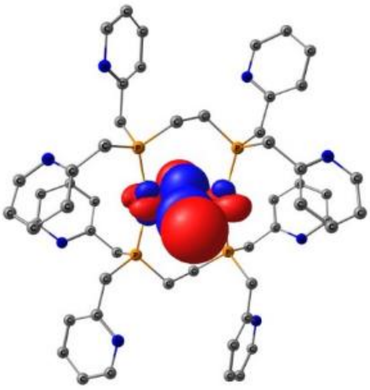	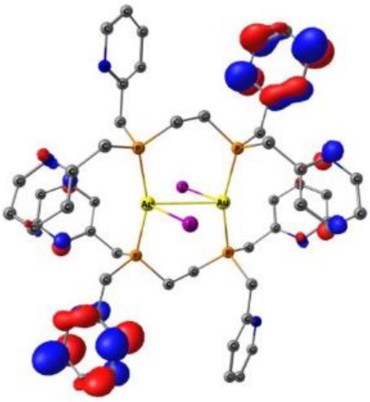

S_7	0.97	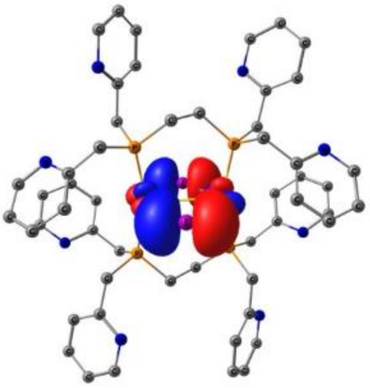	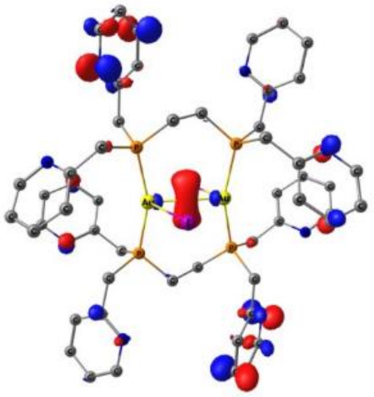

Table S5. The dominant NTO pairs for the excited singlet states of complex **3a**.

Excited state number	W	Hole	Particle
S_1 *f* = 0	0.74	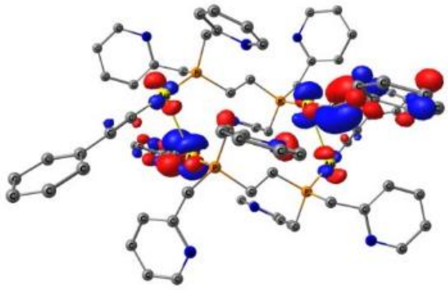	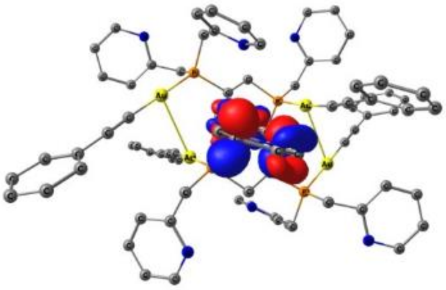
	0.25	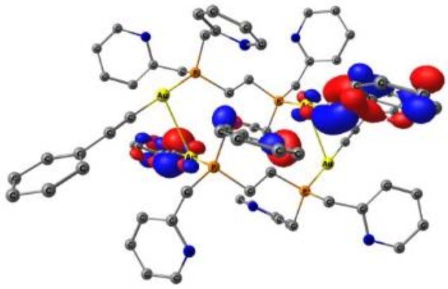	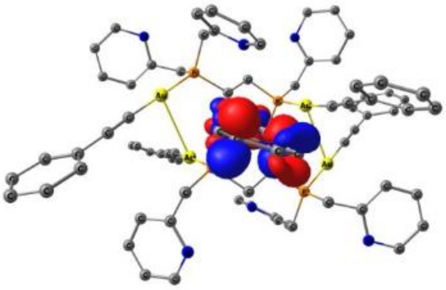
S_2	0.51	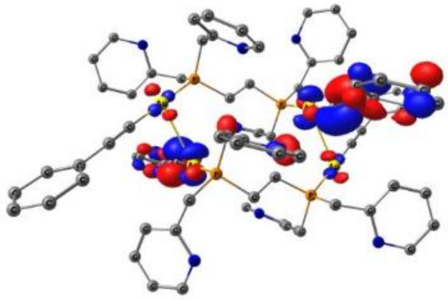	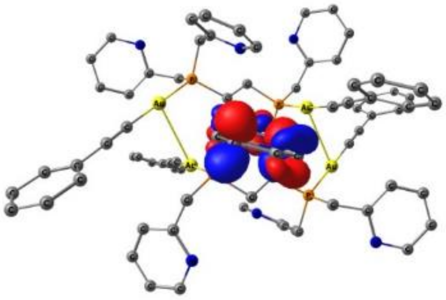
	0.49	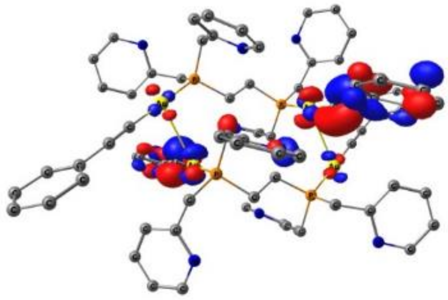	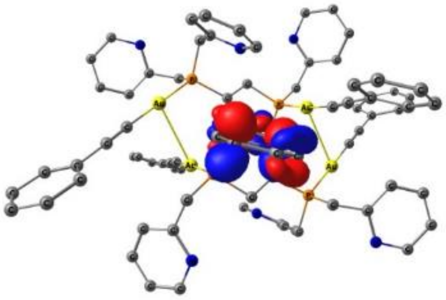

S_3	0.65	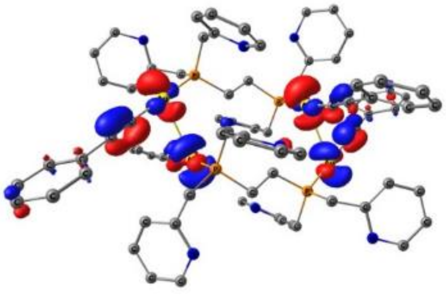	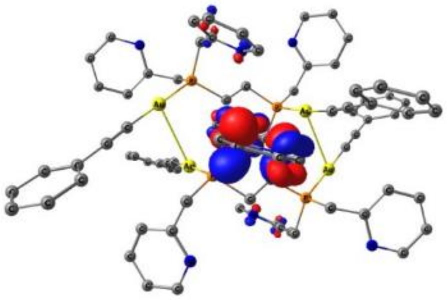
	0.34	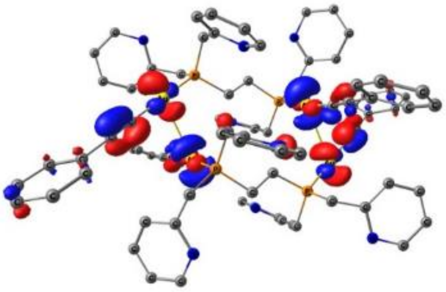	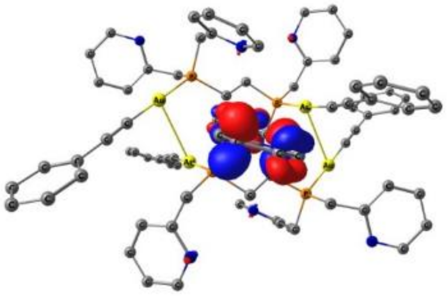
S_7	0.61	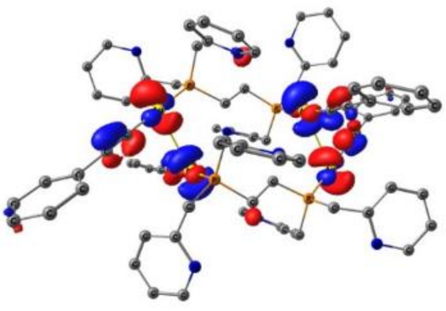	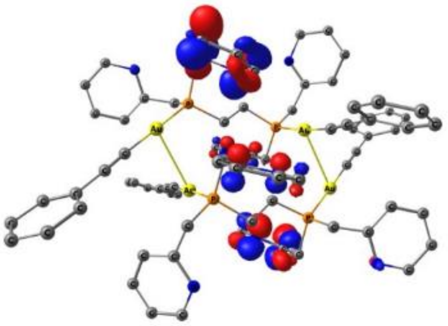
	0.33	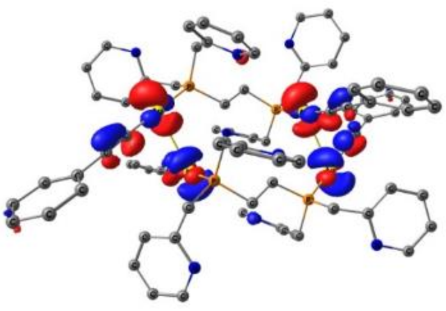	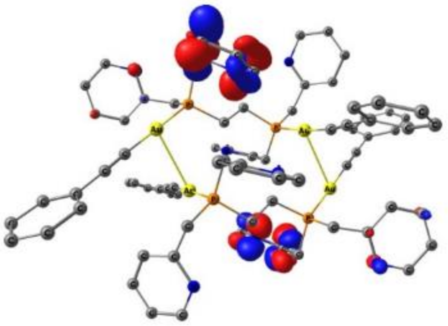
S_{16}	0.45	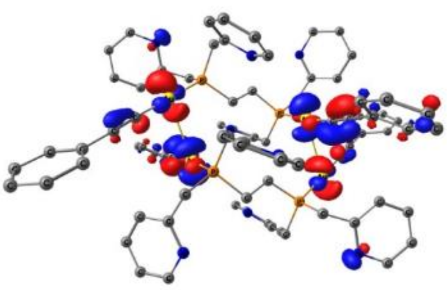	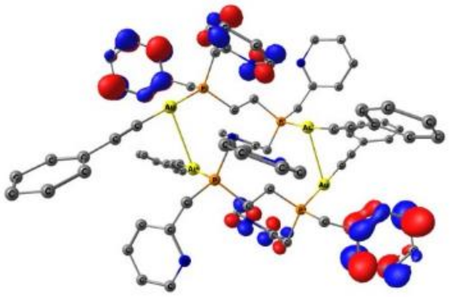
	0.37	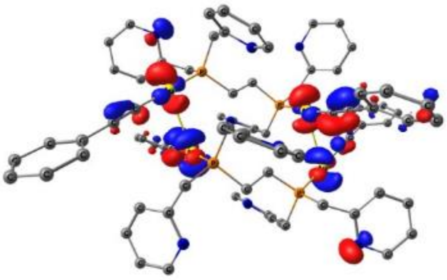	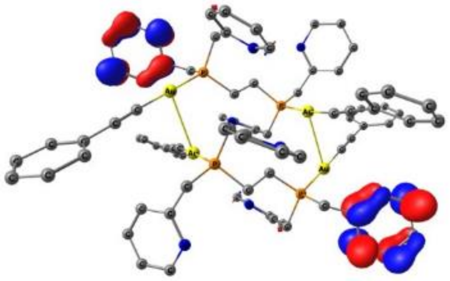

S$_{24}$	0.67	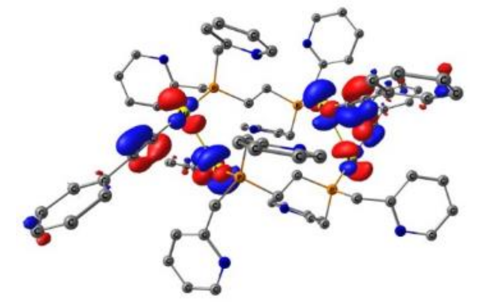	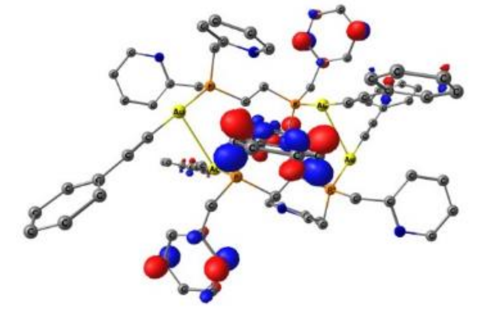
	0.25	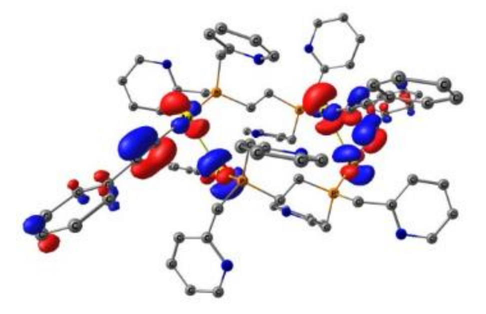	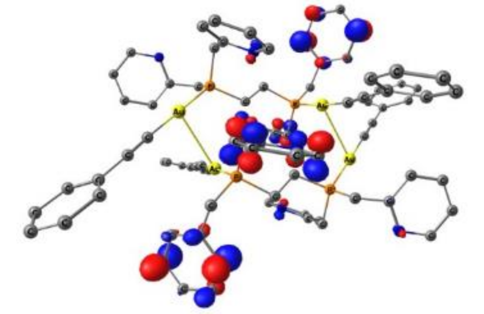

Table S6. The dominant NTO pairs for the excited singlet states of complex **4**.

Excited state number	W	Hole	Particle
S$_1$	0.99	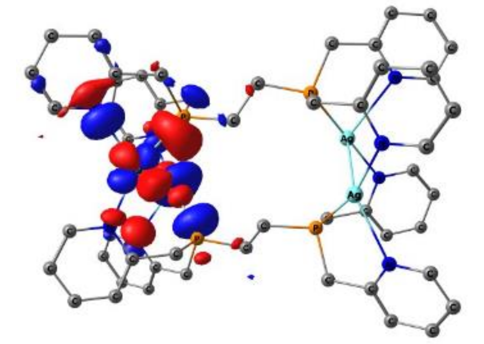	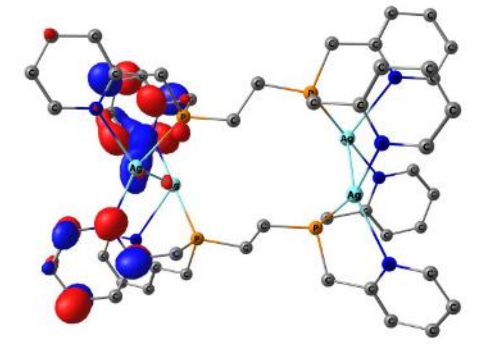
S$_2$	0.99	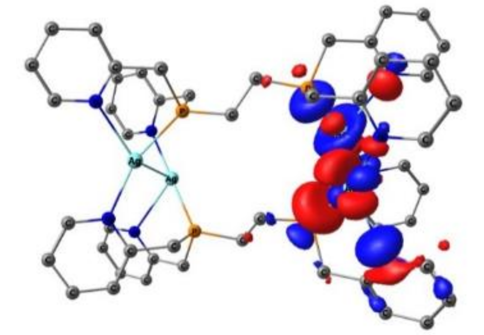	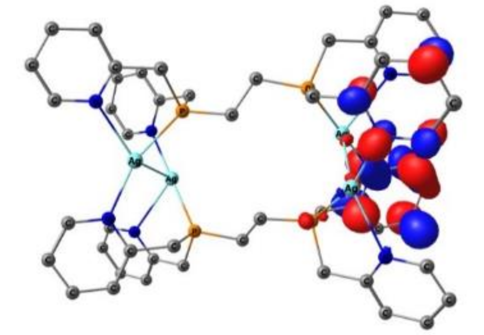
S$_6$	0.59	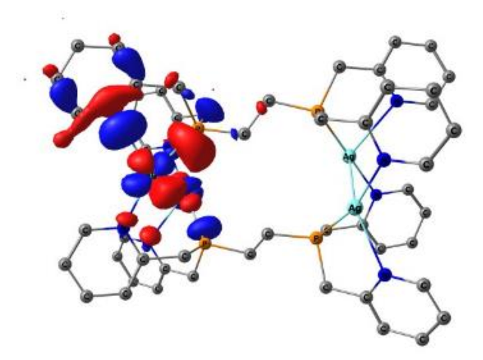	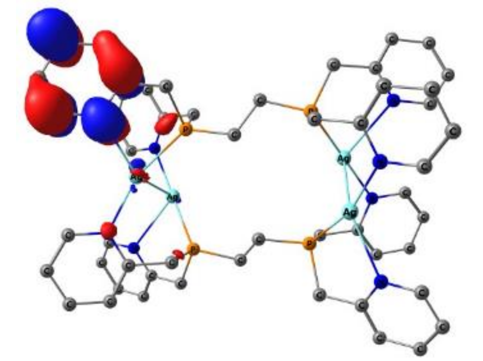

	0.38	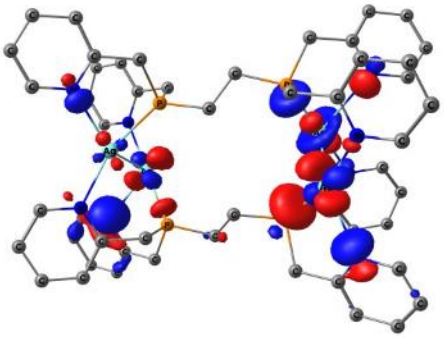	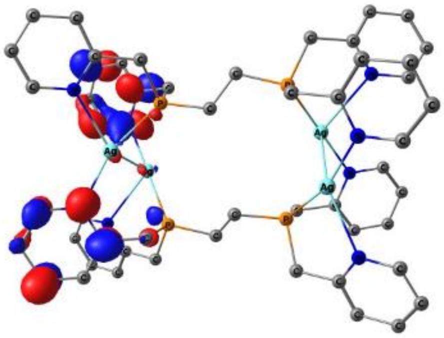
S_8	0.62	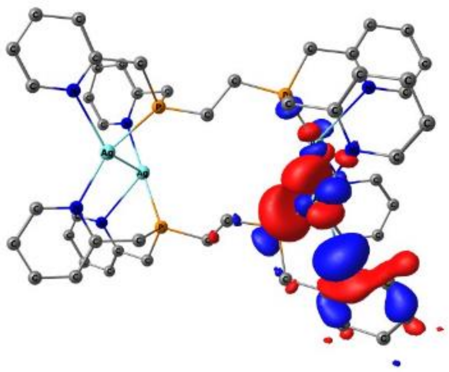	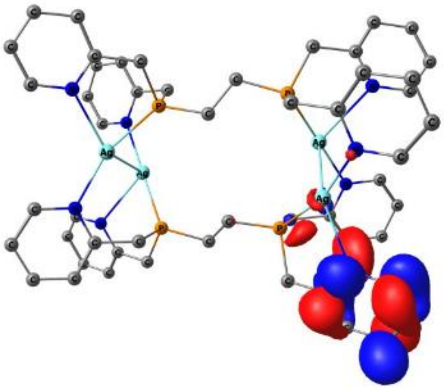
	0.36	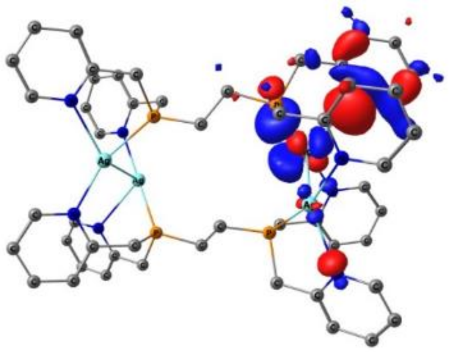	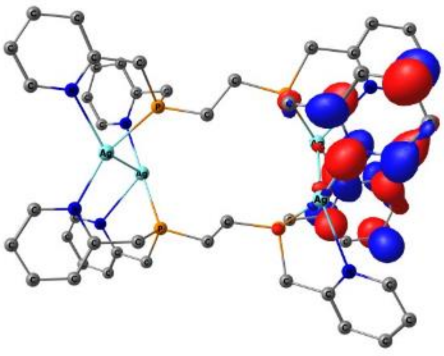
S_{10}	0.69	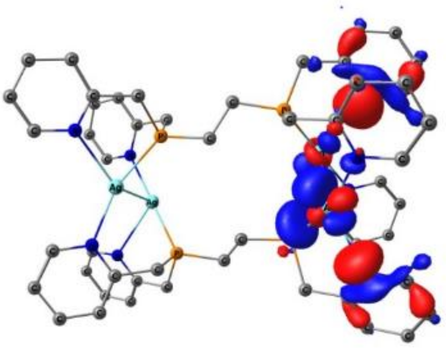	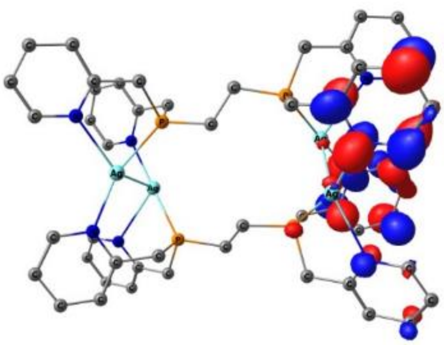

	0.29	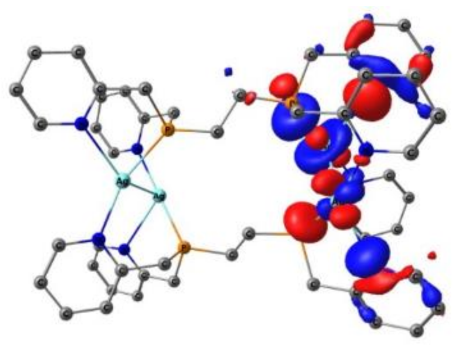	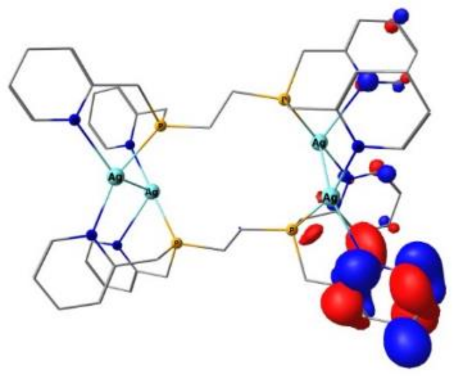
S_{13}	0.86	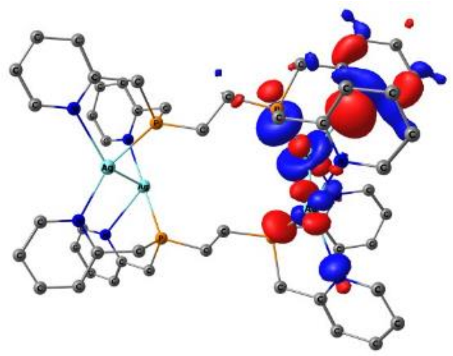	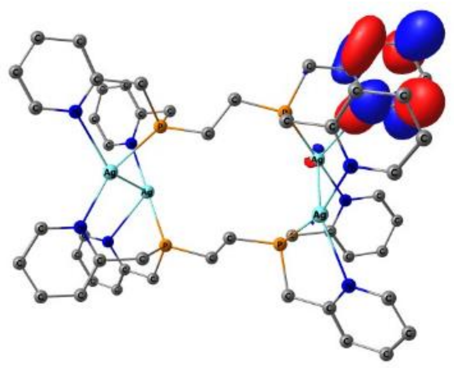

Table S7. The dominant NTO pairs for the excited singlet states of complex **5**.

Excited state number	W	Hole	Particle
S_1 ($f = 0$)	1.00	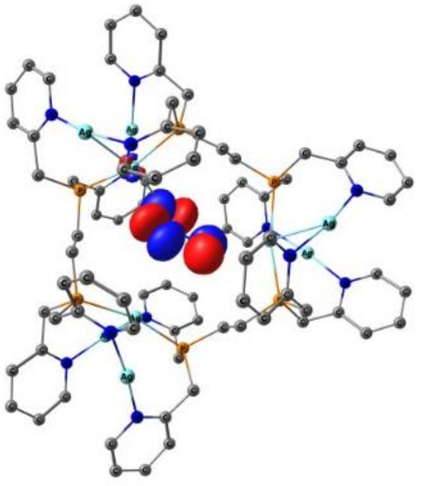	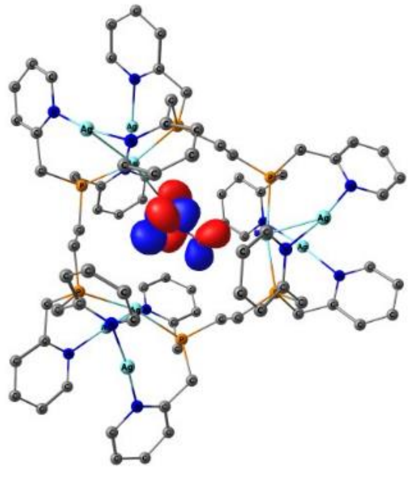

S$_2$	0.76	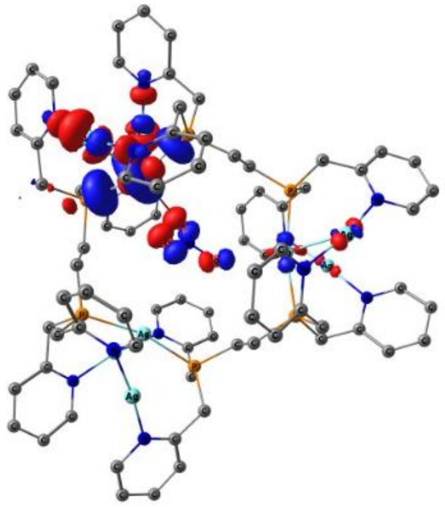	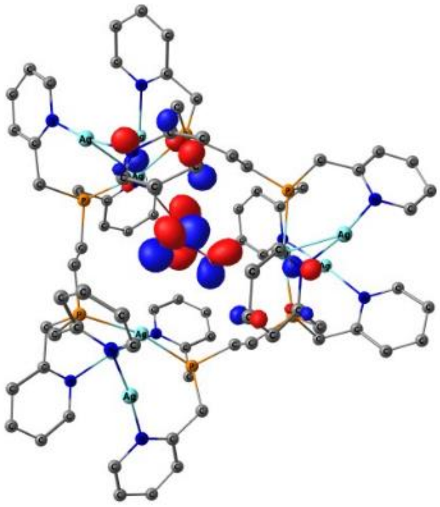
	0.22	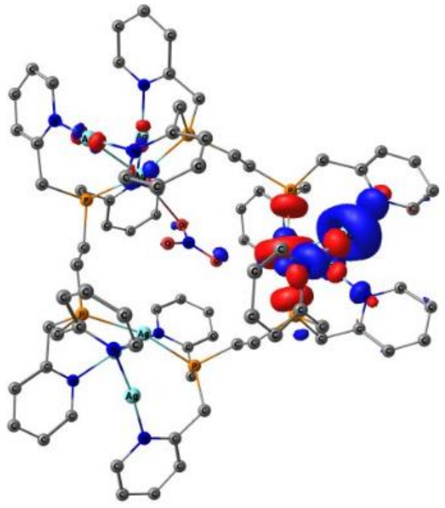	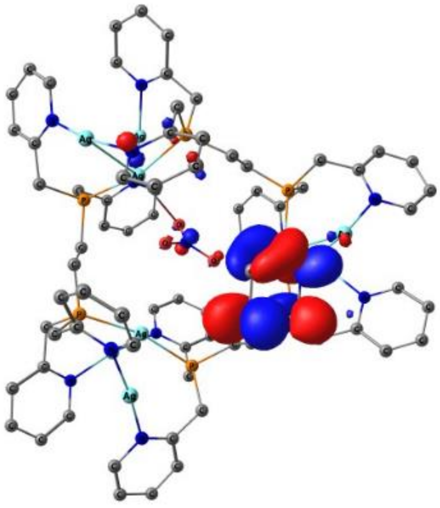
S$_3$	0.79	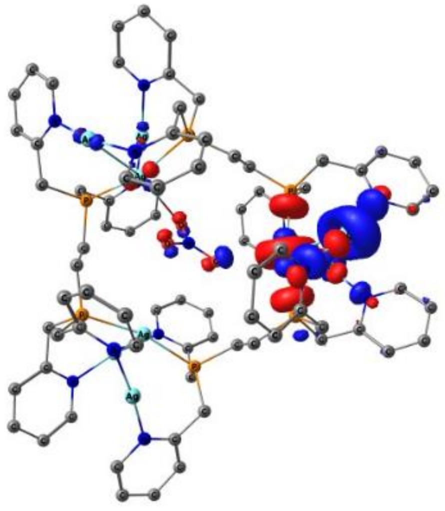	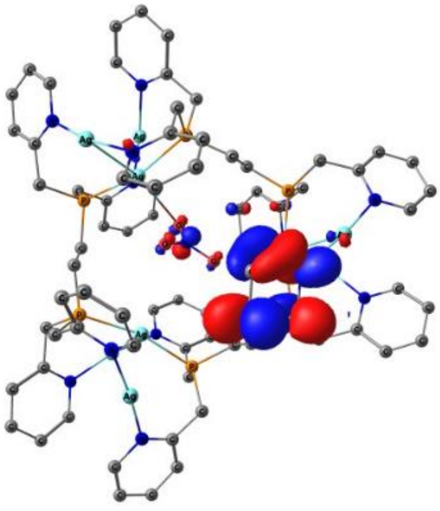

S_4	0.94	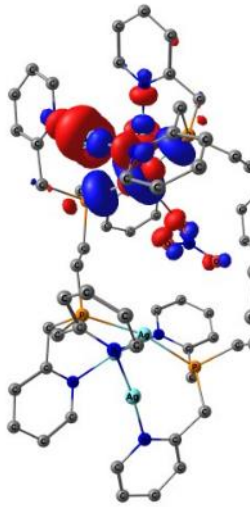	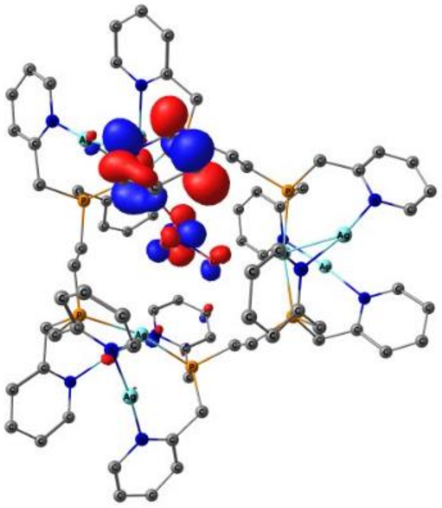
S_8	0.96	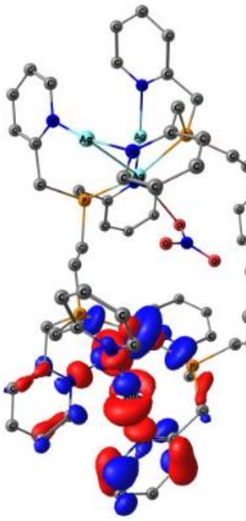	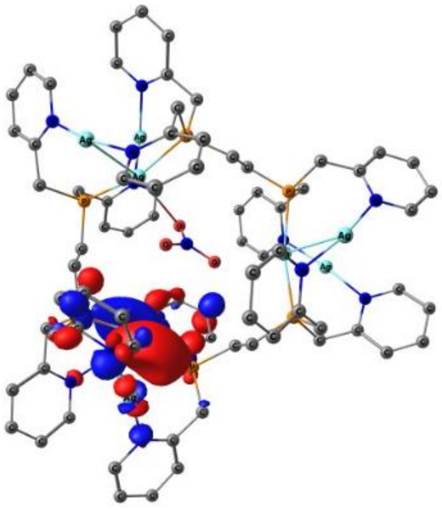

Table S8. The dominant NTO pairs for the excited singlet states of complex **6**.

Excited state number	W	Hole	Particle
S_1	0.69	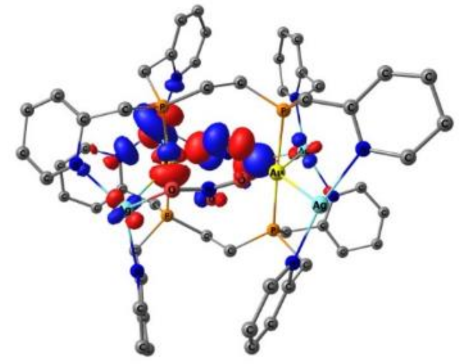	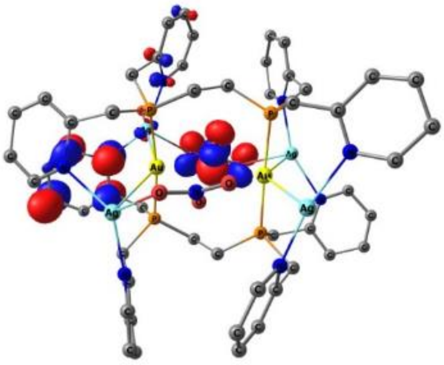

	0.30	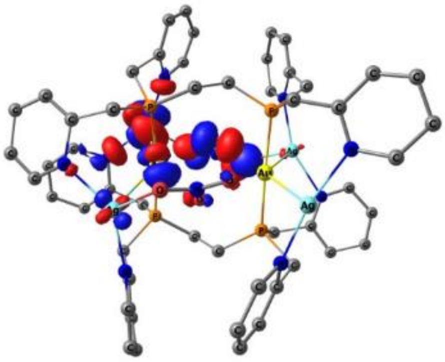	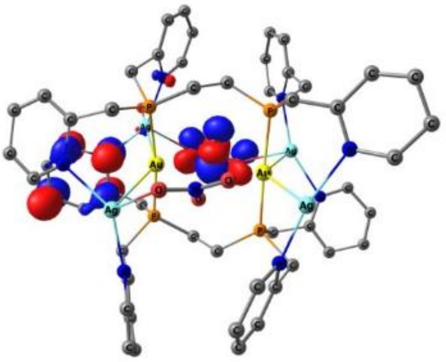
S_2	0.62	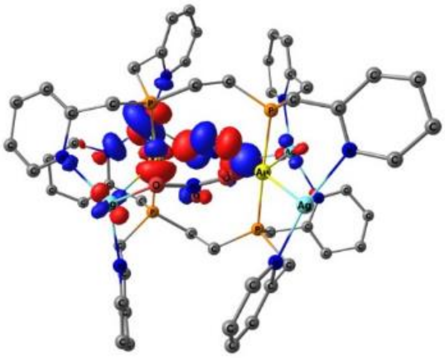	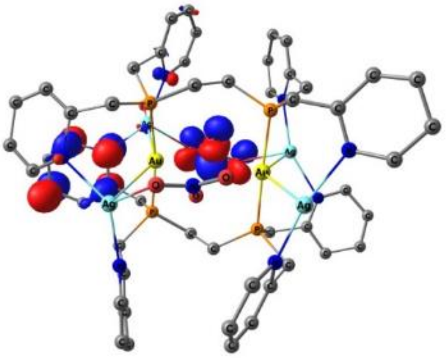
	0.36	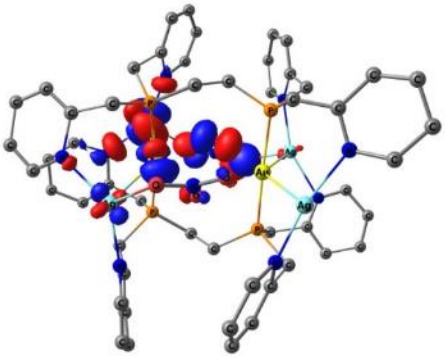	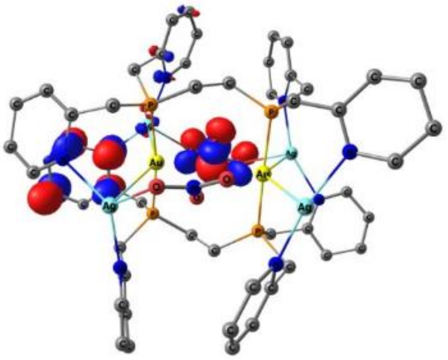
S_4	0.90	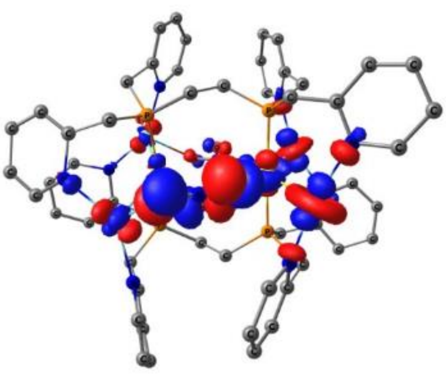	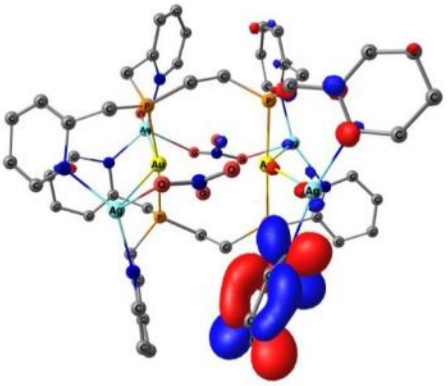
S_6	0.71	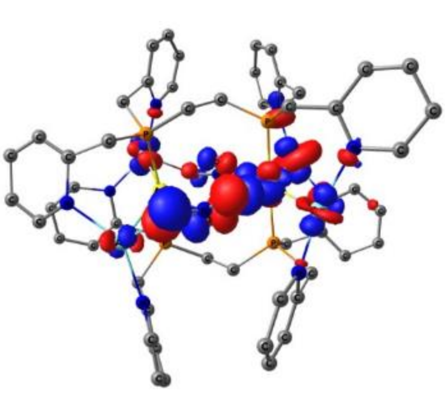	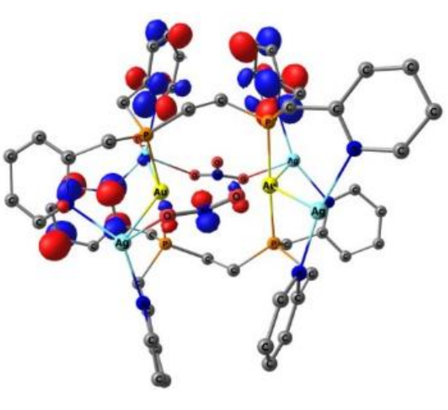

Table S9. The dominant NTO pairs for the excited singlet states of complex **7**.

Excited state number	W	Hole	Particle
S_1	0.83	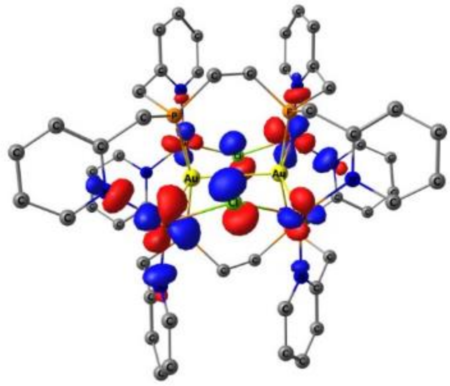	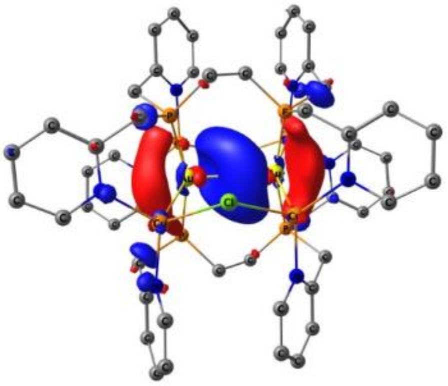
S_4	0.59	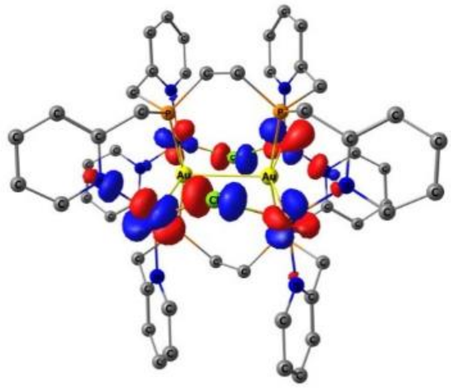	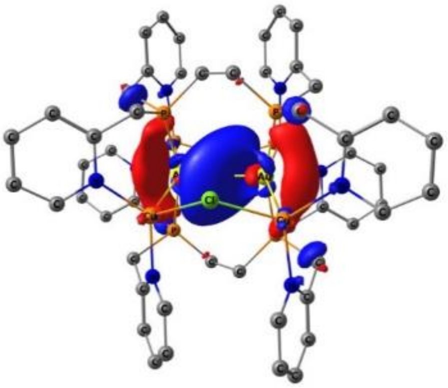
	0.39	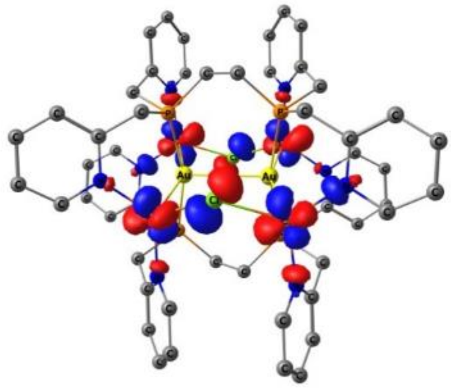	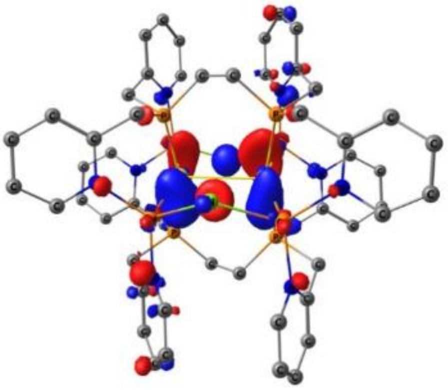
S_7	0.82	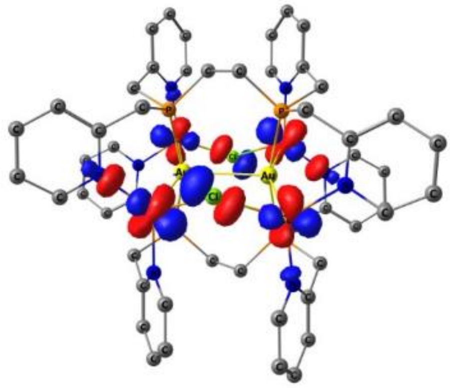	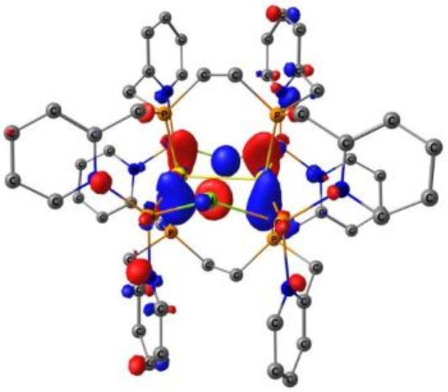

S_{10}	0.61	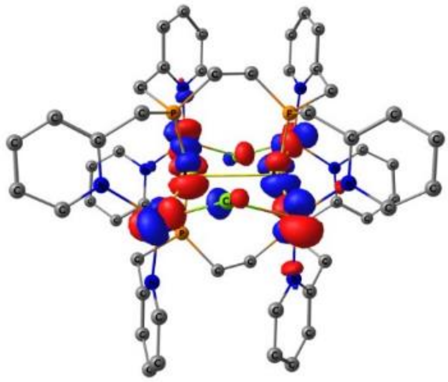	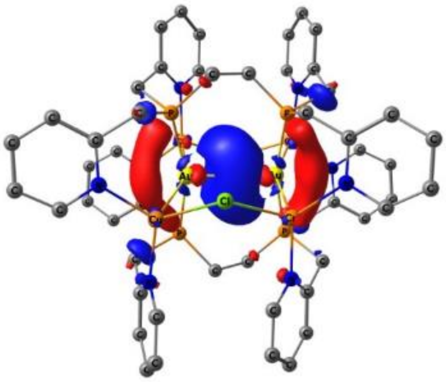
	0.21	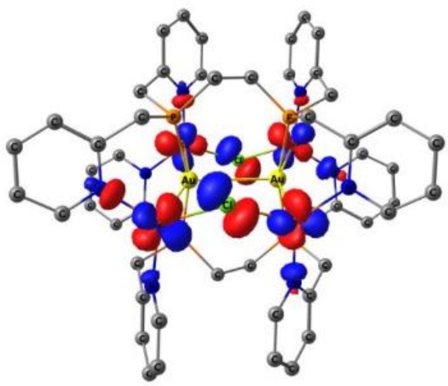	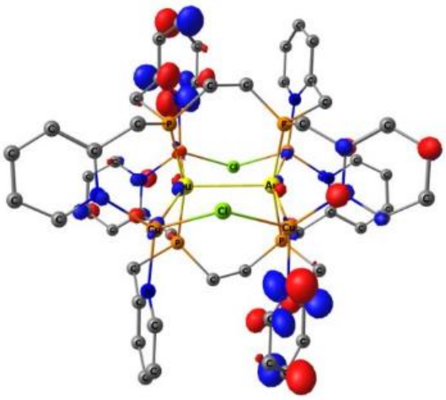
S_{12}	0.40	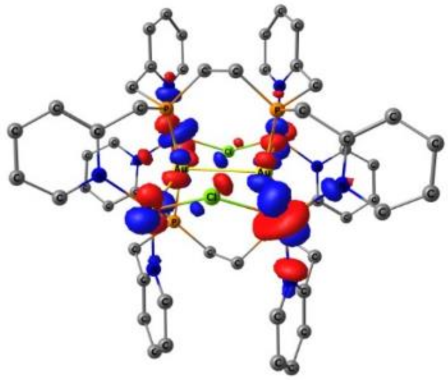	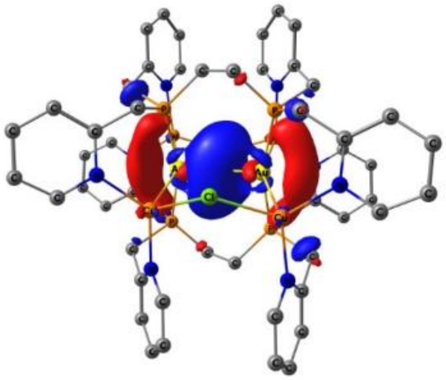
	0.29	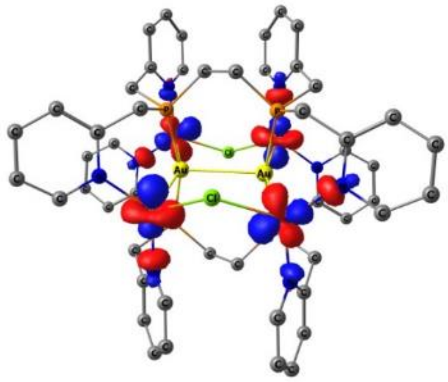	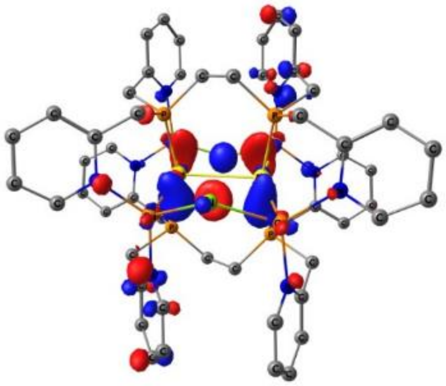
	0.25	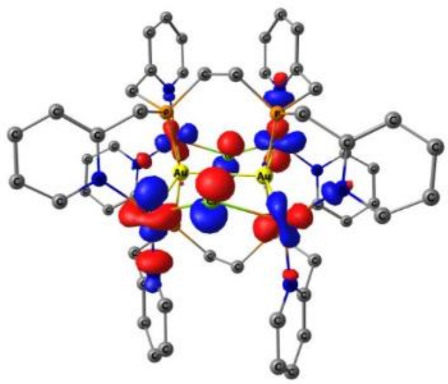	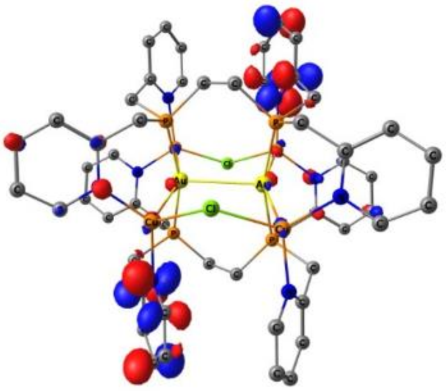

S_{16}	0.31	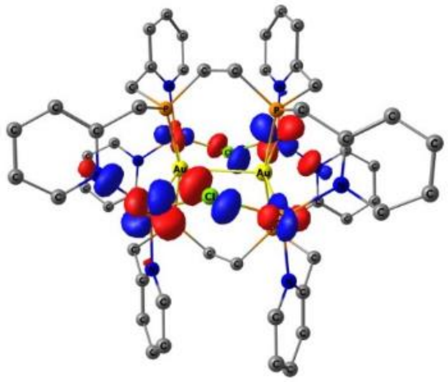	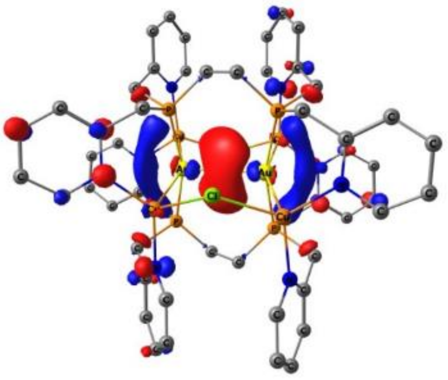
	0.30	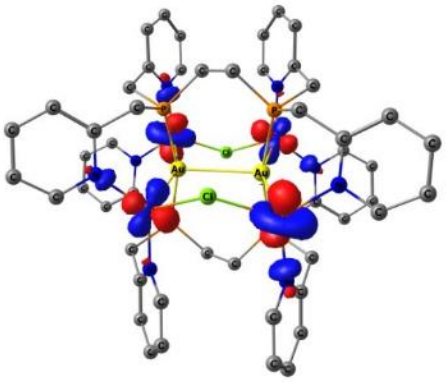	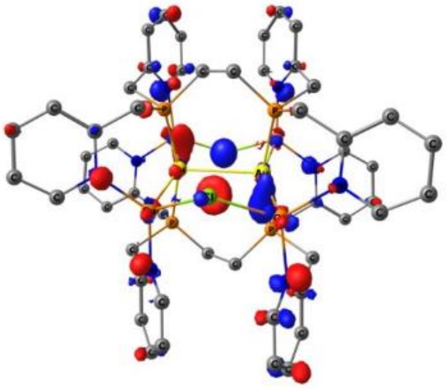
	0.17	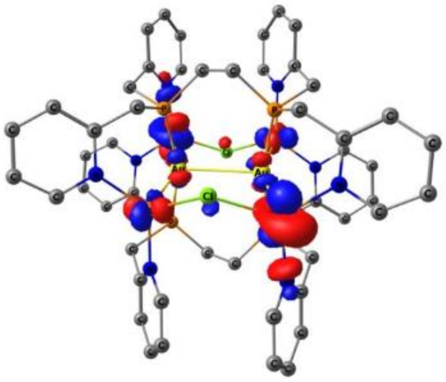	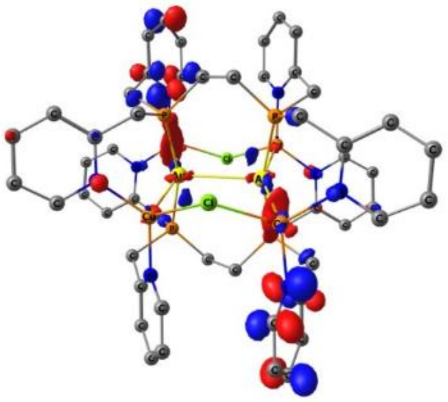

Table S10. The dominant NTO pairs for the excited singlet states of complex **8**.

Excited state number	W	Hole	Particle
S_1	0.96	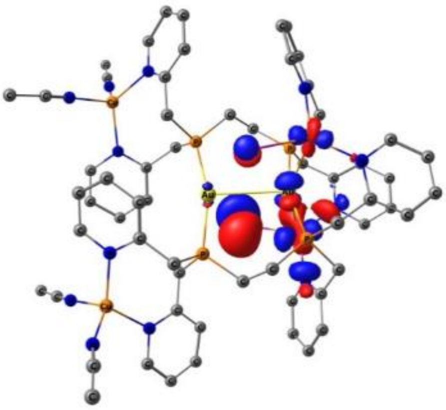	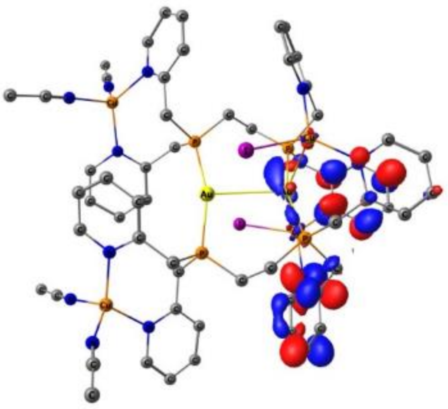

S_2	0.85	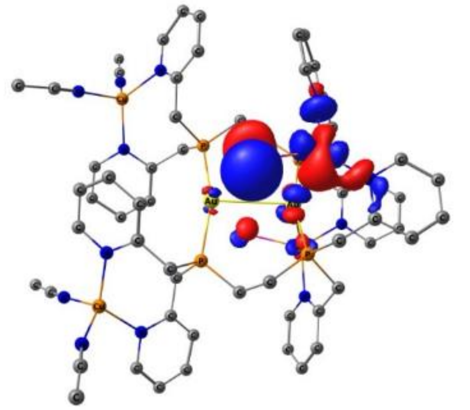	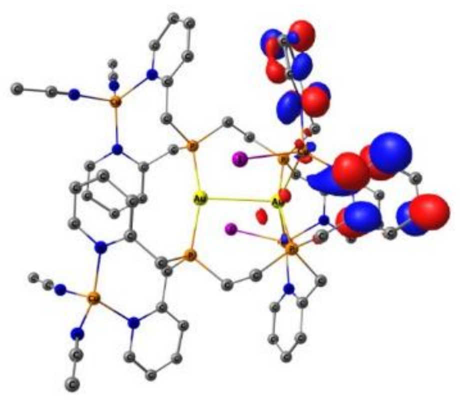
S_3	1.00	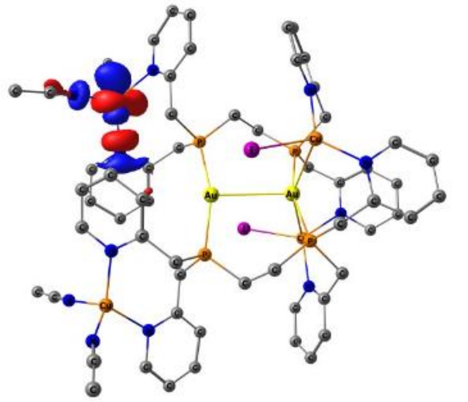	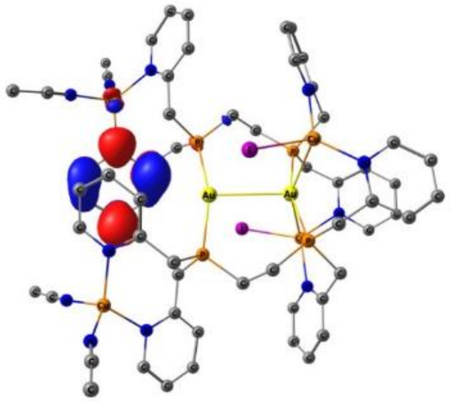
S_4	0.83	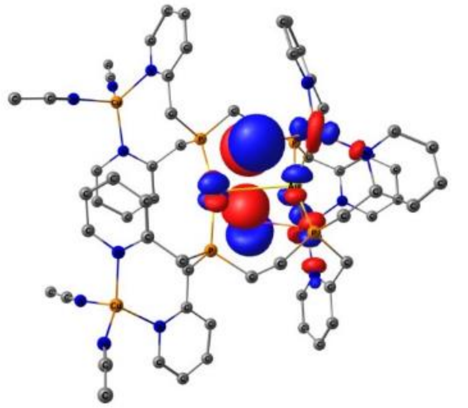	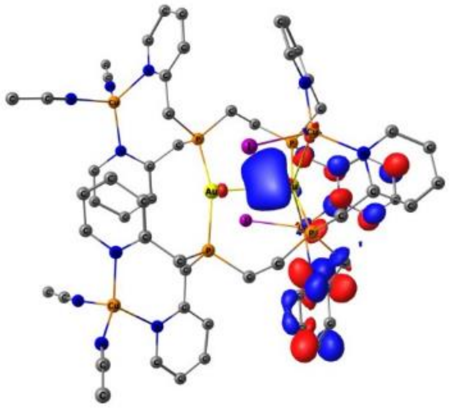
S_5	0.97	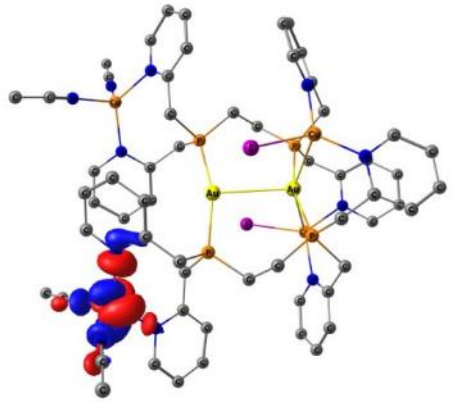	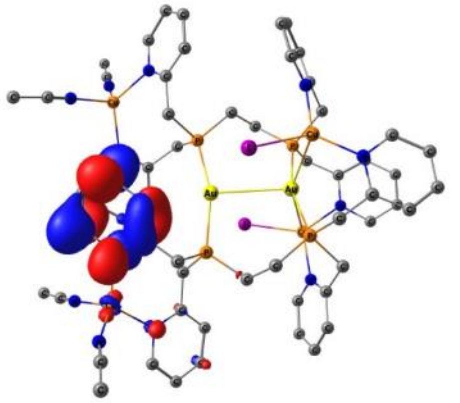

S_6	0.62	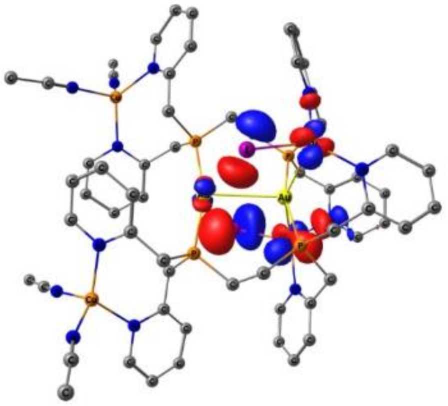	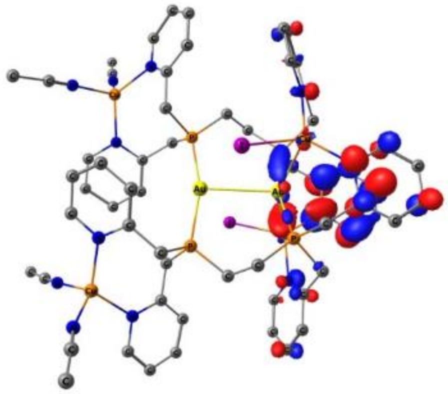
	0.30	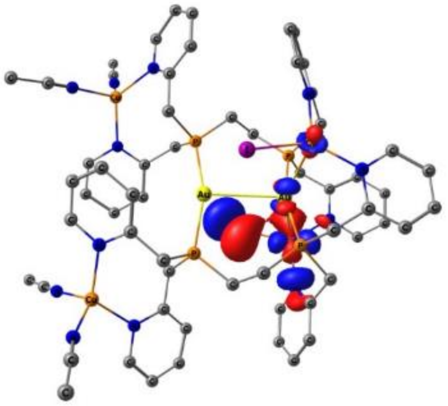	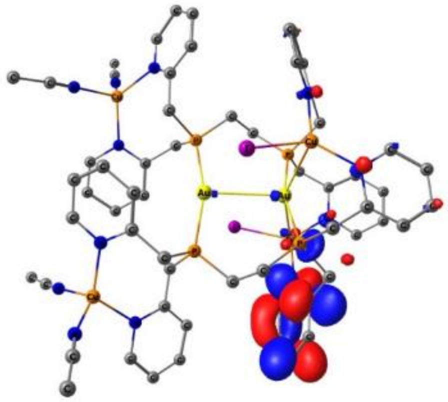
S_9	0.92	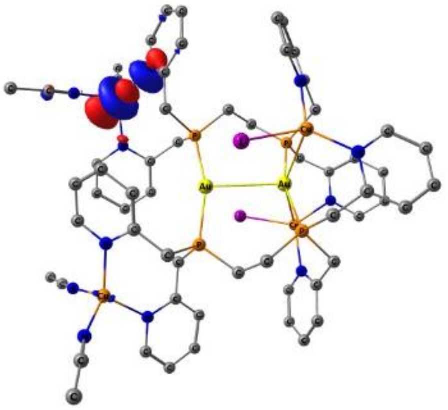	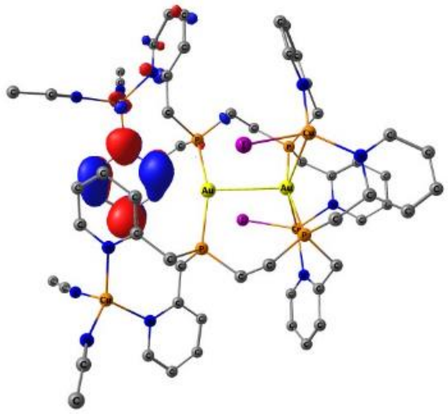
S_{14}	0.64	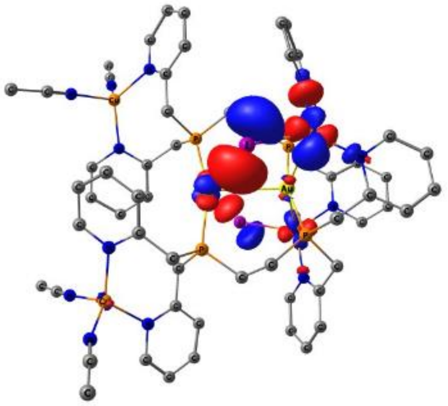	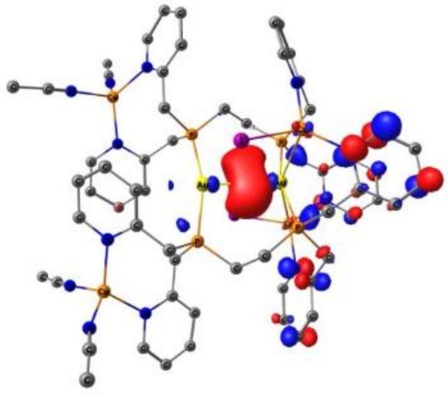

	0.24	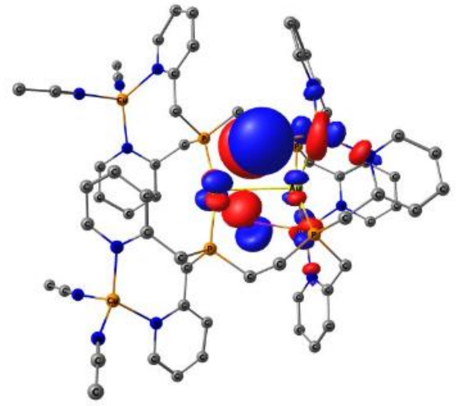	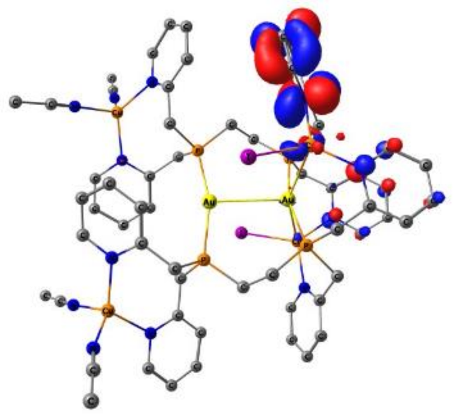

Table S11. The dominant NTO pairs for the first excited triplet states of complexes **1–8**.

Complex	W	Hole	Particle
1	0.96	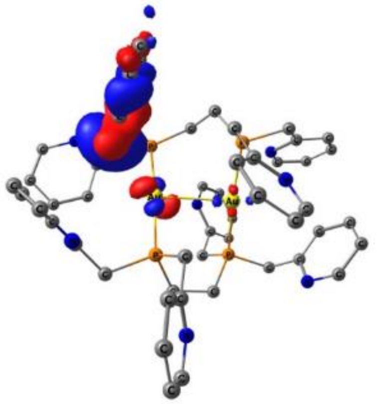	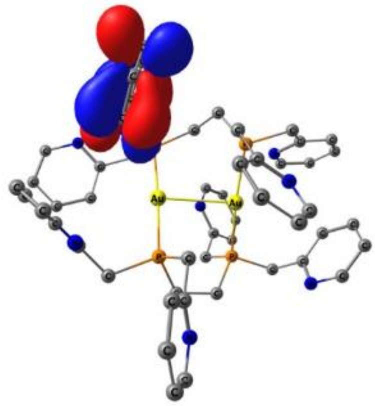
2	0.99	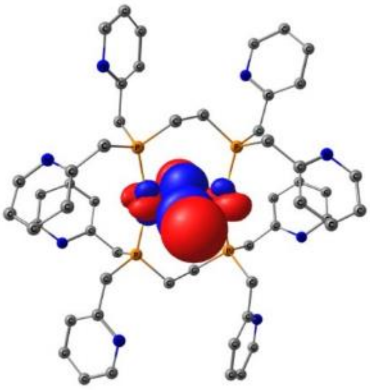	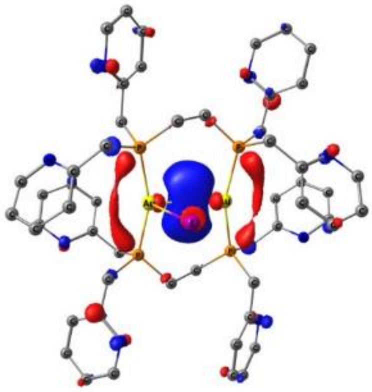
3a	0.39	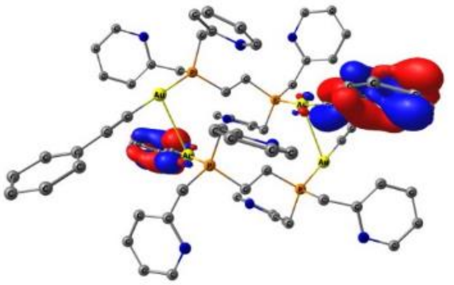	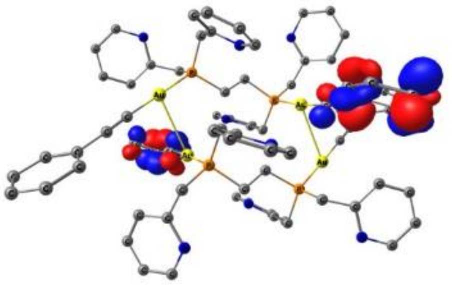
	0.38	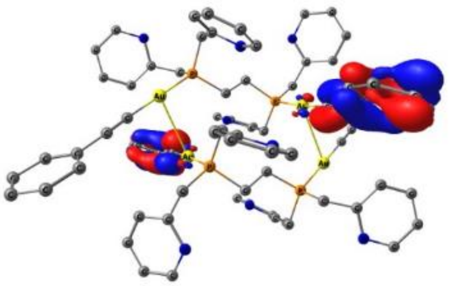	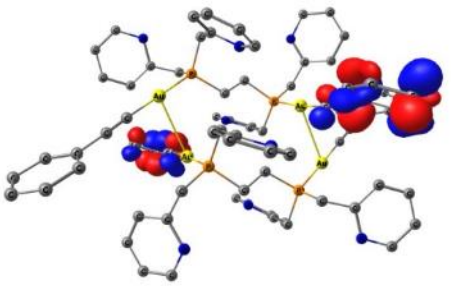

4	0.70	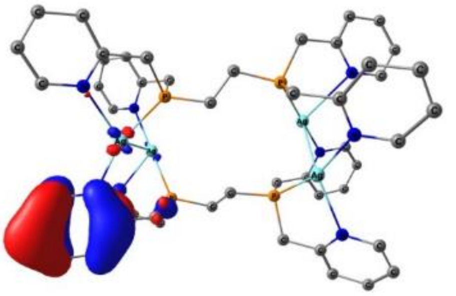	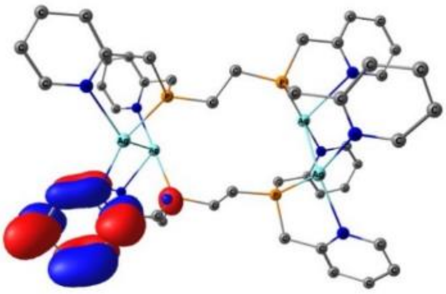
	0.26	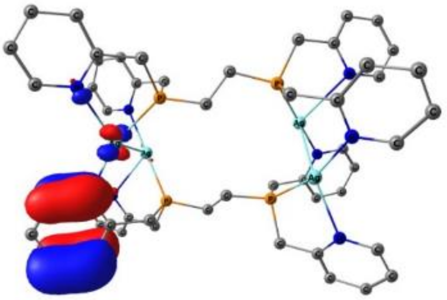	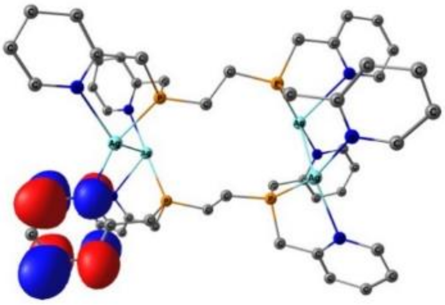
5	1.00	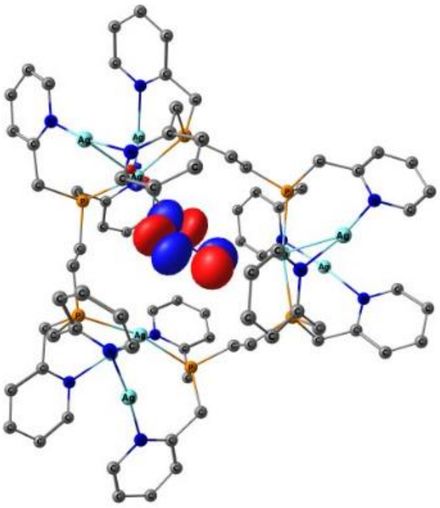	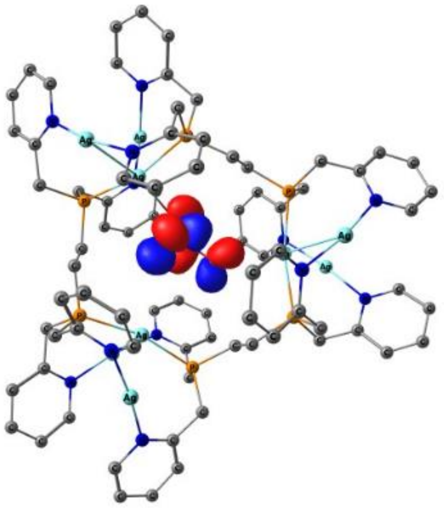
6	1.00	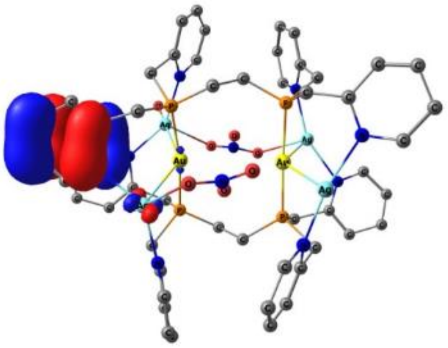	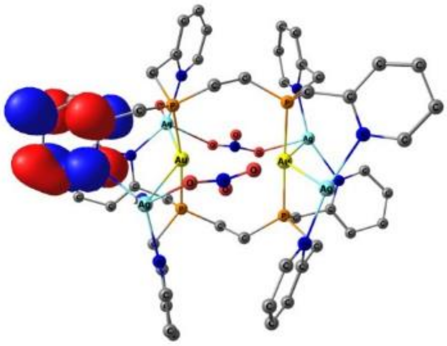
7	0.70	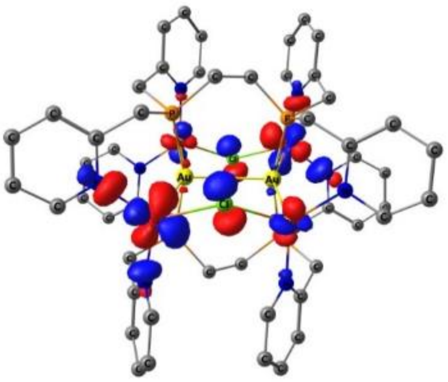	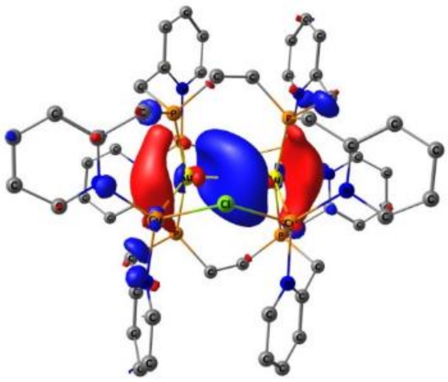

	0.28	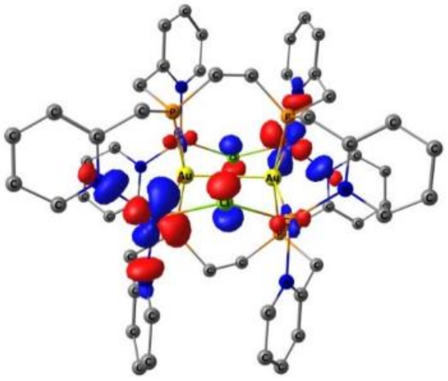	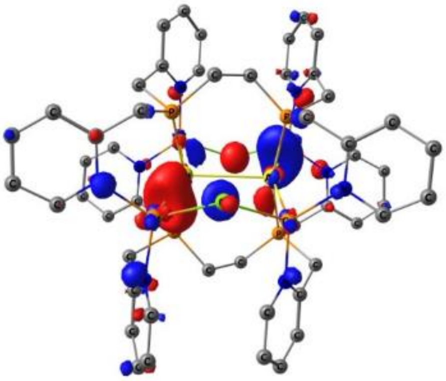
8	0.91	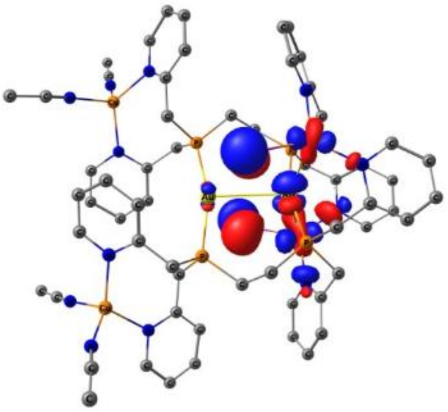	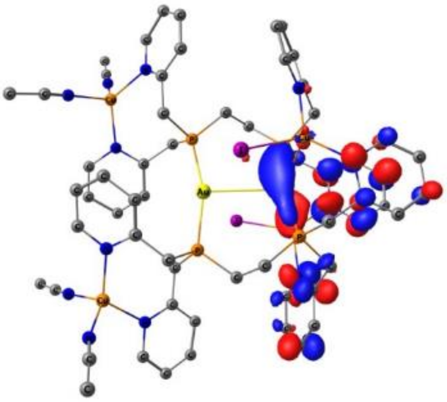

§10. Photophysical data

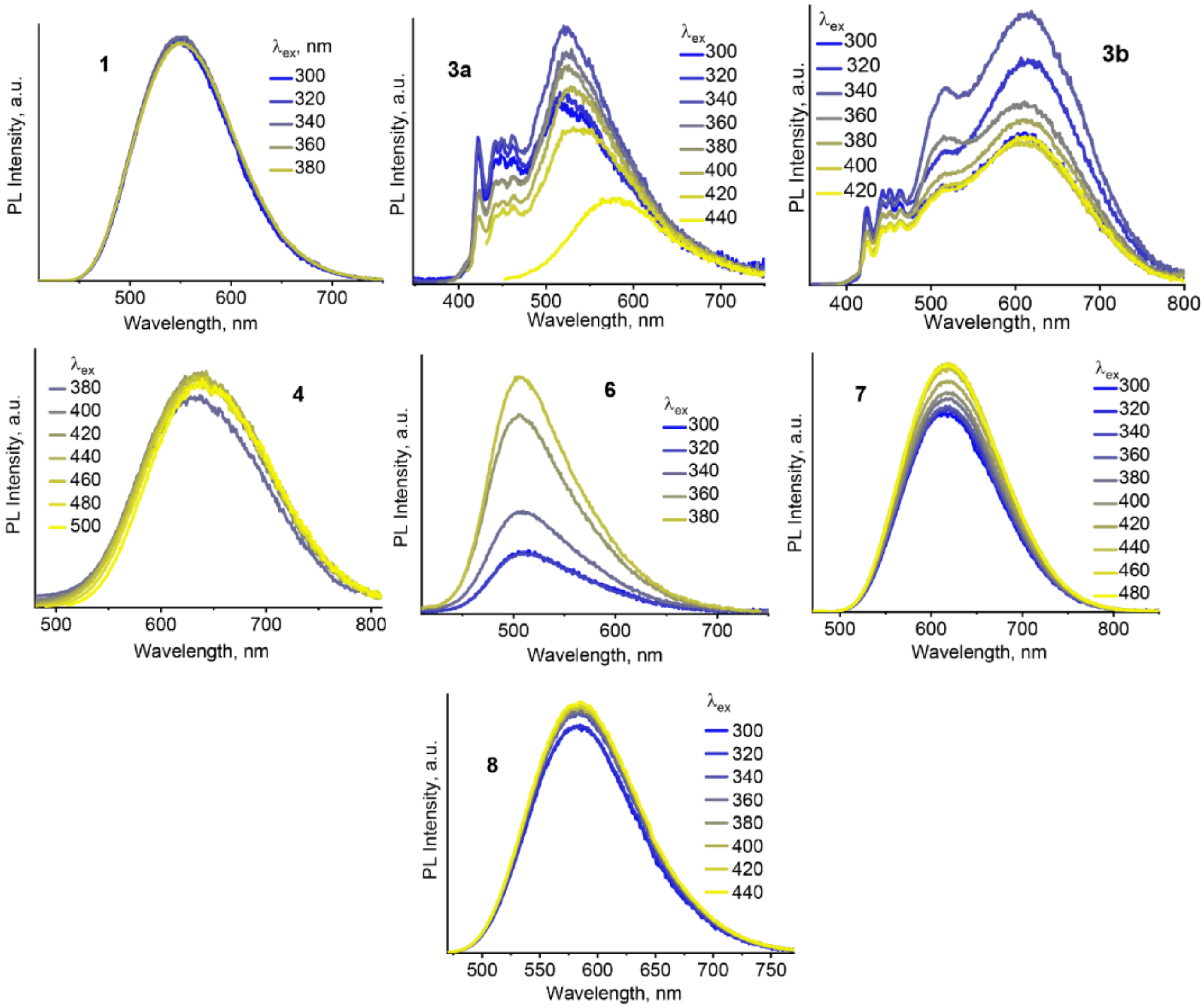

Figure S44. Excitation-dependent PL spectra of solid samples **2**–**4** and **6**–**8** (298 K).

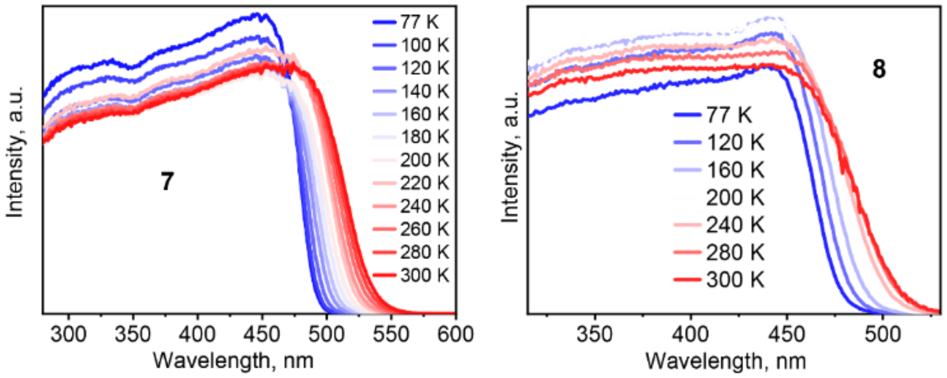

Figure S45. Temperature-dependent excitation spectra of solid samples **7** and **8**.

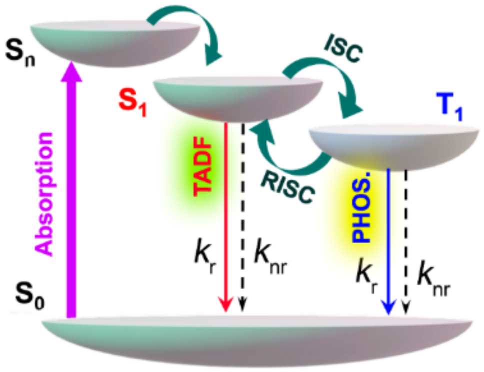

Figure S46. Simplified diagram of the TADF mechanism.

The singlet-triplet splitting energies, $\Delta E(S_1–T_1)$, for **7** and **8** were estimated by fitting the experimental $\tau(T)$ datasets (Fig. 5g in the main document) with the equation (Eq. 1)[16] proposed for the TADF model:

$$\tau(T) = (3 + \exp\left(-\frac{\Delta E(S_1\text{-}T_1)}{k_B T}\right))/(\frac{3}{\tau(T_1)} + \frac{1}{\tau(S_1)}\exp\left(-\frac{\Delta E(S_1\text{-}T_1)}{k_B T}\right)) \quad \text{Eq. 1}$$

where $\tau(T)$ is the observed emission lifetime, $\tau(S_1)$ and $\tau(T_1)$ are the decay times of the S_1 and T_1 excited states, respectively, k_B is the Boltzmann constant, and T is temperature. The evaluated values of $\Delta E(S_1–T_1)$ are 518 and 506 cm^{-1} for **7** and **8**, respectively.

As mentioned in the main text, the NTQ behavior of 8 is related to the fact that the ratio of the non-radiative decay rate to the radiative decay rate (k_{nr}/k_r) for the T_1 state (at 77 K) is higher than that for the S_1 state (at 298 K). In other words, the longer-lived T_1 state of 8 is much more susceptible to non-radiative decay than the shorter-lived S_1 state. In contrast, **7** exhibits ZTQ behavior, showing comparable PL intensities at 77 K and 298 K, which suggests that its T_1 and S_1 states have similar k_{nr}/k_r ratios. To verify these assumptions, we calculated the k_{nr}/k_r ratios for the S_1 states of 7 and 8 using the data in Table 1. For the T_1 states, the k_{nr}/k_r ratios were estimated by assuming that the PLQY is proportional to the integrated PL intensities (**Fig. 5f** in the main text). As seen in **Table S12**, the calculated and estimated k_{nr}/k_r values support our hypothesis. Indeed, for 8, the k_{nr}/k_r ratio for the T_1 state (2.47) is significantly higher than that for the S_1 state (1.63). In the case of 7, the k_{nr}/k_r ratios for the S_1 and T_1 states are nearly identical (1.5 and 1.45, respectively).

Table S12. The calculated radiative and non-radiative rate constants for **7** and **8** at 77 and 298 K.[a]

	k_r (298 K) [10^4 s^{-1}]	k_{nr} (298 K) [10^4 s^{-1}]	k_r (77 K) [10^4 s^{-1}]	k_{nr} (77 K) [10^4 s^{-1}]
7	7.4	11.1	2.2	3.2
8	9.5	15.5	3.6	8.9

[a] The k_n and k_{nr} values were calculated according to k_r = PLQY/τ and k_{nr} = (1 – PLQY)/τ, respectively.

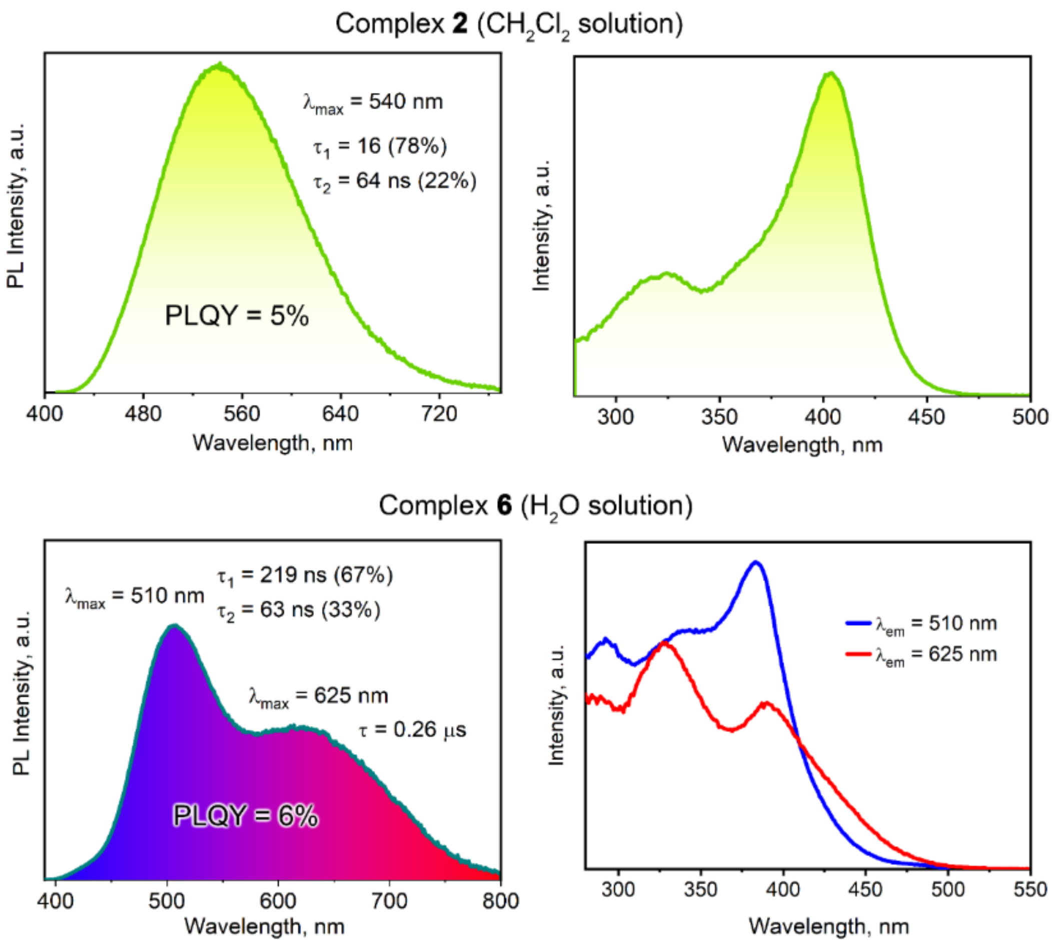

Figure S47. Excitation and emission spectra for solutions of **2** and **6** in CH_2Cl_2 and H_2O, respectively (298 K).

§11. References

1. G. J. Kubas, B. Monzyk, A. L. Crumbliss, *Inorg. Synth.,* **1979**, *19*, 90–92.
2. A. Yu. Baranov, T. S. Sukhikh, A. V. Artem’ev, *J. Struct. Chem.*, **2022**, *63*, 524–526.
3. R. Uson, A. Laguna, M. Laguna, D. A. Briggs, H. H. Murray, J. P. Fackler Jr., *Inorg. Synth.,* **1989**, *26*, 85–91.
4. M. Wilfling and K. W. Klinkhammer, *Angew. Chem., Int. Ed.,* **2010**, *49*, 3219–3223.
5. K. J. Kilpin, R. Horvath, G. B. Jameson, S. G. Telfer, K. C. Gordon, J. D. Crowley, *Organometallics*, **2010**, *29*, 6186–6195.
6. (a) A. V. Alexeev, S. A. Gromilov, *Russ. J. Coord. Chem*., **2010**, *51*, 156–165; (b) A. V. Alexeev, S. A. Gromilov, *J. Struct. Chem*., **2010**, *51*, 744–757.
7. C. Prescher, V. B. Prakapenka, *High Press. Res*., **2015**, *35*, 223–230.
8. G. M. Sheldrick, *Acta Crystallogr., Sect. C: Struct. Chem.*, **2015**, *71*, 3–8.
9. SADABS, v. 2008-1, Bruker AXS, Madison, WI, USA, 2008.
10. A. L. Spek, *Acta Crystallogr.* C, **2015**, *71*, 9–18.
11. M. J. Frisch et al. Gaussian 09, Revision C.01, Gaussian Inc., Wallingford, CT, 2010.

12. (a) C. Adamo, V. Barone, *J. Chem. Phys*. **1999**, *110*, 6158; (b) J.P. Perdew, K. Burke, M. Ernzerhof, *Phys. Rev. Lett*. **1996**, *77*, 3865.
13. P. J. Hay, W.R. Wadt, *J. Chem. Phys*., **1985**, *82*, 299–310.
14. G. A. Petersson, M. A. Al-Laham, *J. Chem. Phys*., **1991**, *94*, 6081–6090.
15. (a) R. Bauernschmitt, R. Ahlrichs, *Chem. Phys. Lett*. **1996**, *256*, 454; (b) C. Van Caillie, R.D. Amos, *Chem. Phys. Lett*. **1999**, *308*, 249; (c) G. Scalmani, M.J. Frisch, B. Mennucci, J. Tomasi, R. Cammi, V. Barone, *J. Chem. Phys*. **2006**, *124*, 094107.
16. H. Yersin, A.F. Rausch, R. Czerwieniec, T. Hofbeck, T. Fischer, *Coord. Chem. Rev.* **2011**, *255*, 2622.